ROLE OF PROGENITOR CELLS IN REGENERATION OF LUNG TISSUE FOLLOWING INFLUENZA INFECTION

YIN LU

(B.Eng., NTU)

A THESIS SUBMITTED

FOR THE DEGREE OF DOCTOR OF PHILOSOPHY

IN COMPUTATION AND SYSTEMS BIOLOGY (CSB)

SINGAPORE-MIT ALLIANCE

NATIONAL UNIVERSITY OF SINGAPORE

2012

DECLARATION

I hereby declare that this thesis is my original work
and it has been written by me in its entirety.
I have duly acknowledged all the sources of
information which have been used in the thesis.

This thesis has also not been submitted for any
degree in any university previously

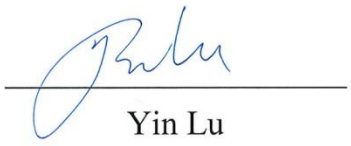

Yin Lu
1 October 2012

ACKNOWLEDGEMENTS

I would like to express my most sincere gratitude to my advisors Prof. Hanry Yu and Prof. Jianzhu Chen for their patient guidance and all-sided supports throughout my candidature. Their infinite passion in exploration of unknown impressed me deeply and inspired me with enthusiasm in science. Their stringent attitude in research served as an excellent illustration to me. It was my great luck and honour to be a part of their teams. I am extremely grateful to Prof. Yu for the freedom he gave to me to work on areas outside of the group's main scope, which encouraged me to grow as an independent researcher. I am thankful to Prof. Chen for carefully directing my project at every critical stage, and giving invaluable suggestions on my future career plans.

I am indebted to my co-advisors Prof. Jagath Rajapakse and Prof. Vincent Chow, who generously provided me with important resources and techniques. Prof. Chow's unreserved sharing of lab produced virus has incredibly accelerated my progress of work and his critical feedbacks on my manuscripts have contributed greatly to my learning process. Prof. Rajapakse and his team provided outstanding technical support in terms of image processing and equipped me with expanded knowledge and skills.

Special thanks to my teammates Dr. Gino Limmon, Dr. Dahai Zheng and Ms. Nicola Leung. It was Dr. Limmon and Dr. Zheng's selfless sharing of

knowledge and experiences and step-by-step demonstrating of experiment that brought me into the field of biology from an engineering background. Working together as a team has greatly promoted my intellectual growth, and I could not have achieved as much as I have without their help. I thank Ms. Leung for her dedicated support to me and the team. Thanks to her timely taking care of orderings, organization of experimental reagents and documentations, and fluency skill with animal work, the team could operate extremely smoothly.

I wish to extend my pure-hearted gratitude to all my colleagues in Chen and Hanry Labs and Singapore-MIT Alliance for Research and Technology (SMART) Infectious Disease Interdisciplinary Research Group (ID-IRG) for all their inputs, discussions, supports and creating a wonderful learning and working environment. I also wish to thank Singapore-MIT Alliance (SMA) and SMART for providing me with a memorable graduate school experience and bountiful funding.

Even the most gorgeous words fail to express my deepest gratitude to my family and friends, who always smooth my sorrow and bring joy to me. This thesis is dedicated to all of them.

TABLE OF CONTENTS

SUMARRY

It is believed that lung tissue regeneration post injury requires a functional pool of stem or progenitor cells. The role of multiple lung progenitor and putative stem cell types in repairing lung tissue have been demonstrated in chemical and physical injury models in recent studies, however, the rare chances in reality of exposure to those injury sources renders the studies less clinically significant. Lung injury caused by influenza virus infection is frequent and globally spreading. In this study, we established a novel lung injury model using Influenza virus to explore the cellular and molecular pathways of lung tissue repair. We carried out comprehensive immunohistochemical analysis during the course of influenza infection and recovery. A novel cell type expressing the Alveolar type II cell (AT2) marker surfactant protein C (SPC) was observed to be induced in bronchioles in the damaged areas of the lung. These cells, referred to as SPC^{+} bronchiolar epithelial cells (SBECs), could be genetically traced to originate from Clara cells. SBECs form the tips of extending bronchioles and differentiate into AT2s during the regeneration of alveolar epithelium in a process similar to development of embryonic alveolar epithelium. These findings demonstrated that influenza-induced lung tissue damage repair involves Clara cell to AT2 differentiation through reactivation of the embryonic lung development program. We also developed imaging-based high throughput tissue informatics methods to quantitatively accessing the extent of lung damage and repair on

tissue level and trace the dynamic responses of the three critical progenitor cells involved in lung repair process. The results supported the novel lung repair mechanism we proposed in a computational and systematic way. Moreover, by applying the developed quantification methods, we obtained preliminary observations to elucidate differences in lung damage repair between adult and aged mice in terms of lung tissue regeneration following injury, with an aim to shed light on the cause of the much more severe disease in the elderly. This study holds great clinical significance since it would lead to the identification of cellular and molecular targets for therapeutic intervention.

LIST OF TABLES

LIST OF FIGURES

LIST OF ACRONYMS

AT1: alveolar type I cell

AT2: alveolar type II cell

BADJ: bronchioalveolar duct junction

BALF: bronchioalveolar lavage fluid

BASC: bronchioalveolar stem cell

CCSP: Clara cell secretory protein

Clara^{v}: variant Clara cell

CYP2F2: cytochrome P450, family 2, subfamily f, polypeptide 2

mT: tomato red

NEB: neuroendocrine body

PDPN: podoplanin

SBEC: SPC^{+} bronchiolar epithelial cell

SPC: surfactant protein C

TMX: tamoxifen

CHAPTER 1 - GENERAL INTRODUCTION

Mammalian respiratory system includes proximal conducting region and distal respiratory region, the lung. The conducting region includes trachea and bronchi, which further divide within the lung to bronchioles and alveoli (Figure 1). Study on the lung is complicated by the diversity of lung epithelial cell types. In murine, basal cell, Clara cell and ciliated cell are the major cell types in proximal conducting region. Non-ciliated columnar Clara cell is the predominant cell type in distal bronchiolar epithelium. The alveolar epithelium is comprised of squamous Alveolar Type I cells (AT1) and cuboidal Alveolar Type II cells (AT2).

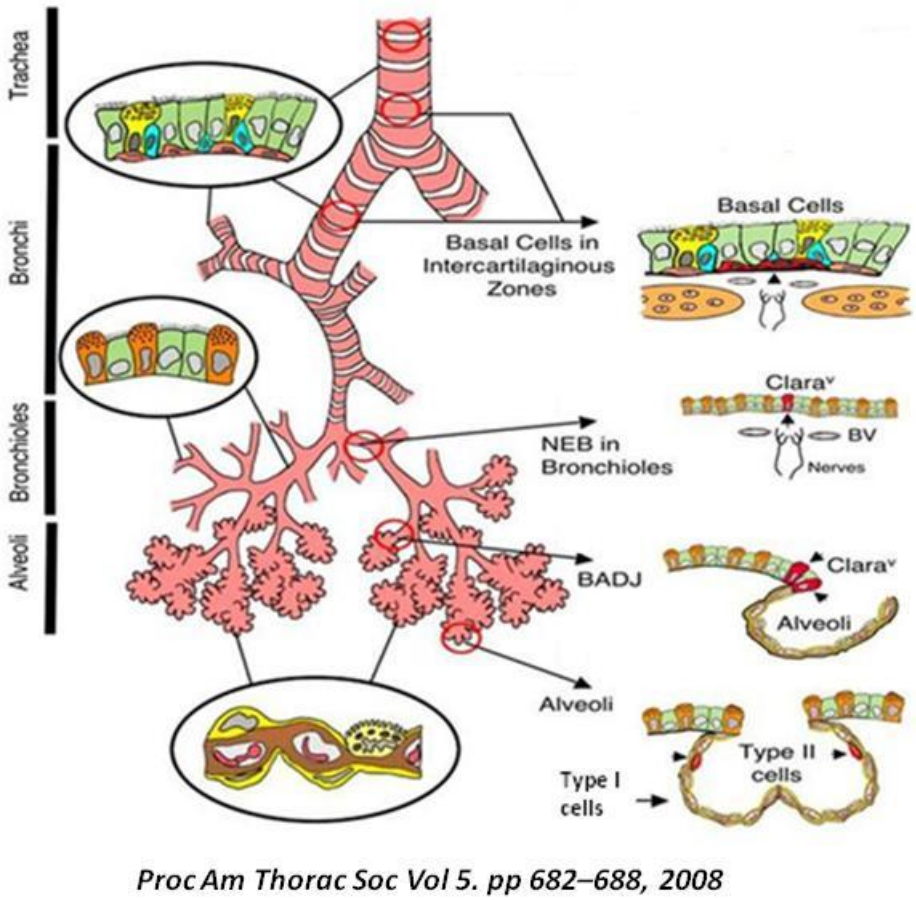

Figure 1. Putative stem and progenitor cells in the lung

The ability of lung tissue to repair itself has been well demonstrated in many studies on injury models. Although little is known about the underlying mechanism, it is believed that lung stem or progenitor cells play crucial roles in this process (Liu et al., 2006). In proximal conducting airway, basal cell is widely accepted as the stem cell population for its ability to renew itself and give rise to almost all other major cell types in this region, including Clara cell, ciliated cell, goblet cell, etc and restore the epithelial structure *in vivo* (Hong et al., 2004; Schoch et al., 2004).

However, previous studies fail to identify a single stem cell type in the lung that can give rise to all the epithelial lineages, and the mechanisms of bronchiolar and alveolar epithelium regeneration, especially under severe physiological conditions, remains unclear. Nevertheless, the functions of Clara cell and AT2 as progenitor cell and capacity for repair lung tissue at their respective residential anatomical locations have been widely studied with various injury models. Evidence has partially proven Clara cell's capacity in maintain and repair bronchiolar epithelium (Rawlins et al., 2009a; Reynolds and Malkinson, 2010; Stripp and Reynolds, 2008). Most current knowledge on regeneration of damaged alveolar epithelium derives from studies on bleomycin-induced lung injuries models, which causes pulmonary toxicity including fibrosis (Azambuja et al., 2005; Gothelf et al., 2003; Woolfenden et al., 1979). Based on histology analysis and *in vitro* culture in these studies, regeneration of alveolar epithelium has long been thought to be mediated by proliferation of AT2s and their subsequent differentiation into AT1s (Adamson, 1976; Aso et al., 1976). However, this concept has been challenged by a recent study using lineage tracing in mice, showing

that the regenerated AT2s are not derived from the pre-existing AT2s (Chapman et al., 2011). Moreover, based on morphological observations, a previous report has also suggested the possibility for bronchiolar cells to give rise to alveolar cells during the regeneration of alveolar epithelium (Aso et al., 1976). However, this concept failed to attract much attention due to lack of definitive evidence.

Recent studies have identified various putative lung stem or progenitor cells. Bronchioalveolar stem cells (BASCs) express markers of both Clara cells and AT2s, and reside at the bronchioalveolar duct junction (BADJ) (Kim et al., 2005). *In vitro*, BASCs can be induced to differentiate into both Clara and AT2s; however, the function of BASCs *in vivo* has been questioned (McQualter et al., 2009; Teisanu et al., 2009). In humans, a c-kit^{+} lung stem cell has been reported to form bronchioles, alveoli and pulmonary vessels after injection into the damaged mouse lung (Kajstura et al., 2011). Similarly, a mouse lung stem cell has been reported to express integrin α6β4 and form clusters of Clara cells and AT2s in kidney capsules when mixed together with fetal lung cells (Chapman et al., 2011). More recently, it was reported that p63^{+} cells in the distal lung in mice might contribute to alveolar repair after influenza virus induced lung injury (Kumar et al., 2011). However, none of these reported lung stem and progenitor cells has been rigorously shown to give rise to AT1s and AT2s for the regeneration of alveolar epithelia by genetic lineage tracing.

In conclusion, the roles of reported putative stem or progenitor cells in repair of lung damage and the underlying mechanism remains a mystery. This thesis attempts to

further investigate this problem with influenza-induced lung injury model through computational systems biological approach.

CHAPTER 2 – CONTRIBUTION OF CLARA CELLS TO LUNG REGENERATION FOLLOWING SEVERE PULMONARY DAMAGE

2.1 Summary

Little is known about repair of alveolar epithelium following severe lung injury. We show that following sublethal influenza virus infection and bleomycin treatment in mice, a novel cell type expressing Alveolar Type II cell (AT2) marker surfactant protein C (SPC) was induced in bronchioles in the damaged areas of the lung. These cells, referred to as SPC^+ bronchiolar epithelial cells (SBECs), initially expressed the Clara cell secretory protein (CCSP), shared the Clara cell transcription profile, and could be genetically traced to Clara cells. *In vivo* genetic lineage tracing revealed that SBECs were the intermediates from Clara cells to AT2s differentiation for regeneration of alveolar epithelium, in a process similar to that of development of embryonic alveolar epithelium. $p63^+$ cells were observed in damaged parenchyma post influenza infection as well as bleomycin treatment. These $p63^+$ cells were also genetically traced back to Clara cells and were intermediates during the regeneration of bronchioles. These findings demonstrated that Clara cells contributed to the regeneration of both alveoli and bronchioles following severe pulmonary damage.

2.2 Introduction

Lung contains an extensive surface of epithelium and other tissues that are constantly exposed to environmental insults. Maintaining the integrity of the alveolar epithelium is critical for lung function in gaseous exchange. Studies have identified different cell

types involved in the maintenance and repair of tracheal, bronchial, bronchiolar and alveolar epithelia (Liu et al., 2006; Rawlins and Hogan, 2006; Rock and Hogan, 2011). In mouse, $p63^+$ basal cells are confined to the trachea, and known to give rise to all major adjacent cell types, including Clara cells, ciliated cells, goblet cells and granular secretory cells (Hong et al., 2004; Rock et al., 2009; Rock et al., 2010; Schoch et al., 2004). Clara cells, which express Clara cell secretory protein (CCSP), constitute the predominant cell type in the bronchiolar epithelium, and are capable of self-renewal (Hong et al., 2001; Rawlins et al., 2009a). Alveolar Type II cells (AT2s), secreting surfactant protein C (SPC), serve as the progenitor cells of alveolar epithelium, and can regenerate Alveolar Type I cells (AT1s) (Adamson and Bowden, 1974; Evans et al., 1973, 1975). Bronchioalveolar stem cells (BASCs) at the bronchioalveolar duct junction (BADJ) (Kim et al., 2005) express both CCSP and SPC, and can be induced to differentiate into both Clara cells and AT2s *in vitro*. However, lineage tracing in transgenic mice suggests that BASCs do not contribute significantly to the repair of alveolar epithelium following oxygen-induced lung injury (Rawlins et al., 2009a). More recently, another lung stem cell type in mouse was reported to express integrin α6β4 (Chapman et al., 2011) and form clusters of Clara cells and AT2s in kidney capsules when mixed together with fetal lung cells. In human, a c-kit-positive lung stem cell was reported to form bronchioles, alveoli and pulmonary vessels after injection into the damaged mouse lung (Kajstura et al., 2011). Another recent report showed that $p63^+$ cells were induced in distal lung in mice and contribute to alveolar repair following influenza infection other than bleomycin treatment (Kumar et al.,

2011).

Studies on the function of lung progenitor and stem cells in lung tissue repair are commonly based on various *in vivo* injury models (Bigby et al., 1985; Borthwick et al., 2001; Dubaybo et al., 1991; Izbicki et al., 2002; Modelska et al., 1999; Randell, 1992; Smith, 1985; Theise et al., 2002; Van Winkle et al., 1999). Bleomycin is one of the most common drugs used to induce pulmonary toxicity including fibrosis. Early studies suggested that the repair of bleomycin-induced alveolar damage occurs via proliferation of AT2s and their subsequent differentiation into AT1s (Adamson, 1976; Aso et al., 1976). A recent study using lineage tracing indicated that after bleomycin-induced injury, newly generated AT2s are not derived from the pre-existing AT2s (Chapman et al., 2011), suggesting the role of other progenitor cells in the repair of bleomycin-induced alveolar damage. Based on morphological observations, previous studies suggested that bronchiolar cells may give rise to AT2s and AT1s during the regeneration of alveolar epithelium after bleomycin injury (Aso et al., 1976), although this idea did not draw significant attention without definitive evidence.

Rare chance of exposure to experimental injury sources in real life compromises their clinical significance. Lung injury caused by influenza virus is frequent and globally spread (Brady, 2010; Lipatov et al., 2004; Marcos et al., 2009; Potter, 2001). Being a generally recoverable disease, influenza infection sometimes leads to severe complications with underlying conditions such as, pneumonia and even death (Eccles,

2005; Taubenberger and Morens, 2008). Infected cells can be killed directly by the virus, and immune responses to the virus-infected cells also lead to additional cell death and tissue damage. However despite the critical importance of such tissue repair, how it comes about subsequent to infection by influenza and other respiratory viruses has yet to be discovered.

In this study, we investigated cellular pathways that are involved in the repair of damaged lung tissue following influenza infection or bleomycin treatment. We show that Clara cells are induced to differentiate into AT2s to regenerate alveolar epithelium through the intermediate SBECs. Clara cells are also induced to form new bronchioles containing regenerated Clara cells and $p63^{+}$ cells in damaged parenchyma.

2.3 Methods

2.3.1 Mice, influenza infection and chemical treatments

C57BL/6 mice were purchased from the Centre for Animal Resources (CARE), Singapore. Transgenic *rCCSP-rtTA* (stock number 006232), *tetO-Cre* (stock number 006234) and *ACTB-mT-EGFP* (stock number 007676) mice on B6 background were purchased from Jackson Laboratories. The transgenic mice were bred to generate triple transgenic mice *rCCSP-rtTA:tetO-Cre:ACTB-mT-EGFP* in the animal facility at National University of Singapore (NUS). The genotype of transgenic mice was determined by PCR, according to a protocol from Jackson Laboratories. Transgenic mouse *CCSP-CreER* on B6 background was obtained from Dr. Brigid Hogan from

Duke University, USA. Double transgenic mice *CCSP-CreER: ACTB-mT-EGFP* were generated by breeding *CCSP-CreER* mice with *ACTB-mT-EGFP* mice and screened according to the protocol provided by Dr. Hogan's laboratory. To induce *Cre*-mediated recombination, *CCSP-CreER: ACTB-mT-EGFP* transgenic mice were treated with tamoxifen (TMX) in corn oil or corn oil only as control every other day for four times at the dose of 0.25mg/g body weight (Rawlins et al., 2009b). TMX-treated mice were infected with influenza virus or bleomycin one week later. B6 and transgenic mice at age of 8-12 weeks were infected with a sublethal dose of influenza virus A/Puerto Rico/8/34 (H1N1) (100 pfu/mouse) or treated with bleomycin (1U/kg body weight for wild type mice and 0.5U/kg body weight for transgenic mice) by intra-tracheal instillation under anesthesia. All animals were housed in biosafety level 2 (BSL2) animal facilities at NUS. All animal protocols were approved by the Institutional Animal Care and Use Committees (IACUC) at NUS and Massachusetts Institute of Technology (MIT).

2.3.2 RNA extraction and real-time fluorescence quantitative PCR

Mice were sacrificed at indicated time points post infection, total RNA was extracted from the lung tissue with TRIZOL reagent (Life Technologies) according to manufacturer's protocol. 2μg of total RNA from each sample was reverse transcribed using Oligo(dT) and Superscript II (Life Technologies). PCR was performed with Bio-Rad CFX-96 real-time system with Sofast Evagreen Supermix (Bio-Rad Laboratories). Primer sequences for the housekeeping gene L32 and influenza virus N

gene were as previously described (Alt et al., 2007; Doyle et al., 2003).

2.3.3 Antibodies

Polyclonal rabbit anti-CCSP antibody (US Biological, C5828) was used at a 1:200 dilution. Polyclonal goat anti-CCSP (Santa Cruz Biotechnology, sc-9772), goat anti-SPC (Santa Cruz Biotechnology, sc-7706), rabbit anti-SPC (Santa Cruz Biotechnology, sc-7705), goat anti-clusterin (R&D Systems, AF2747), goat anti-PDPN (R&D Systems, AF3244), rabbit anti GFP (Abcam, ab290), monoclonal rat anti-Ki67 (Dako, M7249), mouse anti-p63 4A4 (Santa Cruz Biotechnology, sc-8431) and mouse anti-BrdU (Leica Microsystems, NCL-BrdU) were used at a 1:50 dilution. Rabbit anti-influenza virus serum was provided by Dr. T. Narasaraju (NUS, Singapore). Secondary antibodies, including donkey anti-rabbit, anti-goat, anti-rat, or anti-mouse, each with different Alexa Fluor conjugations were all purchased from Life Technologies and used at a 1:200 dilution.

2.3.4 Histopathology and immunochemical staining

Mice were sacrificed at indicated post infection time points, and lung tissues were harvested and fixed in 10% neutral buffered formalin solution (Sigma-Aldrich) for 24 hours. The tissues were processed with Tissue Processor (Leica Microsystems) and embedded in paraffin. Sections were cut at a 5μm thickness, mounted on polylysine coated slides (ThermalFisher Scientific), de-waxed, rehydrated, and stained for H&E according to standard protocol. For immunofluorescent staining, antigen retrieval was

carried out by either microwaving the slides in 0.01M sodium citric acid buffer (pH 6.0) for 30min (for anti-Ki67 and p63) or by digesting the slides in proteinase K solution (Sigma-Aldrich, 20mg/ml, in 50mM Tris-Cl,1mM EDTA, pH 8.0) at 37^{o}C for 30min (for all other antibodies). For BrdU staining, sections were firstly processed according to the manufacturer's protocol. After treatments, all sections were then immersed for 1 hour in blocking buffer (3% BSA, 0.2% Triton X-100 in PBS), then incubated in primary antibody (diluted with blocking buffer) at 4^{o}C overnight, followed by incubation in secondary antibody (diluted with blocking buffer) at 4^{o}C for 1h. All lung sections were counter-stained with DAPI (blue). Sections were mounted with antifade reagent (Life Technologies) and then scanned with high-resolution MIRAX MIDI system (Carl Zeiss) equipped with both bright field and fluorescence illumination. Images were analyzed by the software Miraxviewer.

2.4 Results

2.4.1 Influenza infection induced lung damage and repair model

To study lung tissue repair mechanisms in response to severe pulmonary damage, we developed a model of influenza-induced lung injury and repair, in which B6 mice were infected intra-tracheally with a sublethal dose of influenza A virus PR8. Infected mice started to lose weight at 3 dpi, reached a peak weight loss of ~25% by 9 dpi, and then gradually recovered (Figure 2A). The viral load in the lung reached maximal levels at 5 dpi, decreased thereafter to undetectable levels at 14 dpi (Figure 2B). H&E staining of lung tissue sections revealed a post-infection infiltration of

inflammatory cells, which peaked around 14 dpi, decreased significantly by 21 dpi, and almost completely gone by 60 dpi (Figure 2C).

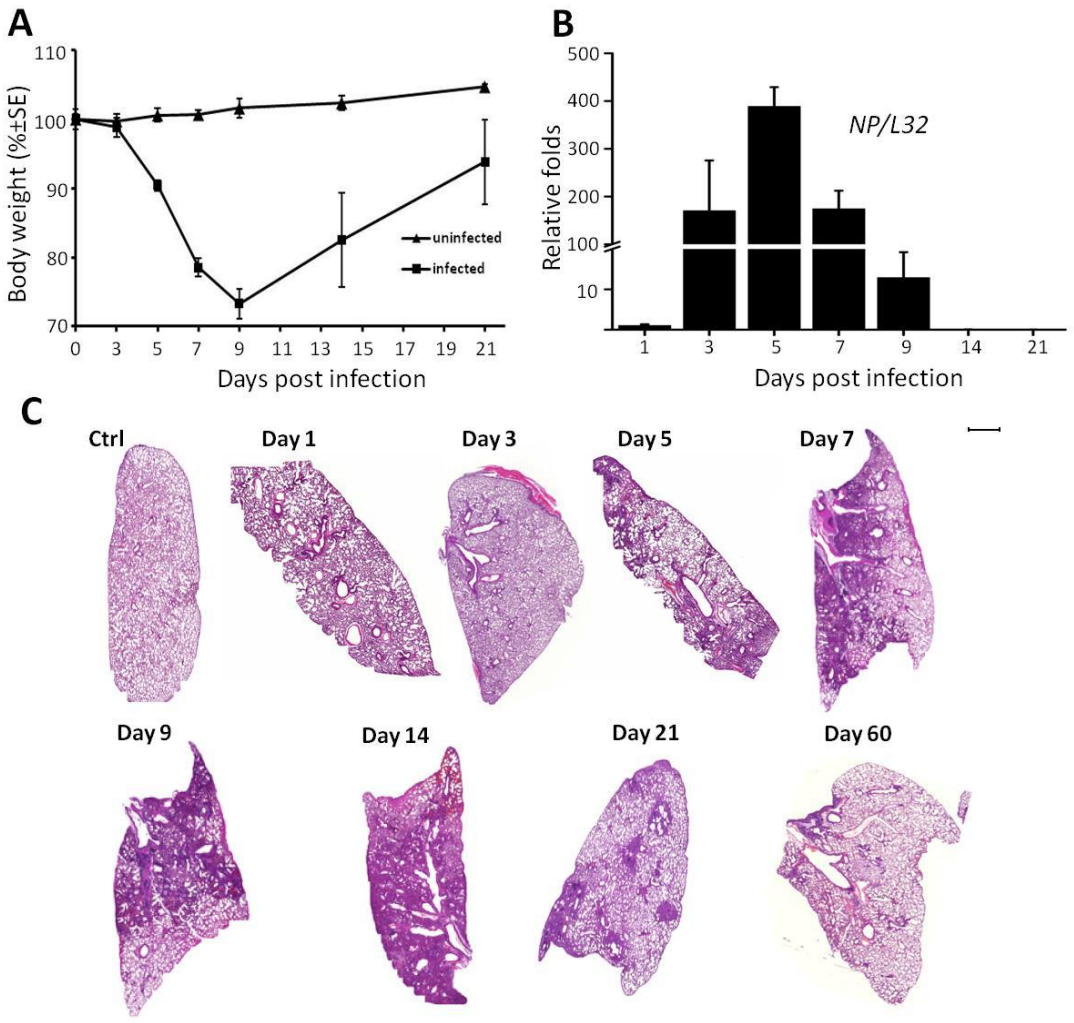

Figure 2. Influenza virus-induced lung damage and repair model (A) Relative (mean ± S.E., n=5 per group) body weight of mice at different dpi. (B) Viral titers in the lung at different dpi. The level of influenza nucleoprotein (NP) RNA in the lung tissues was quantified by real-time PCR. Data were normalized to the level of ribosomal protein L32 RNA and expressed as fold changes (mean ± S.E., n=3 mice per time point) over that of 1 dpi. (C) Representative H&E staining of lung sections of uninfected (control) and infected mice at the indicated dpi. Scale bars: (C) 1000μm.

In healthy lung, Clara cells line the bronchiolar epithelium, whereas AT1s cover more than 95% of the area of alveolar epithelium with AT2s dispersed among them.

Consistently, staining of the Clara cell marker CCSP was confined to bronchiolar epithelium (Figures 3A and 3B); staining of the AT1 cell marker PDPN marked the entire alveolar epithelia; while staining of the AT2 cell marker SPC was dispersed among $PDPN^{+}$ AT1 cells (Figure 3C).

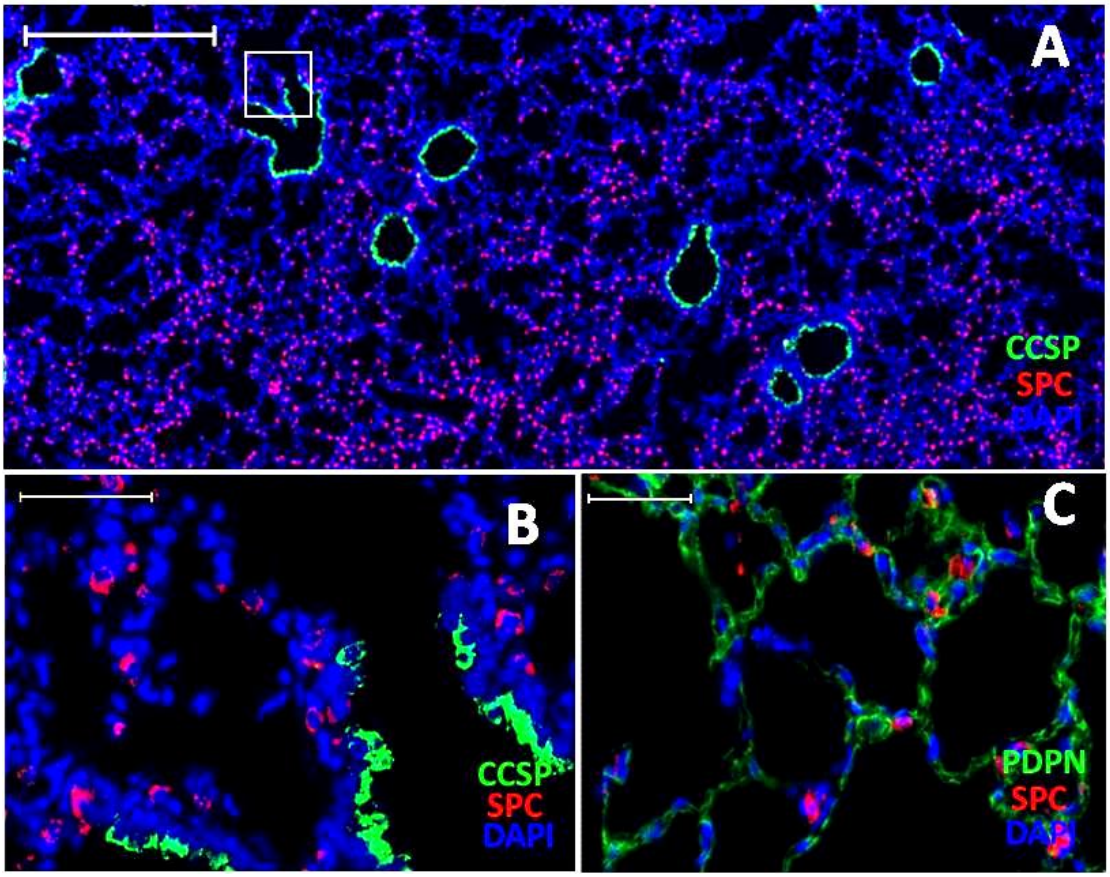

Figure 3. Staining of bronchial and alveolar epithelial cells in healthy lung (A) Representative CCSP (green), SPC (red) and and DAPI (blue) staining of the lung sections of uninfected mice. Higher magnification of boxed area in (A) is shown in (B). (C) Representative images of PDPN (green), SPC (red) and DAPI (blue) staining of B6 mice without injury. Scale bars: (A) 500μm; (B and C) 50μm.

As early as 3 dpi, both Clara cells and AT2s were observed positive for influenza virus (Figures 4A and 4B, arrows). Sloughing off of epithelial cells from bronchioles was evident in the infected areas of the lung (Figure 4A, arrowheads). At 7 dpi, the

damage was so severe that most bronchioles in the infected areas (indicated by dense DAPI staining of nuclei of infiltrating cells) were depleted of $CCSP^+$ Clara cells, while the infiltrated parenchyma was almost completely devoid of SPC staining (Figure 4C). To determine whether AT2s were depleted or merely turned off the expression of SPC after infection, we utilized *rCCSP-rtTA:tetO-Cre:ACTB-mT-EGFP* transgenic mice. In this system, transcription of the *rtTA* transactivator is under the control of a *CCSP* promoter, transcription of *Cre* is under control of the *tetO* and doxycycline, and transcription of a membrane-bound form of tomato red (mT) or EGFP is under the control of *β-actin* promoter (Perl et al., 2005). Without *Cre*-mediated recombination, cells express tomato red; after doxycycline treatment and recombination, Clara cells switch to EGFP expression. The signals of EGFP and mT could be directly detected without staining. Because of system leakage, many AT2s were also induced to express EGFP after doxycycline treatment (Figure 4D). However, as early as 7 dpi, no SPC^+ or $EGFP^+$ cells were detected in the infiltrated parenchyma (Figure 4E). Because EGFP was driven by the housekeeping gene *β-actin* promoter, these results suggested that after infecting by influenza virus, AT2s were not merely turned off SPC expression, but depleted from infected areas of the lung. Thus, influenza infection induced severe damage in both bronchiolar and alveolar epithelia.

Proliferation and differentiation of progenitor cells are necessary for tissue repair. We used Ki67 staining to evaluate proliferation of $CCSP^+$ and SPC^+ cells at various time points following influenza infection. As early as 5 dpi, some $CCSP^+$ cells in the

bronchiolar epithelia were Ki67$^+$ (data not shown). At 9 dpi, many CCSP$^+$ cells in the damaged areas were Ki67$^+$ (Figure 4F), indicating extensive proliferation. At 14 dpi, most bronchioles were covered with CCSP$^+$ Clara cells (data not shown). In contrast, very few SPC$^+$ AT2s were Ki67$^+$ through the course of infection (data not shown). During 21-60 dpi, as infiltration in the damaged areas of the lung gradually reduced, normal alveolar structure appeared (Figure 2C). Collectively, these results showed that influenza infection caused severe lung tissue damage in mice, and the damage was repaired as the animals recovered from the infection.

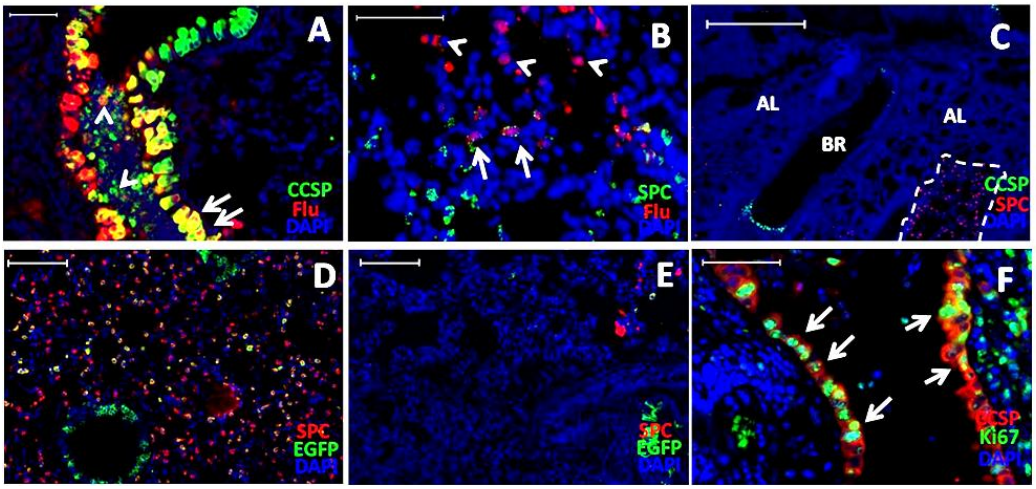

Figure 4. Loss and proliferation of Clara cell and AT2 post influenza infection (A and B) Representative immunofluorescent images of lung sections stained for Flu (red), CCSP (green) and DAPI (blue) or Flu (red), SPC (green) and DAPI (blue) at 3 dpi. Arrows indicate CCSP and Flu (A) or SPC and Flu (B) double positive cells; arrowheads indicate Clara cells that sloughed off from the bronchiolar epithelium (A) or the Flu single positive cells in alveolar epithelium (B). (C) Representative immunofluorescent images of lung sections stained for CCSP (green), SPC (red) and DAPI (blue) at 7 dpi. AL, alveolus; BR, bronchiole. Broken white line demarcates the infiltrated area (upper) from the normal area (lower) of the lung. (D and E) *rCCSP-rtTA:tetO-Cre:ACTB-mT-EGFP* transgenic mice were given doxycycline-containing water for 7 days and then infected intra-tracheally with PR8 virus. At 7 dpi, lung sections were analyzed for EGFP (green), SPC (red) and DAPI (blue). Shown are representative images of lung sections of uninfected (D) and infected (E) mice. For better visualization of immunofluorescence, tomato red channel

is not shown. (F) Representative images of co-staining for Ki67 (green), CCSP (red) and DAPI (blue) in sections through the lungs of mice at 9 dpi, Arrows indicate cells that are double positive for CCSP and Ki67. Scale bars: (A and B) 50µm; (C) 500µm; (D and E) 100µm. (F) 50µm.

2.4.2 SBECs are induced in response to severe alveolar damage

After influenza infection, both Clara cells and AT2s were infected and depleted (Figures 4A-4C). However, at 14 dpi, in the bronchiolar epithelium, we noticed large number of cells that expressed the AT2 marker SPC, but exhibited the characteristic cytomorphology of Clara cells (Figures 5A-5E). We refer to these cells as SPC^{+} bronchiolar epithelial cells (SBECs). Some of the SBECs were positive for CCSP while some others were negative for CCSP (Figures 5B-5E).

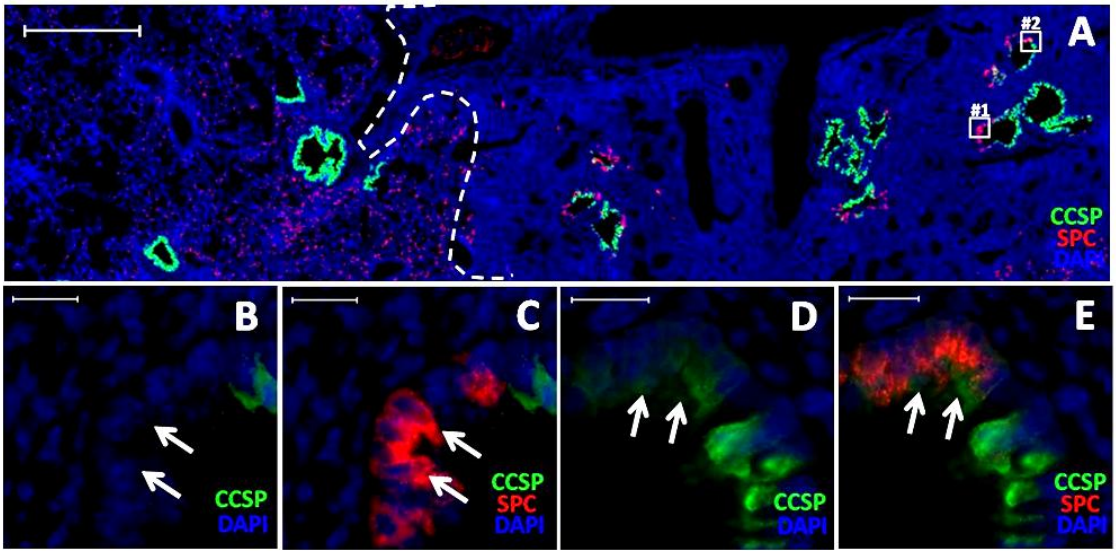

Figure 5. Induction of SBECs after influenza-induced lung injury (A) Representative CCSP (green), SPC (red) and and DAPI (blue) staining of the lung sections of mice 14 dpi. The white broken line in demarcates the infiltrated area (to the right) and healthy area (to the left). (B and C) Higher magnifications of the boxed area #1 from (A) either without (B) or with (C) the SPC channel. Arrows indicate SPC single positive cells. (D and E) Higher magnifications of the boxed area #2 from (A), imaged without (D) or with (E) the SPC channel. Arrows indicate CCSP and SPC double positive cells. Scale bars: (A) 500µm; (B-E) 20µm.

In another alveolar epithelium injury model induced by bleomycin treatment in mouse, the lung tissue was also severely infiltrated, depletion of AT2s and AT1s were evident (Figures 6A and 6B), while there was no significant depletion of Clara cells in bronchioles. Large amount of SBECs were also observed in this injury model (Figure 6B).

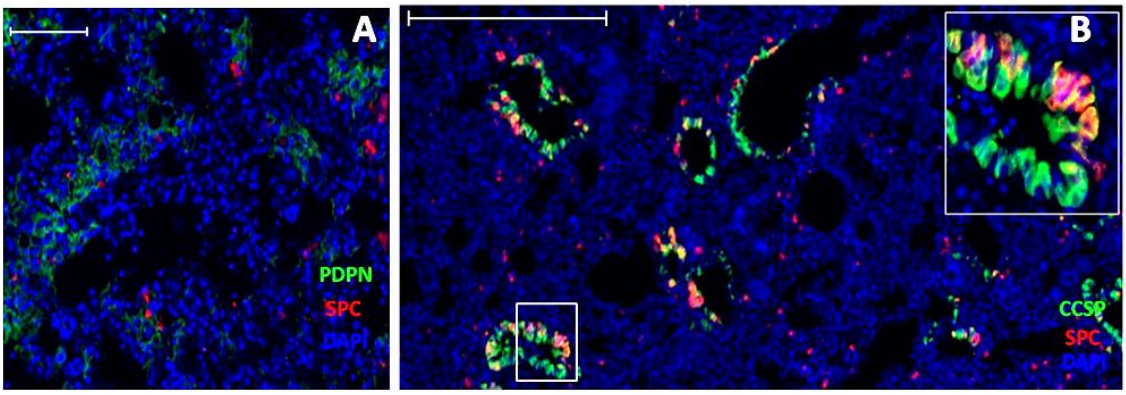

Figure 6. Induction of SBECs after bleomycin-induced lung injury (A) Representative images of PDPN (green), SPC (red) and DAPI (blue) staining of B6 mice at 7 day post bleomycin treatment. (B) Representative CCSP (green), SPC (red) and DAPI (blue) staining of the lung sections of mice at 7 day post bleomycin treatment, higher magnification of the boxed area is shown at the upper-right corner. Scale bars: (A) 100μm; (B) 500μm.

Clara cells are heterogeneous, with one subset identified as variant Clara cells (Clara^{v}), which are lack of the protein cytochrome P450, family 2, subfamily f, polypeptide 2 (CYP2F2), and believed to regenerate other Clara cells (Giangreco et al., 2002; Hong et al., 2001; Reynolds et al., 2000). Co-staining of SPC and CYP2F2 showed that most of the SBECs expressed CYP2F2 following influenza virus infection (data not shown) or bleomycin treatment (Figure 7), suggesting that these SBECs were not Clara^{v} cells.

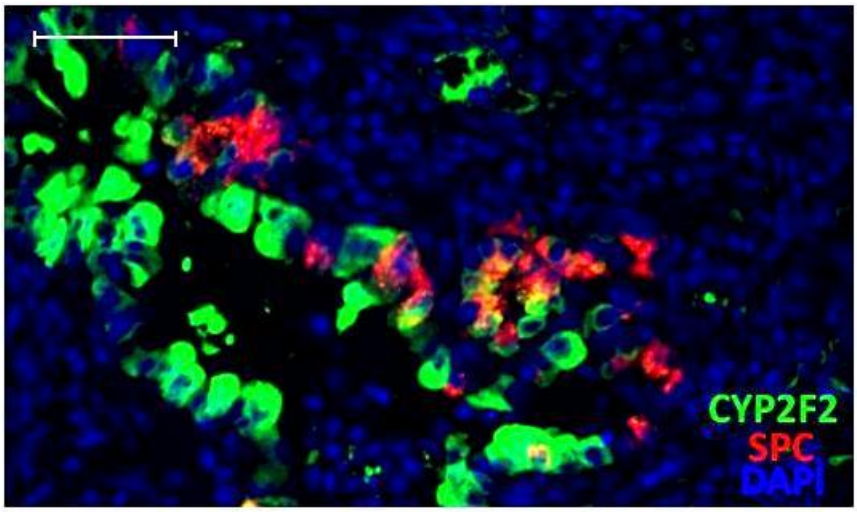

Figure 7. SBECs are distinct from Clara^{v} A representative image for CYP2F2 (green), SPC (red) and DAPI (blue) staining of lung sections of mice at 14 days post bleomycin treatment. Scale bar: 50μm.

A kinetic analysis over the time course post infection showed that SBECs were initially CCSP^{+}. No SBECs were detected before 7 dpi, and all of them at 7 dpi were CCSP^{+}. At 11 dpi, CCSP^{-} SBECs were also detected, and their proportion increased with time (Figures 8A and 8B). At 14 and 21 dpi, most SBECs were CCSP^{-} (Figure 8B). Similarly, in bleomycin-induced lung injury model, SBECs were detected as early as 3 days post bleomycin treatment in ~8% of bronchioles, and they were all CCSP^{+} (Figures 8C and 8D). At day 7 post treatment, SBECs were detected in 50% of bronchioles, and majority of them were CCSP^{+}. At day 14 and 21, more than half of SBECs ceased to express CCSP (Figures 8C and 8D).

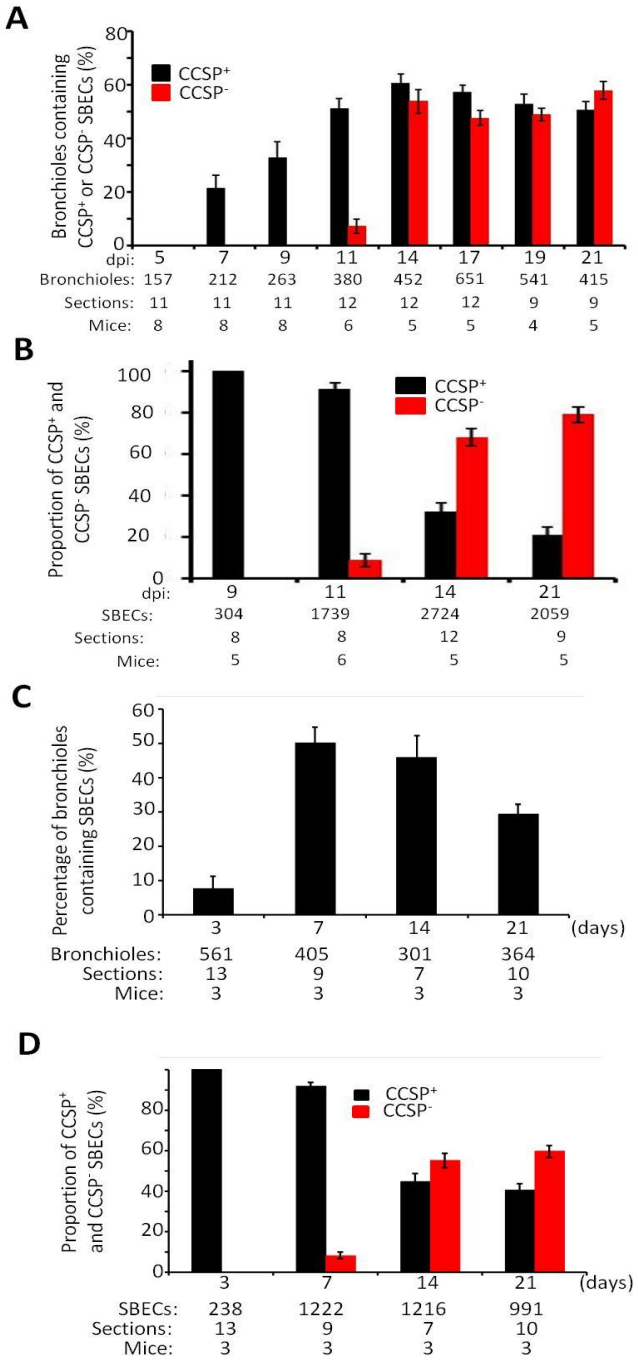

Figure 8. Dynamic analysis of SBECs (A) Percentages (mean ± S.E.) of bronchioles in the infiltrated area containing $CCSP^+$ (black bars) and $CCSP^-$ (red bars) SBECs. (B) Proportions of $CCSP^+$ and $CCSP^-$ SBECs in a given lung section at the indicated dpi. Results are expressed as mean ± S.E. (C) Percentages (means ± S.E.) of bronchioles containing SBECs at the indicated days post bleomycin treatment. (D) Proportions of $CCSP^+$ and $CCSP^-$ SBECs in a given lung section at the indicated days post bleomycin treatment. Results are expressed as means ± S.E. The numbers in (A-D) indicate the number of SBECs, bronchioles, lung sections, and mice from which the data are obtained.

In naphthalene-induced lung injury model, as reported previously, most Clara cells were depleted from the bronchiolar epithelium without significant depletion of alveolar epithelial cells following naphthalene treatment (Figure 9A). At 9 and 12 days post treatment, the remaining Clara cells in bronchioles were actively proliferating (Figures 9C and 9D). However, no SBECs were observed during the entire process. $CCSP^{+}SPC^{+}$ positive cells were occasionally detected at the BADJ of terminal bronchioles (Figure 9B). These cells were likely to be BASCs given that they were weakly positive for SPC (Kim et al., 2005), and their frequency (1%) was similar to that observed in mice without treatment. Thus, we infer that the induction of SBECs might be a common cellular process in response to severe alveolar damage.

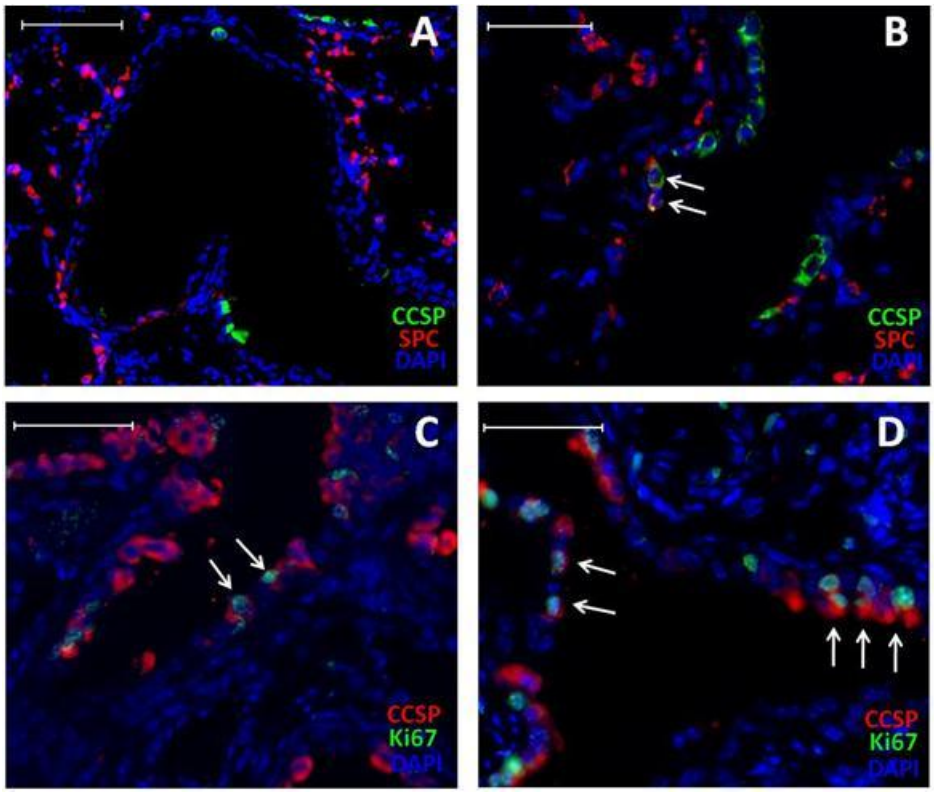

Figure 9. SBECs are not induced following naphthalene treatment in mice (A-B) Representative CCSP (green), SPC (red) and DAPI (blue) staining of lung sections of mice at 6 days post naphthalene treatment. Arrows in (B) indicate BASCs at BADJ. (C-D) Representative staining for CCSP (red), Ki67 (green) and DAPI (blue) of lung sections of mice at 9 (A) or 12 (B) days post naphthalene treatment. Arrows indicate the CCSP and Ki67 double positive cells. Scale bars: (A) 100μm; (B-D) 50μm.

2.4.3 SBECs originate from Clara cells

Based on their Clara cell cytomorphology, localization in the bronchioles, and initial expression of CCSP, SBECs are likely derived from Clara cells. To obtain direct evidence, we performed lineage tracing using *CCSP-CreER:ACTB-mT-EGFP* double transgenic mice (Rawlins et al., 2009a). In this transgenic system, the CreER is expressed in $CCSP^+$ cells but retained in the cytoplasm. Only upon binding to tamoxifen (TMX), the CreER is translocated to the nucleus where it catalyzes recombination to delete mT transgene. Thus, without TMX treatment to the mice, all transgenic cells, including $CCSP^+$ Clara cells, expressed mT. After TMX treatment, Clara cells lose mT expression and become $EGFP^+$. Consistent with the previous report (Rawlins et al., 2009a), without TMX treatment, no $EGFP^+$ cells were found in the alveolar region and only a small fraction (~10%) of Clara cells in the bronchioles were $EGFP^+$ (Figures 10A and 10E). After TMX treatment, ~85% (ranging from 79% to 100%) of Clara cells in the bronchioles expressed EGFP and evenly distributed in all bronchioles (Figures 10B and 10E). Thus, the transgenic system yielded a satisfactory dynamic range (~8-fold) of $EGFP^+$ Clara cells induction after TMX treatment.

To determine whether SBECs were derived from Clara cells,

CCSP-CreER:ACTB-mT-EGFP transgenic mice were given TMX to label Clara cells and then infected with influenza virus to induce the generation of SBECs. Mice infected without TMX treatment were used as controls. Mice were sacrificed at 9, 14 and 21 dpi; lung sections were stained for SPC and CCSP, and visualized for EGFP, mT, SPC and CCSP. In control mice, the fraction of $EGFP^+$ Clara cells remained low (~16%) at 9, 14 and 21 dpi (Figure 10E). The slight increase (from 10% to 16%) was likely caused by expansion of pre-existing $EGFP^+$ Clara cells following the damage of bronchiolar epithelium (Rawlins et al., 2009a). Supporting this notion, $EGFP^+$ cells in the bronchioles tended to cluster together (Figure 11). With TMX treatment, the fraction of $EGFP^+$ Clara cells increased to ~75%. The fraction did not vary much following infection (Figure 10E), indicating majority of Clara cells in the transgenic mice were labeled with EGFP following TMX treatment and infection. Correspondingly, ~10% of SBECs were $EGFP^+$ in infected mice without TMX treatment, whereas ~75% of SBECs were $EGFP^+$ in infected mice treated with TMX, (Figure 10F). All SBECs in the transgenic mice were $CCSP^+$ at 9 dpi and the fraction of $CCSP^-$ SBECs increased to more than 70% at 14 and 21 dpi (Figures 10C, 10D and 10G).

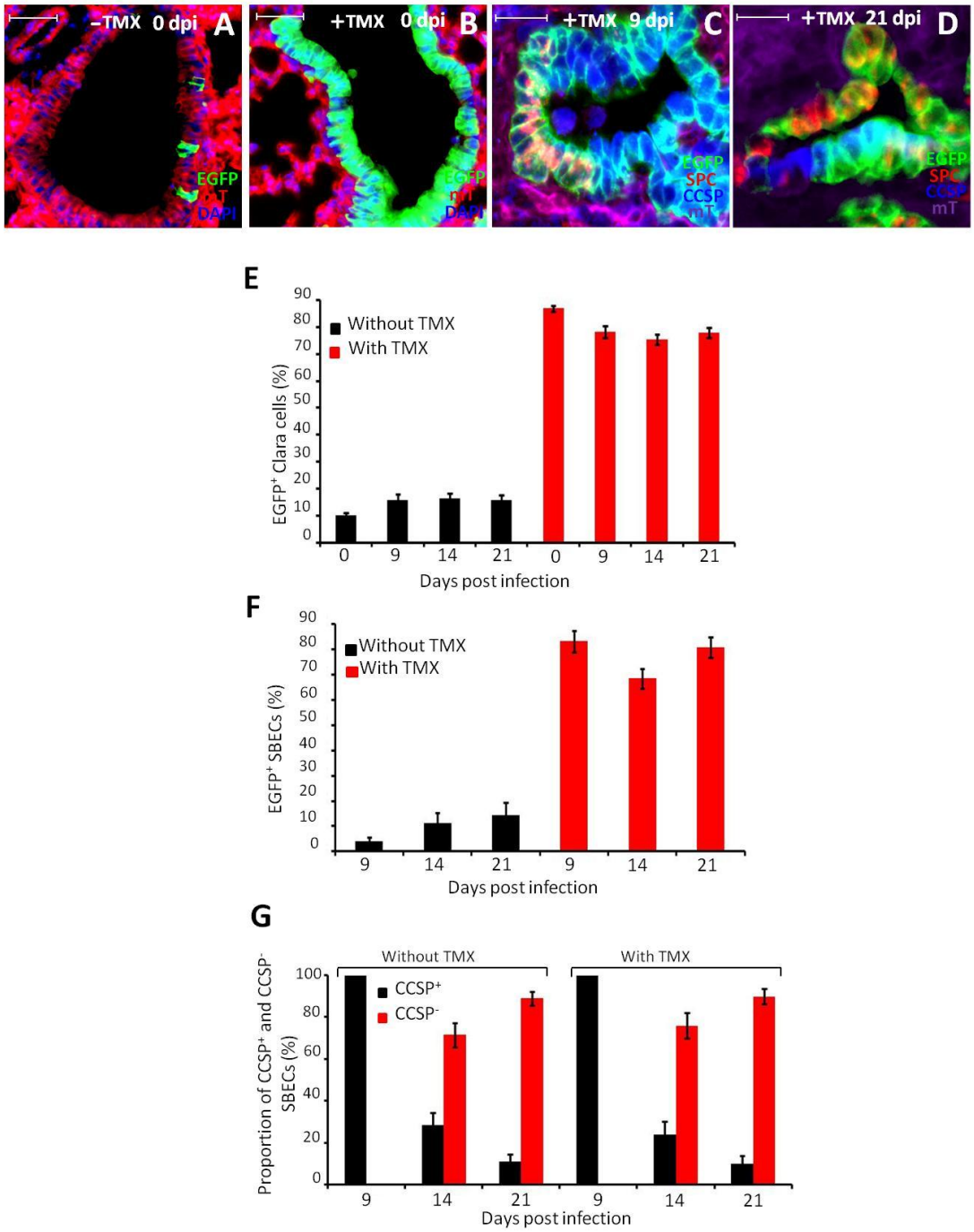

Figure 10. SBECs originated from Clara cells post influenza-induced lung injury
(A and B) Representative images of bronchioles of *CCSP-CreER:ACTB-mT-EGFP* transgenic mice without (A) or with (B) TMX treatment. Expression of EGFP (green) and tomato red (mT, red) are shown. Sections are counter-stained by DAPI (blue). (C and D) *CCSP-CreER:ACTB-mT-EGFP* transgenic mice were given TMX and then infected with influenza virus. Shown are representative images of lung sections analyzed for expression of EGFP (green) and tomato red (purple) and stained for SPC (red) and CCSP (blue) 9 (C) or 21 (D) dpi. (E) Percentages (mean ± S.E.) of Clara cells per bronchiole that expressed EGFP in *CCSP-CreER:ACTB-mT-EGFP*

transgenic mice without (black columns) or with (red columns) TMX treatment at different time points post influenza infection. Data at each time point was obtained by counting 2551 to 7980 Clara cells ($CCSP^+$ SPC^-) from at least 6 lung sections of 2 mice. (F) Percentages (mean ± S.E.) of SBECs that expressed EGFP in *CCSP-CreER:ACTB-mT-EGFP* transgenic mice without (black columns) or with (red columns) TMX treatment at different days post influenza infection. (G) Proportion of SBECs that are $CCSP^+$ (black columns) or $CCSP^-$ (red columns) in *CCSP-CreER:ACTB-mT-EGFP* transgenic mice without or with tamoxifen treatment at different days post influenza infection. Each data of (F) and (G) was obtained by counting 180 to 998 cells from at least 7 sections of 2 mice. Scale bars: (A and B) 100μm; (C, D) 50μm.

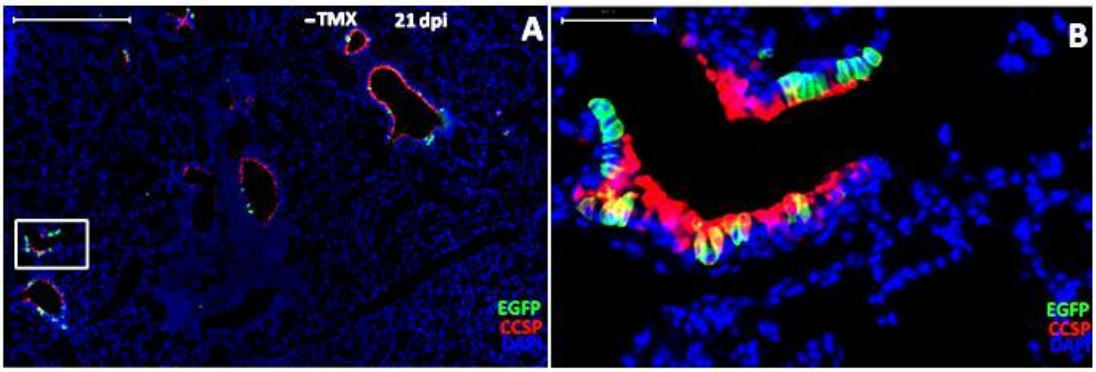

Figure 11. $EGFP^+$ Clara cells tend to form cluster (A and B) *CCSP-CreER:ACTB-mT-EGFP* transgenic mice without TMX treatment were infected with influenza virus. Shown are representative images of lung sections of mice at 21 dpi analyzed for expression of EGFP (green) and stained for CCSP (red) and DAPI (blue). Tomato red channel is not shown. Higher magnification image of boxed area in (A) is shown as (B). Scale bars: (A) 500μm; (B) 50μm.

Similarity was observed in bleomycin-induced injury model. ~9% of the SBECs were $EGFP^+$ in transgenic mice without TMX, and the fraction increased to ~80% after TMX treatment (Figure 12A). All SBECs expressed CCSP in transgenic mice at 3 days post bleomycin treatment, and following TMX treatment, 50-60% of them became $CCSP^-$ at days 14 and 21 post bleomycin treatment (Figure 12B). These results revealed that SBECs were derived from Clara cells, and transited from $CCSP^+$ to $CCSP^-$ phase.

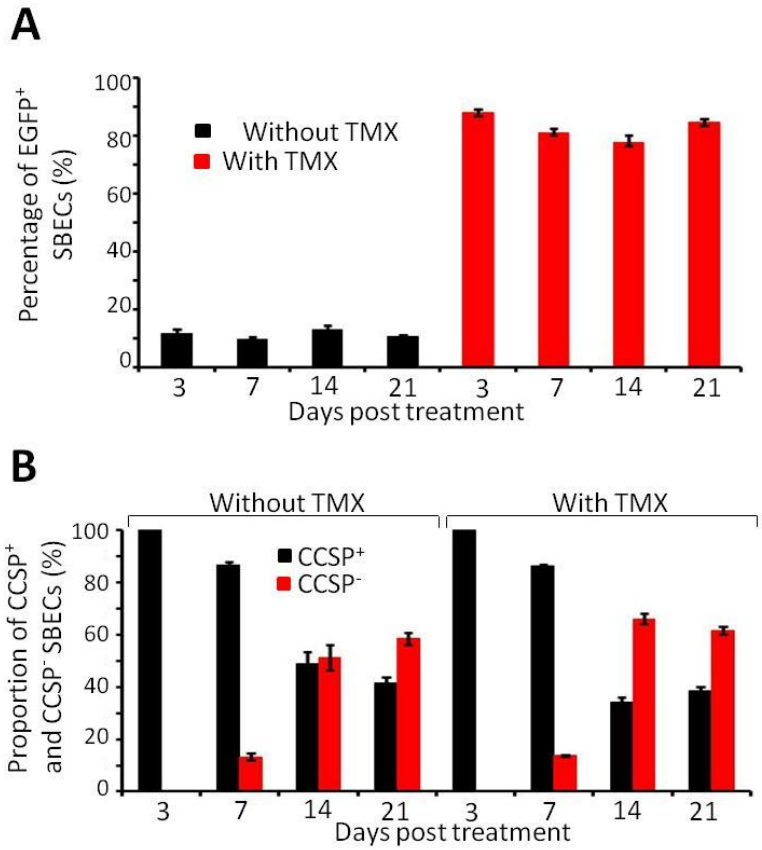

Figure 12. SBECs originated from Clara cells post bleomycin-induced lung injury (A) Percentages (means ± S.E.) of SBECs that expressed EGFP in *CCSP-CreER:ACTB-mT-EGFP* transgenic mice without (black columns) or with (red columns) tamoxifen (TMX) treatment at different days post bleomycin treatment. (B) Proportions (means ± S.E.) of SBECs that were $CCSP^+$ (black columns) or $CCSP^-$ (red columns) in *CCSP-CreER:ACTB-mT-EGFP* transgenic mice without or with tamoxifen treatment at different days post-bleomycin treatment. Each data of (H) and (I) was obtained by counting 351 to 1323 SBECs from at least 6 lung sections of at least 2 mice.

2.4.4 Regeneration of alveolar epithelium

Repair of damaged alveolar epithelium is critical for recovery of lung function. As described above, almost all AT2s were depleted in the damaged alveolar areas by 7-9 dpi (Figures 4C and 5A). We noticed, however, that SPC^+ cells re-appeared in the damaged alveolar areas starting around 11 dpi and expanded to considerable amount

by 17 dpi (Figure 13A). The SPC^+ cells were either dispersed in clusters or formed ring-like structures of various size (Figure 13B) in damaged alveolar areas. Clusters of $CCSP^-$ SBECs at the tips of bronchioles also formed similar ring-like structures (Figure 13C), indicating that they might be the source of SPC^+ cells in damaged alveolar areas. Few ring-like structures could be observed at 11 dpi, but they became more abundant after 15 dpi (Figure 13D), coinciding with the development of $CCSP^-$ SBECs (Figures 8A and 8B). Moreover, PDPN were detected in the same region of damaged parenchyma where large number of SPC^+ cells existed (Figure 13E). Importantly, PDPN signals were associated with cells exhibiting characteristic morphology of AT1s and SPC^+ cells were cuboidal in shape and interspersed among $PDPN^+$ cells. These results suggested that these cells were regenerated AT2s and AT1s for the repair of alveolar epithelium.

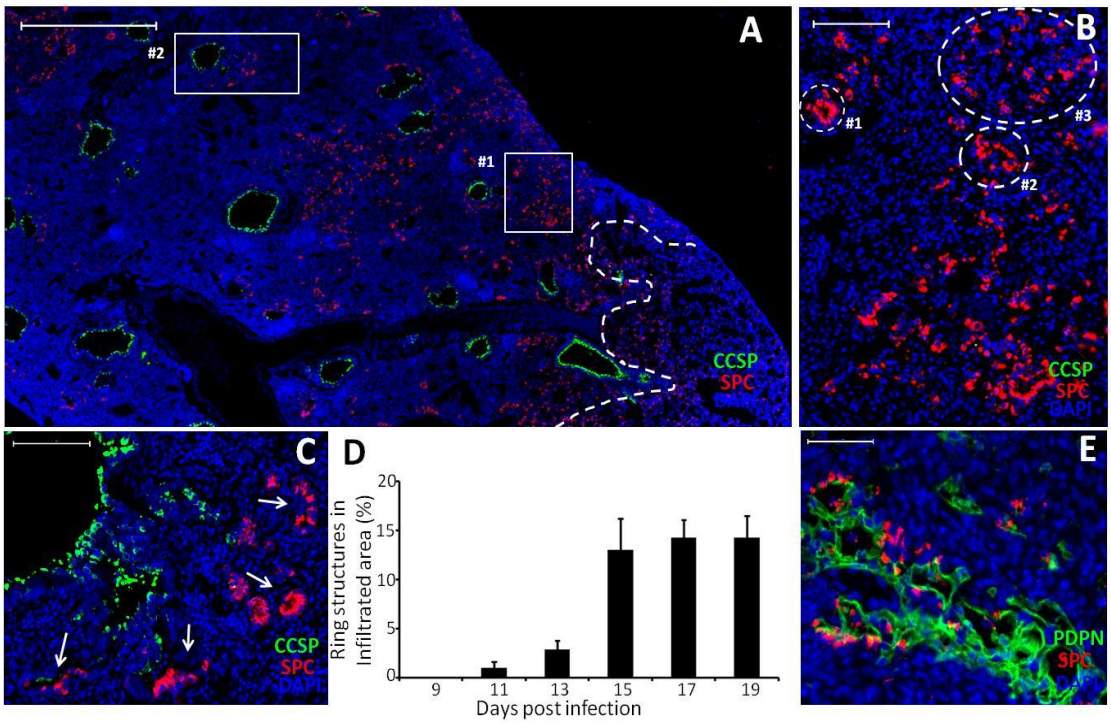

Figure 13. Regeneration of damaged alveolar epithelium cells post influenza-induced lung injury (A-C) Representative images of SPC (red), CCSP (green) and DAPI (blue) staining of lung sections of B6 mice 17 dpi. Higher magnification of the boxed areas #1 and #2 in (A) are shown as (B) and (C) respectively. White broken line in (A) demarcates the infiltrated area (to the left) and normal area (to the right). Arrows in (C) indicate SPC^{+} cells at the tips of bronchioles. (D) Frequency (mean ± S.E.) of ring-like structures in the infiltrated areas of the lung at different dpi. Data (mean ± S.E.) at each time point was obtained from 7 to 15 lung sections of 3 to 8 mice. (E) Representative images of PDPN (green), SPC (red) and DAPI (blue) staining of B6 mice at 21 dpi. Scale bars: (A) 1000μm; (B, C) 100μm; (E) 50μm;

Similar phenomena were also observed in bleomycin induced lung injury model. In this model, mice were visibly sick 7 days post bleomycin treatment; with some of them showing severe clinical signs after 14 days and had to be euthanized. By 21 days post bleomycin treatment, the survived animals appeared to have recovered from bleomycin treatment, and immunofluorescent analysis of lung sections at day 21 revealed reduced immune cell infiltration in the lung. Large number of regenerated AT2s were also detected in the damaged parenchyma (Figure 14A), which was

consistent with previous reports (Adamson, 1976; Aso et al., 1976; Chapman et al., 2011). SPC^+ clusters (Figure 14B), SPC^+ ring-like structures (Figure 14C), $CCSP^-$ SBECs formed ring-like structures (Figure 14D), as well as $PDPN^+$ cells (Figure 14E) were observed in the same respective areas as described in influenza model.

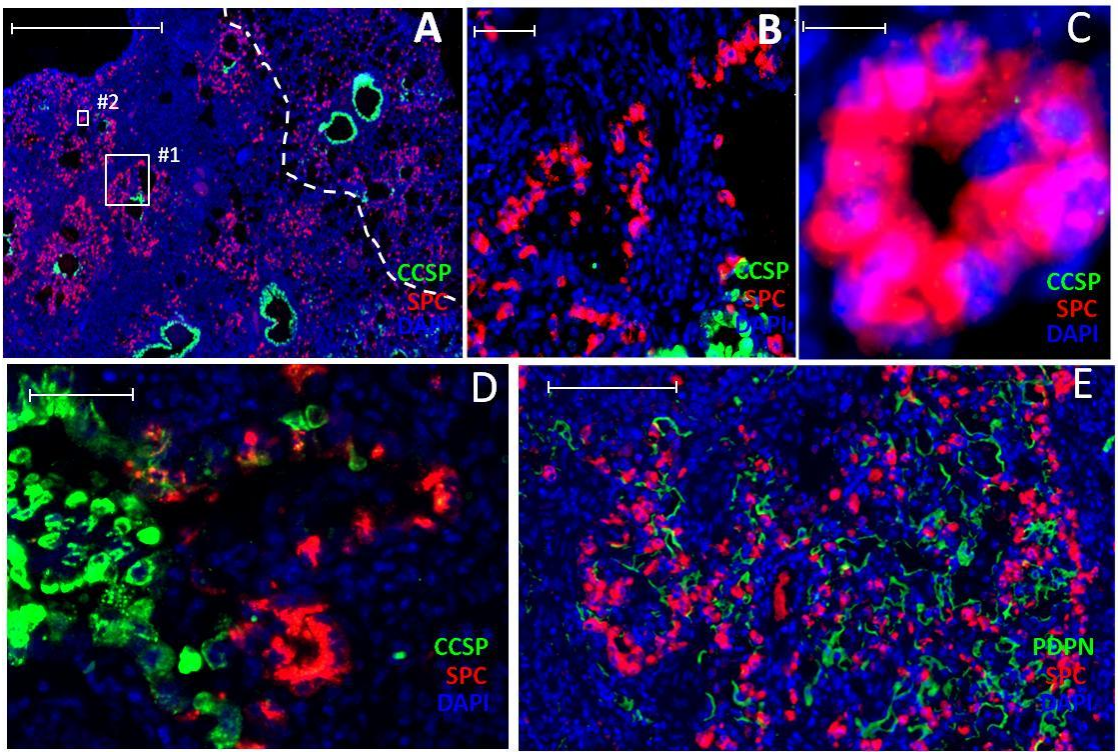

Figure 14. Regeneration of damaged alveolar epithelium cells post bleomycin-induced lung injury (A-D) Representative images of CCSP (green), SPC (red) and DAPI (blue) staining of lung sections of B6 mice at 21 days post bleomycin treatment. High magnification of the boxed areas #1 and #2 in (A) are shown as (B) and (C) respectively. White broken line in (A) demarcates the infiltrated area (left) from the normal area (right) of the lung. Scale bars: (A) 1000 μm; (B and D) 50μm; (C) 10μm.

2.4.5 SBECs give rise to AT2s during the regeneration of damaged alveolar epithelium

Based on anatomical locations of all the SPC^+ cells in damaged parenchyma, the

regenerated AT2s might be the result of dilation of SPC^+ ring-like structures which were associated with the $CCSP^-$ SBECs and were traced back to Clara cells. If this hypothesis is true, the regenerated AT2s and ring-like structures would be $EGFP^+$ in the transgenic mice. To verify this, we performed lineage tracing in *CCSP-CreER:ACTB-mT-EGFP* transgenic mice. In mice without TMX treatment, $EGFP^+SPC^+$ ring-like structures (16%) and clusters (10%) were observed in the damaged parenchyma at 21 dpi (Figures 15A and 15B; and Table 1). Importantly, $EGFP^+$ AT2s were also found in the recovered areas with normal alveolar structure (Figure 15C). In addition, $EGFP^+$ AT1-like cells were detected besides the $EGFP^+$ AT2s (Figure 15C, arrows). Staining of adjacent sections confirmed that the $EGFP^+$ AT1-like cells were $PDPN^+$ (Figure 15D, arrows). Since without TMX treatment no $EGFP^+$ cells was detected in alveolar epithelium before injury, the regenerated $EGFP^+$ AT2s, AT1s and ring-like structures after injury were derived from the genetically labeled Clara cells.

Table 1 Percentage of different cell types before and after infection with or without TMX treatment (%)

Percentage of $EGFP^+$ Cells (mean±SE)	before infection		after infection (21 dpi)	
	without TMX	with TMX	without TMX	with TMX
Clara	10.3±0.9	86.8±1.1	16.0±1.8	77.9±2.0
SBECs	*N.A.	N.A.	14.4±5.0	80.8±4.0
#Ring structures	N.A.	N.A.	10	70
&SPC^+ cells in clusters	N.A.	N.A.	10.1±1.3	48.1±3.0

* N.A. stands for Not Applicable; # Each data is obtained from at least 8 sections of 2 mice; & Each data is obtained from total 3162 SPC^+ cells in 4 sections (without TMX) or 6799 SPC^+ cells in 10 sections (wth TMX) of 2 mice.

Following TMX treatment, ~70% of SPC^+ ring-like structures and 50% of regenerated

AT2s in damaged parenchyma were EGFP$^+$ at 21 dpi (Table 1). EGFP$^+$ AT2s were observed in areas with normal alveolar structure (Figure 16C-16E). Although ~7% of AT2s were EGFP$^+$ in TMX-treated transgenic mice before infection as previously reported (Rawlins et al., 2009a), it was unlikely that these AT2s gave rise to as much as 50% of regenerated SPC$^+$ cells in the damaged alveolar areas during repair (Table 1). Considerable amount of EGFP$^+$ SBECs at the tips of bronchioles and EGFP$^+$SPC$^+$ cells in dilating ring-like structures were observed in the damaged alveolar areas (Figures 15E-15G).

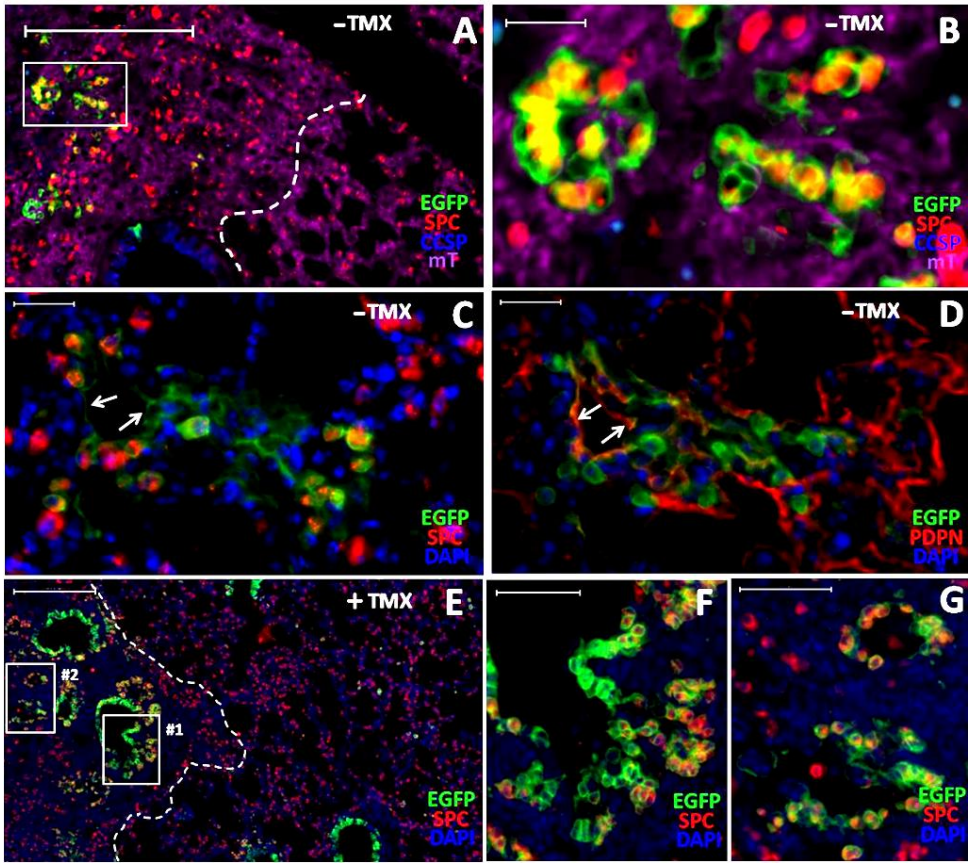

Figure 15. SBECs give rise to AT2s to repair alveolar damaged post influenza infection (A and B) *CCSP-CreER:ACTB-mT-EGFP* transgenic mice without tamoxifen treatment were infected with influenza virus. Shown are representative images of lung sections were analyzed for EGFP (green), SPC (red),CCSP (Blue) and tomato red (mT, purple) 21 dpi. White broken line in (A) demarcates the infiltrated

area (to the left) and normal area (to the right). Higher magnification of the boxed area in (A) is shown as (B). (C and D) *CCSP-CreER:ACTB-mT-EGFP* transgenic mice without tamoxifen treatment were infected with influenza virus. Shown are representative images of adjacent lung sections from mice 21 dpi analyzed for expression of EGFP (green) and SPC (red) (C) or EGFP (green) and PDPN (red) (D). Both sections are counterstained with DAPI (blue). Tomato red channel is not shown. Arrows point to EGFP+ AT1s. (E-G) *CCSP-CreER:ACTB-mT-EGFP* transgenic mice were treated with TMX and then infected with influenza virus. Lung sections were analyzed for EGFP (green), SPC (red) and DAPI (blue) 21 dpi. White broken line in (A) demarcates the infiltrated area (to the left) and normal area (to the right). Higher magnification of the boxed areas are shown in (F) and (G) respectively. Tomato red channel is not shown. Scale bars: (A and E) 200μm; (B-D) 20μm; (F and G) 50μm.

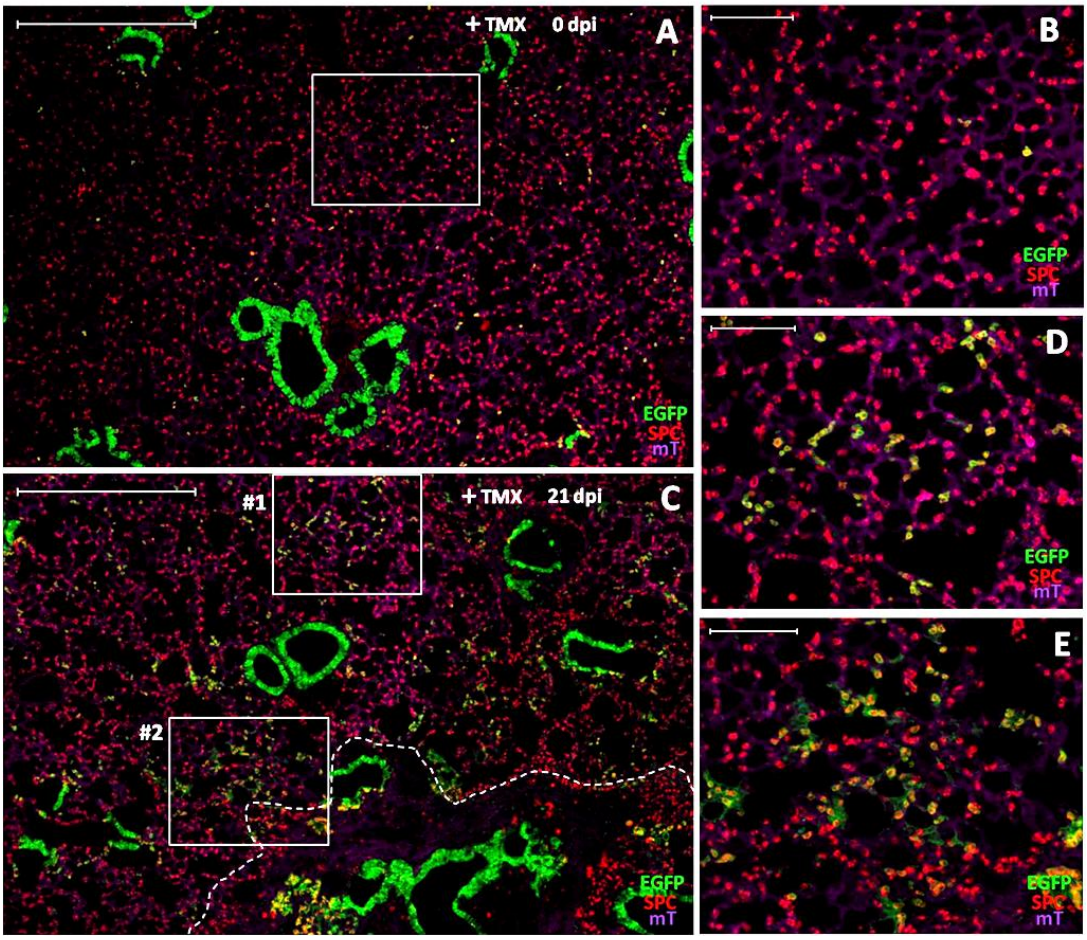

Figure 16. Increase of EGFP+ AT2s after repair Representative images of *CCSP-CreER:ACTB-mT-EGFP* transgenic mice with (TMX) treatment before (A and B) and after (C-E) influenza infection at 21 dpi. Expression of EGFP (green), tomato red (purple) and SPC (red) are analyzed. Higher magnification image of boxed area in (A) is shown as (B); higher magnification images of boxed areas in (C) are shown as (D) and (E) respectively. White broken line in (C) demarcates the infiltrated area (below) and normal area (above). Scale bars: (A and C) 500μm; (B, D and E) 100μm.

With TMX administration, large number of regenerated AT2s cells were observed $EGFP^+$ throughout the alveolar areas (Figures 17A and 17B) at 21 days post bleomycin treatment. Similar results were obtained when a stack of 10 lung sections spanning more than 600μm depth were stained. Most of the regenerated AT2s were found in alveolar areas that had not fully repaired yet. Some of them formed clusters or ring-like structures (Figure 17C). Besides the $EGFP^+$ AT2s, large number of AT1 cells also expressed EGFP (Figures 17D and 17E). Even without TMX administration, small patches of $EGFP^+$ AT2s and AT1s were observed (data not shown). These results showed that the majority of regenerated AT2s in the damaged parenchyma were derived from Clara cells with SBECs being the intermediate phase from Clara cells to AT2s. $EGFP^+$ AT1s might also originate from $EGFP^+$ Clara cells, perhaps via $EGFP^+$ AT2s according to previous reports (Adamson and Bowden, 1974; Aso et al., 1976; Mason et al., 1997). Ciliated cells could also be labeled by EGFP in this transgenic system, however, the labeling was so rare (~0.3% without TMX treatment and ~0.4% with TMX treatment) (Rawlins et al., 2009a) that they might not contribute much to the $EGFP^+$ SBECs nor AT2s.

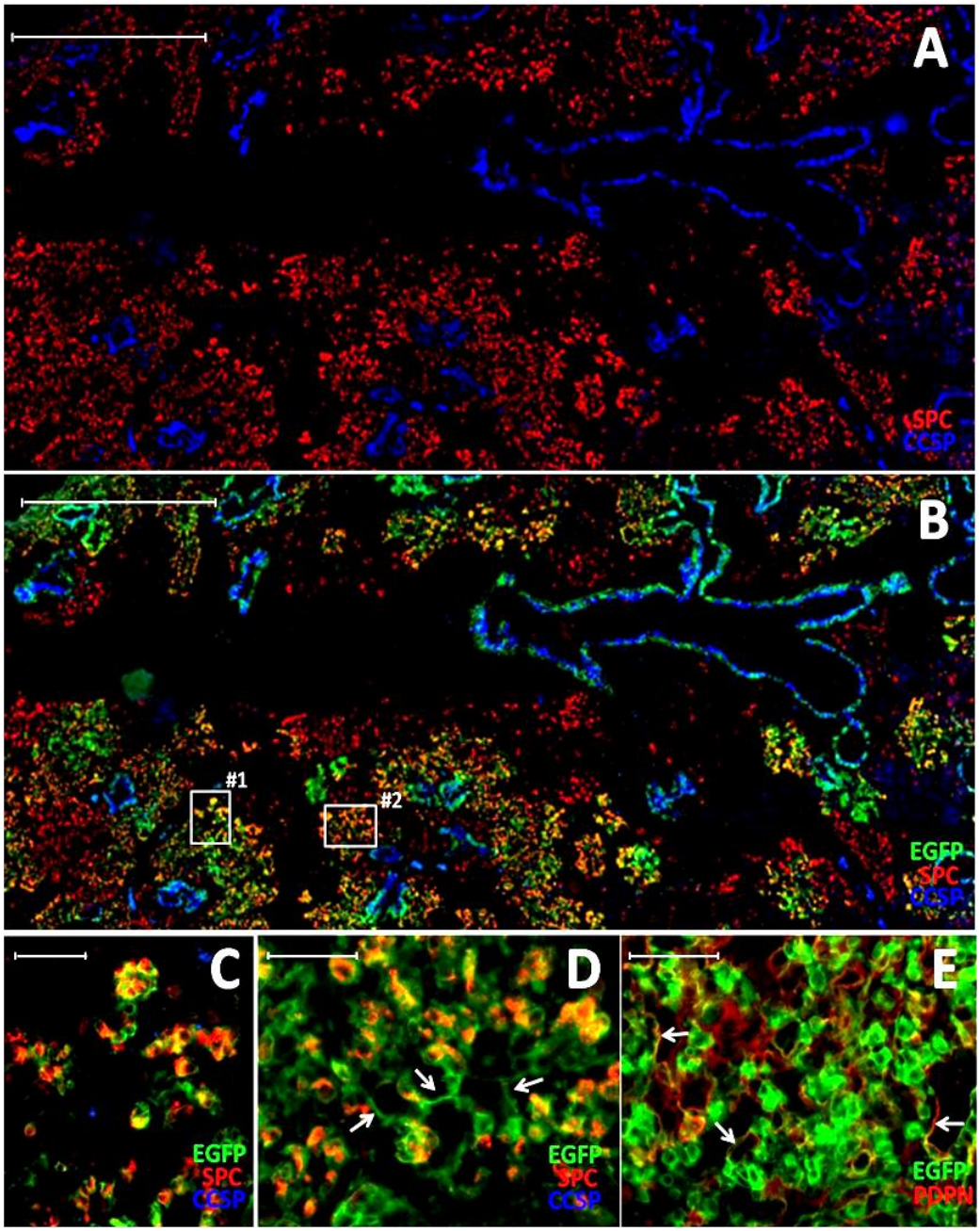

Figure 17. SBECs give rise to AT2s to repair alveolar damaged post bleomycin treatment (A-D) *CCSP-CreER:ACTB-mT-EGFP* transgenic mice were given TMX and treated with bleomycin. Shown are representative images of lung sections analyzed for EGFP (green) (B-D), SPC (red) and CCSP (blue) at 21 days post bleomycin treatment. Tomato red is not shown. High magnification of boxed areas #1 and #2 in (B) are shown in (C) and (D), respectively. Arrows in (C) indicate EGFP+ AT1-like cells. (E) A representative image of EGFP (green) and PDPN (red) of lung tissues of TMX treated transgenic mice at 21 days post bleomycin treatment. Arrows in (E) indicate EGFP and PDPN double-positive AT1s. Scale bars: (A and B) 1000μm; (C-E) 50μm.

The differentiation of SBECs into AT2s, as a strategy for regenerating alveolar epithelia, closely resembles the process of development of alveolar epithelium in embryonic lungs. At gestational day 15, lung is in the pseudoglandular stage and filled with developing tubules, many of the which are lined with SPC^+ cuboidal cells in ring structures (Figures 18A and 18B) that form the tips of developing bronchioles (Figure 18C), similar to the SPC^+ ring structures observed in the damaged alveolar areas (Figures 13B, 14C and 15B). *Clusterin* is transiently but highly expressed in the developing lung and pancreas, where it promotes tissue morphogenesis (French et al., 1993; Min et al., 1998). We also detected intense positive staining for Clusterin at the termini of developing bronchioles in the pseudoglandular stage of embryonic lung development (Figure 18D). In contrast, virtually no cells were Clusterin+ in adult lung in the absence of influenza infection (Figure 18E). Following influenza infection, however, Clusterin expression was induced in the lung (Figure 18F). Some SBECs, including those in ring structures, stained positive for Clusterin (Figures 18G and 18H). Different from the embryonic lung, the expression pattern of Clusterin in the damaged lung was not restricted to tips of bronchioles, but had a more dispersed distribution throughout the damaged tissue (Figure 18F). These results suggested that the repair of damaged lung tissue in adult animals underwent a process which was at least partially parallel to that of embryonic lung development, and $CCSP^-$ SBECs in the infected adult lung were phenotypically and functionally similar to SPC^+ cuboidal cells in the embryonic lung.

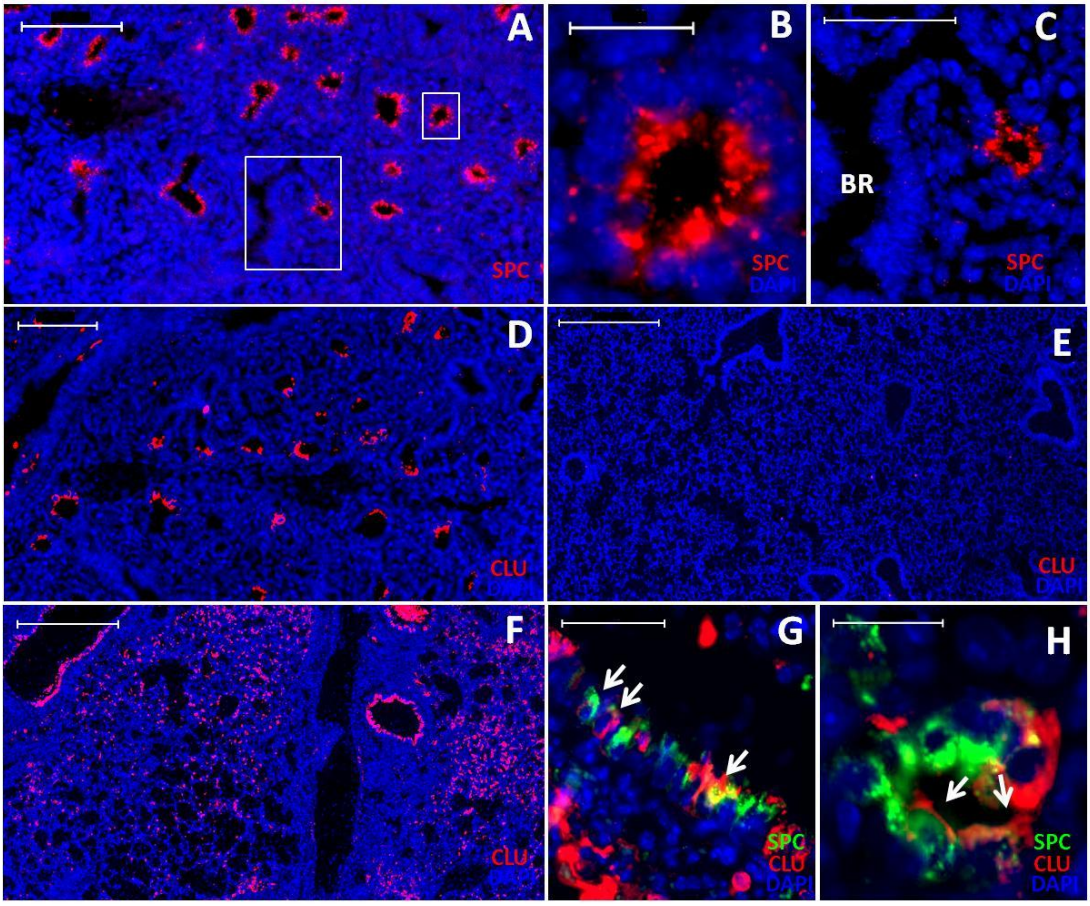

Figure 18. Lung damage repair goes through a process similar to embryonic lung development (A-C) Representative images of SPC (red) and DAPI (blue) staining of a fetal lung at gestational day 15. Arrows point to SPC+ ring structures. Higher maganification showing cuboidal shape of SPC+ cells (B) and a tip of developing bronchiole (C). (D) A representative Image of immunofluorescent staining of Clusterin (red) and DAPI (blue) in fetal lung sections at gestational day 16. (E and F) Representative images of immunofluorescent staining of Clusterin (red) and DAPI (blue) in the lung sections of adult mice without infection (E) or at 9 dpi (F). (G and H) Co-staining of Clusterin (red), SPC (green) and DAPI (blue) in the lung sections of mice at 9 (G) or 15 (H) dpi. Arrows point to Clusterin+ SBECs in a bronchiole (G) or a ring structure (H). All tissues were counterstained with DAPI (blue). Scale bars: (A and D) 100μm; (B and H) 20μm; (C and G) 50μm; (E and F) 500μm.

2.4.6 Clara cells contribute to generation of new bronchioles

Consistent with recent report (Kumar et al., 2011), $p63^{+}$ cells were observed in damaged parenchyma after influenza virus infection (Figure 19A). These cells were in

clusters or patches with some of them forming lumen structures (Figure 19B). Both $p63^+$ cells and SPC^+ cells were observed in patches in infiltrated parenchyma, but they were consistently segregated into different regions (Figure 19C). In comparison, SPC^+ cells and $PDPN^+$ cells co-localized in damaged parenchyma representing the regeneration of alveolar epithelium (Figures 19D, 13E and 14E). Expression of p63 and PDPN signals were detected to be associated in the same infiltrated regions. However, the PDPN signal was from the $p63^+$ cells themselves and was much weaker compared to those from $PDPN^+$ cells co-localizing with SPC^+ cells or that were in the healthy alveolar region (Figure 19E and 19F). The observed expression of PDPN by $p63^+$ cells was congruent with a recent report showing that $p63^+$ basal cells from mouse trachea express PDPN (Rock et al., 2011). Therefore the lumen-like structures might not relate to alveoli. Similar observations were made in damaged parenchyma at day 21 post bleomycin treatment (Figure 19G and 19H)

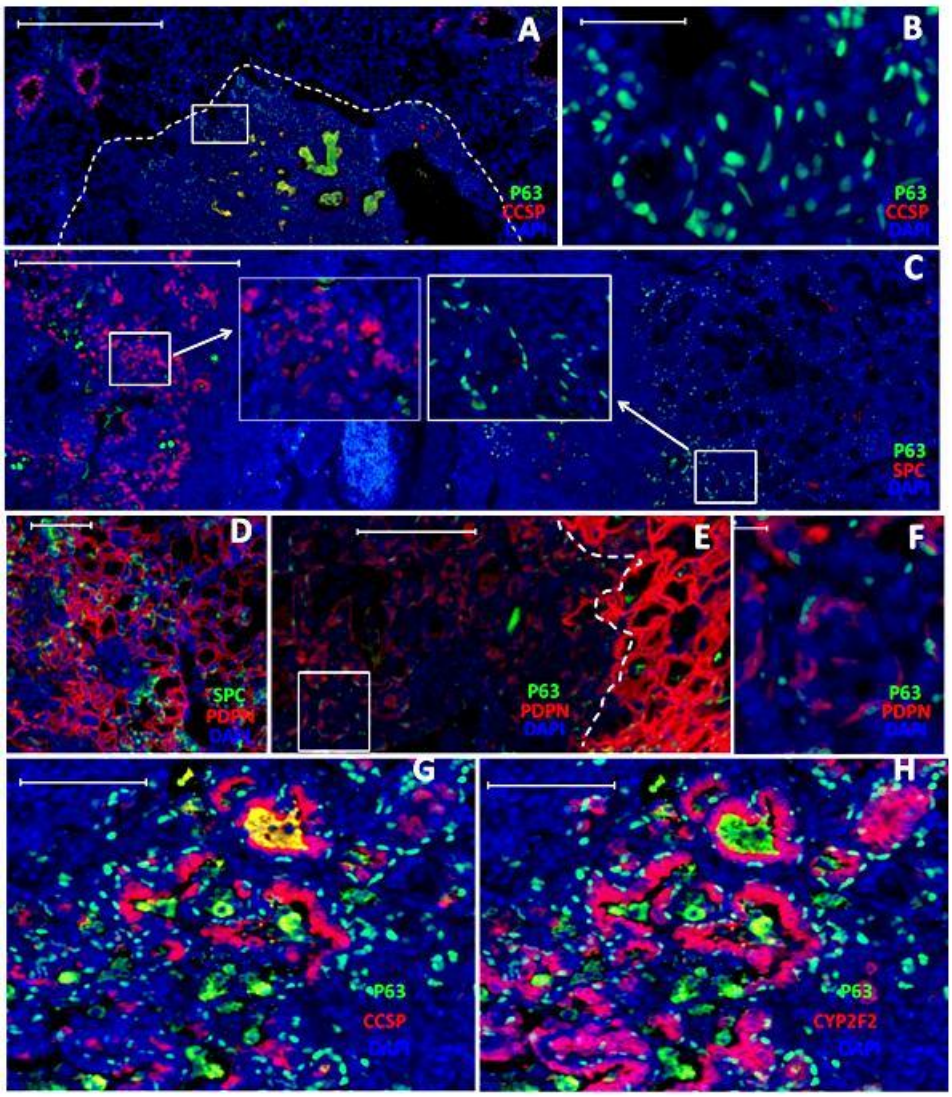

Figure 19. Induction of p63+ cells in damaged parenchyma (A, B) Representative immunofluorescent images of lung sections stained for P63 (green), CCSP (red) and DAPI (blue) at 17dpi. Higher magnification of boxed areas in (A) are shown in (B), white broken line in (A) demarcates the infiltrated area (below) from the normal looking area (upper) of the lung. (C) A representative immunofluorescent image of lung sections stained for P63 (green), SPC (red) and DAPI (blue) at 17 dpi. Higher magnifications of boxed areas are shown as indicated. (D) Representative immunofluorescent images of lung sections stained for SPC (green), PDPN (red) and DAPI (blue) at 17 dpi. (E, F) Representative immunofluorescent images of lung sections stained for P63 (green), PDPN (red) and DAPI (blue) at 17 dpi. Higher magnification of boxed area in (E) is shown in (F). White broken line in (E) demarcates the $p63^{+}$ region (left) from the alveoli region (right) of the lung. (G) and (H) show staining for P63, CCSP, CYP2F2 and DAPI of the same section. (G) shows channels of P63 (green), CCSP (red) and DAPI (blue). (H) shows channels of P63 (green), CYP2F2 (red) and DAPI (blue). Scale bars: (A, C) 500µm (B) 50µm; (D, E, G, H) 100µm; (F) 20µm.

In the lumen-like structures formed by $p63^+$ cells, although very few cells were stained positive for CCSP (Figures 20A-20C), most of them were positive for CYP2F2 (Figures 20D-20F), suggesting the lumen-like structures might relate to bronchioles instead.

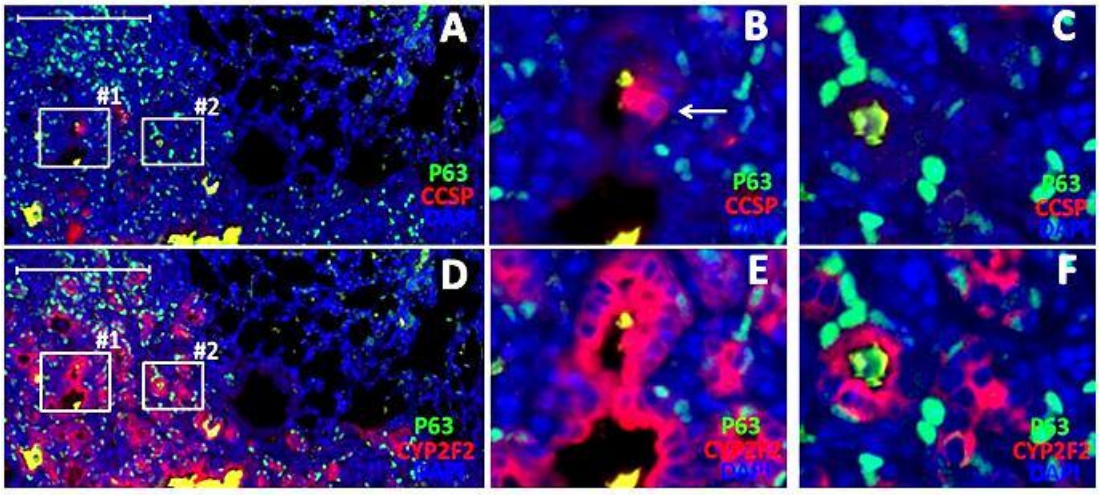

Figure 20. $p63^+$ lumen-like structures in damaged parenchyma induced by influenza infection are related to bronchioles Representative immunofluorescent images of lung sections at 17 dpi. (A) and (D) show staining for P63, CCSP, CYP2F2 and DAPI of the same section. (A) shows channels of P63 (green), CCSP (red) and DAPI (blue), higher magnifications of boxed areas #1 and #2 are shown in (B) and (C) respectively. The arrow in (B) indicates a $CCSP^+$ cell. (D) shows channels of P63 (green), CYP2F2 (red) and DAPI (blue), higher magnification of boxed areas #1 and #2 are shown in (E) and (F) respectively. Scale bars: 200μm.

The $CCSP^-CYP2F2^+$ cells forming lumen-like structures, which are also positive for p63, were similar to the Clara cells during embryonic lung development. At gestational day 17, some of the developing Clara cells were CYP2F2+, but most of them had yet to express CCSP (Figures 21A and 21B). In some damaged parenchyma, the lumen-like structures extended to normal-looking alveolar areas to form terminal bronchioles (Figures 21C and 21D). These results suggested that following influenza virus infection the $CCSP^-$ $CYP2F2^+$ cells in the lumen-like

structures were developing Clara cells; and the lumen-like structures were the regenerated small bronchioles.

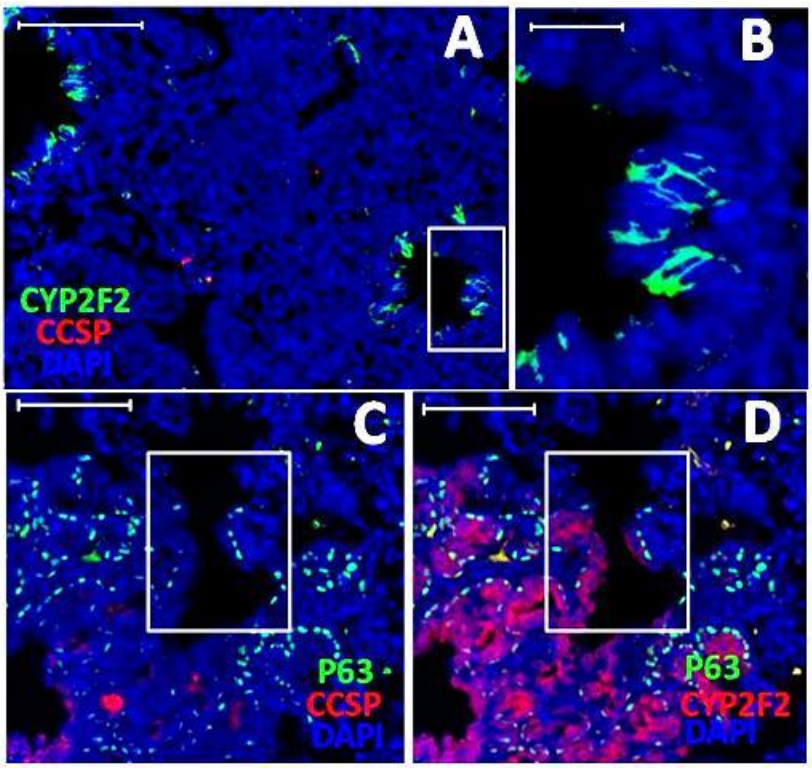

Figure 21. CCSP^{-}CYP2F2^{+} cells forming lumen-like structures were similar to the Clara cells during embryonic lung development (A, B) Representative immunofluorescent images of embryonic lung sections stained for CYP2F2 (green), CCSP (red) and DAPI (blue) at gestational day 17. Higher magnification of boxed area in (A) is shown in (B). (C, D) Representative immunofluorescent images of lung sections at 17 dpi. (C) and (D) show staining for P63, CCSP, CYP2F2 and DAPI of the same section. (C) shows channels of P63 (green), PDPN (red) and DAPI (blue). (D) shows channels of P63 (green), CCSP (red) and DAPI (blue). The box in (C) and (D) indicates a terminal bronchiole. Scale bars: (A, C, D) 100μm; (B) 20μm.

Similar observations were made in damaged parenchyma at day 21 post bleomycin treatment (Figure 19G and 19H), however, in another lung injury model induced by naphthalene treatment, p63^{+} cells were not detected in bronchioles and no massive infiltration was observed (data not shown).

$p63^+$ basal cells are important for the regeneration of stratified epithelium, therefore, the $p63^+$ cells occurred in damaged parenchyma might be the source of regenerated Clara cells. In *CCSP-CreER:ACTB-mT-EGFP* transgenic mice, under normal condition $p63^+$ basal cells were confined in trachea and not labeled by EGFP either without or with TMX treatment (data not shown), which was consistent with previous report (Rawlins et al., 2009a). If $p63^+$ cells in infiltrated parenchyma were derived from pre-existing $p63^+$ cells, they should be $EGFP^-$. Similarly, if the regenerated Clara cells were derived from $p63^+$ cells in damaged parenchyma, they should also be $EGFP^-$. Unexpectedly, in transgenic mice with or without TMX treatment we found $p63^+$ patches labeled by EGFP after influenza or bleomycin-induced injury. In $EGFP^+$ $p63^+$ patches, majority of regenerated Clara cells were $EGFP^+$ (Figures 22A and 22B), and ~80% of the $p63^+$ cells around were also $EGFP^+$ (Figures 22C and 22D). While in $EGFP^-$ $p63^+$ patches, both regenerated Clara and $p63^+$ cells were $EGFP^-$ (Figures 22E-22H). In transgenic mice treated with TMX, ~63% and ~56% of the $p63^+$ patches were $EGFP^+$ at day 21 post bleomycin treatment or at 14 dpi. In comparison, in mice without TMX treatment only ~17% and ~4% of the $p63^+$ patches were $EGFP^+$ post bleomycin treatment and infection respectively (Figure 22I). As mentioned above, the rarely labeled ciliated cell might not contribute much to the $EGFP^+$ $p63^+$ cells either. Therefore, majority of these regenerated Clara cells and $p63^+$ cells, if not all, were derived from pre-existing Clara cells, and forming new bronchioles in damaged parenchyma.

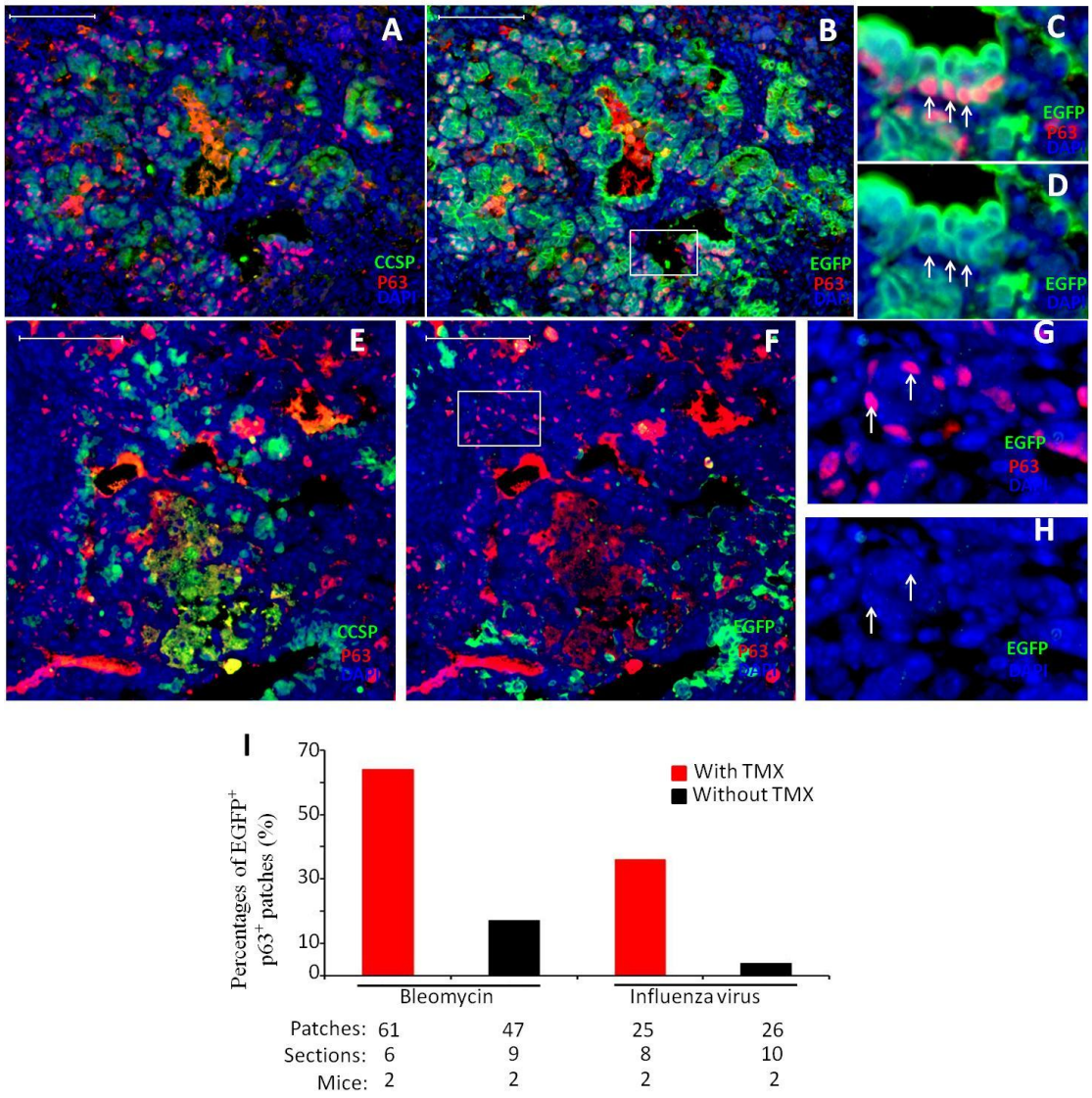

Figure 22. p63+ cells and regenerated Clara cells are originated from pre-existing Clara cells (A) shows channels of CCSP (green), p63 (red) and DAPI (blue); (B) shows channels of EGFP (green), p63 (red) and DAPI (blue). Higher magnification of boxed areas in (B) are shown in (C) and (D). (C) shows channels of EGFP (green), p63 (red) and DAPI (blue); (D) shows channels of EGFP (green) and DAPI (blue). (K) and (L) show staining for p63, CCSP, EGFP and DAPI of the same section. (E) shows channels of CCSP (green), p63 (red) and DAPI (blue); (F) shows channels of EGFP (green), p63 (red) and DAPI (blue). Higher magnification of boxed area in (F) is shown in (G) and (H). (G) shows channels of EGFP (green), p63 (red) and DAPI (blue); (H) shows channels of EGFP (green) and DAPI (blue) (I) Percentages of EGFP+ P63+ patches in transgenic mice with (red columns) or without (black columns) TMX treatment at 14 dpi or at 21 day post bleomycin treatment. The numbers indicate the number of patches, sections and mice from which the data were obtained. Scale bars: (A, B, E, F) 100μm.

2.5 Discussion

Studies of chemically induced lung injuries have identified roles of basal cells, Clara^{v} cells and AT2s in repair and regeneration of tracheal, bronchiolar and alveolar epithelia respectively. However, little is known about the restoration of lung structure following severe damage at distinct anatomical regions simultaneously in the lung, despite the clinical implications of such damage. In this study, we have investigated a cellular pathways involved in repair of lung damage subsequent to both influenza infection and bleomycin treatment. We show that following severe epithelial damage, Clara cells are induced to differentiate into AT2s to restore alveolar epithelium through the intermediate SBECs. Clara cells also regenerate bronchioles in damaged parenchyma.

In healthy lung, CCSP^{+} Clara cells reside in the bronchiolar epithelium, whereas SPC^{+} AT2s reside in the alveolar epithelium. Few CCSP^{+}SPC^{+} cells (BASCs) observed at BADJ. However, following influenza infection or bleomycin treatment, SPC^{+} cells (SBECs) are rapidly induced in the bronchioles of the damaged areas. Our kinetic study shows that SBECs initially express CCSP and possess the cytomorphology of Clara cells, but CCSP expression is lost as cells differentiate to repair the alveolar damage. SBECs are unlikely to be derived from AT2s since SBECs are only observed in the damaged areas where AT2s are almost depleted (Figure 5A). Furthermore, no SBECs were induced following naphthalene treatment which does not cause significant damage to alveolar epithelium. Although BASCs may contribute to some

CCSP^{+} SBECs at terminal bronchioles, their low frequency (~1%) can hardly account for the rapid induction of SBECs throughout the bronchioles. Our lineage tracing study provides definitive evidence to support that SBECs are induced from Clara cells following injury (Figure 10 and 12). Clara cells are known to be heterogeneous, with a subset identified as variant Clara cells (Clara^{v}) which are thought to play a critical role in repair of naphthalene-induced injury. Clara^{v} reside at BADJ or NEB (neuroepithelial body), and are CYP2F2^{-} (Giangreco et al., 2002; Hong et al., 2001; Reynolds et al., 2000). In contrast, SBECs are CYP2F2^{+}; therefore it is unclear if Clara^{v} give rise to SBECs. Although future studies are required to resolve this issue, our current findings definitively demonstrate that majority of SBECs, if not all, are derived from Clara cells.

Our study further shows that regenerated AT2s are also derived from Clara cells. The critical observation of our study is the appearance of large amount of EGFP^{+} AT2s in damaged parenchyma during repair as well as in recovered alveolar epithelium in transgenic mice treated with TMX (Figures 15, 16 and 17). It is noticeable that a small fraction (~7%) of AT2s was also EGFP^{+} if the transgenic mice were given TMX without injury. This result raises the issue that some regenerated EGFP^{+} AT2s might be originated to pre-existing EGFP^{+} AT2s. However, a recent study using lineage tracing in *SPC-CreER* mice following bleomycin injury denies this possibility (Chapman et al., 2011). Therefore, majority of the regenerated AT2s, if not all, are also derived from Clara cells.

Ring-like structures are visualized when $CCSP^-$ SBECs at the tip of the bronchioles are sectioned (Figures 13C, 15E-15G). Initially, the rings are small and tight. As they dilate, they become diffused and eventually turn to clusters of SPC^+ cells in the damaged alveolar areas (Figures 13A and 13B). EGFP labeling in ring-like structures and clusters of AT2s in damaged parenchyma further proves this differentiation process which resembles embryonic development of alveolar epithelium. At gestational day 15 in mouse, lung is at pseudoglandular stage and is filled with developing tubules, most of which contain SPC^+ multi-potent embryonic progenitor cells (Lu et al., 2008; Ten Have-Opbroek, 1979; Wuenschell et al., 1996). These progenitor cells eventually develop into both bronchiolar and alveolar epithelia (Perl et al., 2002; Rawlins et al., 2009a). After severe alveolar injury, the damaged area resembles the pseudoglandular stage of the embryonic lung, where SPC^+ cells also form ring-like structures (Figure 13, 14 and 18). Influenza infection induces the re-expression of lung embryonic specific gene *Clusterin* in adult lung tissue, including SBECs (Figure 18). Together, these observations underscore that repair and regeneration of alveolar epithelium following severe lung damage is similar to the development of alveolar epithelium in embryonic lung. The two processes are not identical, but they do share many common features. In pancreas, another important branching tissue, adult pancreatic duct cells similarly contribute to the repair of the pancreas by recapitulating some aspects of embryonic pancreas development (Inada et al., 2008; Li et al., 2010). Thus, branching organs may share some common strategies for repair and regeneration, namely, reactivation of certain aspects of the embryonic

development program.

A recent study reports that following oxygen induced alveolar damage, Clara cells and BASCs do not contribute significantly to the repair of alveolar epithelium (Rawlins et al., 2009a), but it is cautioned that the data do not exclude the possibility in case of severe alveolar damage. Comparison among lung damage and repair in different models is instructive. We show that while influenza infection and bleomycin treatment induce SBECs, naphthalene treatment does not, indicating that Clara cell-SBEC-AT2 differentiation might be a common cellular mechanism induced by severe alveolar damage. It is tempting to speculate that oxygen-induced lung damage may also not induce SBECs. Contribution of Clara cells in the regeneration of AT2s through an intermediate phase of SBECs during severe alveolar damage is compatible with the anatomy, since it would ensure that the newly regenerated alveolar space in the damaged areas is connected to bronchioles, thus sustain the function of gas exchange.

Another recent report shows that after influenza infection $p63^+$ cells in infiltrated parenchyma are $PDPN^+$ and form lumen structures or "pods" (Kumar et al., 2011). However, since the expression of PDPN in these $p63^+$ cells are much lower than that in alveolar epithelium (Figure 19E), and there is no SPC^+ AT2s around (Figure 19C), the lumen structures are likely to be different from alveoli. In support to this, CYP2F2 staining clearly shows that these lumen structures are bronchioles and $p63^+$ cells line the basement of the lumens with columnar cells at lumen side (Figure 20). Previous report mentioned that such $p63^+$ cells were not observed in bleomycin induced lung

injury model (Kumar et al., 2011), however, in this study we observed large amount of $p63^+$ cells in infiltrated parenchyma at day 21 post bleomycin treatment (Figure 19G and 19H). Studies have proved that Clara cells can be derived from $p63^+$ basal cells, however, a question is also raised that whether columnar cells in adult airways can generate basal cells under some conditions, since they are able to do so during early postnatal development (Rock and Hogan, 2011). In this study, we use *CCSP-CreER:ACTB-mT-EGFP* transgenic mice to genetically trace Clara cells. The results show that pre-existing Clara cells can generate new bronchioles containing both new Clara cells and $p63^+$ cells in damaged parenchyma. Since both influenza virus and bleomycin other than naphthalene can induce severe damage in alveolar epithelium, the generation of new bronchioles containing $p63^+$ cells in infiltrated parenchyma may also be a common repair mechanism in response to severe lung injury.

Clara cells are heterogeneous and multifunctional. They are progenitor cells that produce additional Clara cells and also ciliated cells. Our findings document that following severe lung damage, Clara cells can contribute to regeneration of both alveoli and bronchioles in a process similar to development of embryonic lung (Figure 23). This study does not exclude the existence of parallel cellular mechanisms serving the same purpose. Further elucidation of cellular pathways involved in the repair of lung tissue damage following influenza infection may provide a basis for future development of new interventions to reduce influenza morbidity and mortality.

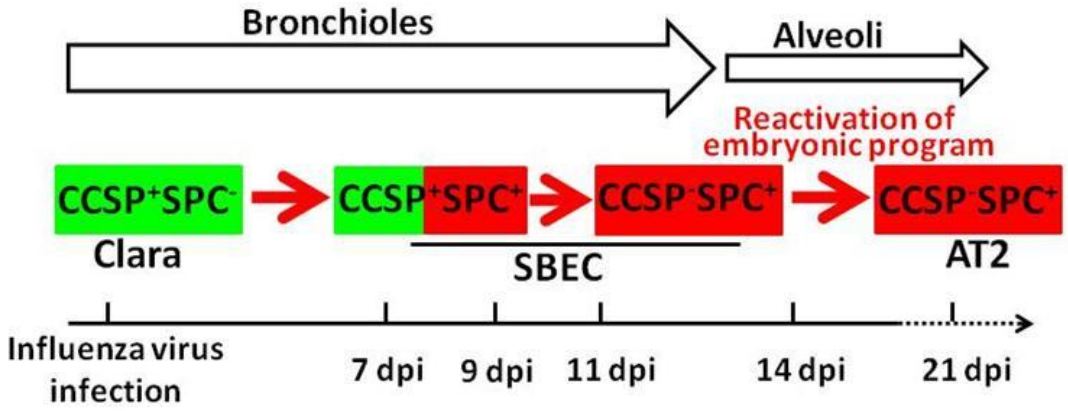

Figure 23. Cellular mechanism of alveolar epithelia regeneration following influenza virus infection In severely damaged areas of the lung following influenza virus infection, Clara cells in bronchiolar epithelia are induced to differentiate into $CCSP^+$ SBECs. $CCSP^+$ SBECs then differentiate into $CCSP^-$ SBECs, which eventually differentiate into AT2s to regenerate alveolar epithelia. CCSP- SBEC to AT2 differentiation goes through a process that resembles the development of alveolar epithelia in embryonic lung.

CHAPTER 3 - IMAGE PROFILING OF PROGENITOR CELL DYNAMICS IN REPAIR OF INFLUENZA-INDUCED LUNG INJURY

3.1 Summary

Lung tissue injury caused by influenza infection is frequent and widely outspread in real life, however, studies on the function of multiple progenitor cells in lung repair have been limited to chemically and physically induced injury models. We established influenza induced lung injury model aiming to quantitatively assess lung damage and repair post infection at tissue and cellular level. For this purpose, high throughput imaging-based tissue informatics study was performed to quantify several aspects, including immune cell infiltration, bronchiolar progenitor Clara cell and AT2 responses, and the frequency of appearance of injury-activated SBECs. We observed temporal difference in the repair of bronchiolar and alveolar epithelium, and the sequential appearance of two phases of transient SBEC, suggesting Clara cell to AT2 trans-differentiation in restoration of alveolar structure post infection. It is also observed that influenza induced lung tissue damage repair progressed simultaneously with immune response.

3.2 Introduction

Studies on the function of lung progenitor cells in lung tissue repair are commonly based on various *in vivo* injury models (Bigby et al., 1985; Borthwick et al., 2001; Dubaybo et al., 1991; Izbicki et al., 2002; Modelska et al., 1999; Randell, 1992; Smith,

1985; Theise et al., 2002; Van Winkle et al., 1999); however, rare chance of exposure to experimental injury sources in real life compromises their clinical significance. Lung injury caused by influenza virus is frequent and globally spread (Brady, 2010; Lipatov et al., 2004; Marcos et al., 2009; Potter, 2001). Being a generally recoverable disease, influenza infection sometimes leads to severe complications with underlying conditions such as, pneumonia and even death (Eccles, 2005; Taubenberger and Morens, 2008). While being the first organ attacked by influenza virus, how lung repairs itself in patients who recover from influenza infection has yet to be discovered. We previously established a lung injury model using H1N1 type A influenza virus to investigate lung tissue repair mechanism post infection. We reported SBECs being induced at injured bronchiolar epithelium following infection, experiencing $SPC^{+}CCSP^{+}$ and $SPC^{+}CCSP^{-}$ status, implying the potential trans-differentiation of bronchiolar Clara cell to AT2 in order to repair the alveolar epithelial structure following severe lung.

Previous study descriptively elucidated the remodeling of lung progenitor Clara cell and AT2 following influenza infection, but was not sufficient for tracing the entire process and obtaining further insights on mutual correlation of their responses. Two possible means could lead to the understanding on continuous scenario of lung repair process: live imaging or serial quantitative study over enough small time intervals for appropriately long period of time. Live imaging of lung at cellular level is complicated with technical difficulties such as movement of lung and staining issue (Chagnon et al., 2010; Parsons et al., 2008).

To quantitatively study the function of progenitor cells in lung repair, it is critical to establish a standard for assessing the extent of lung damage repair over time. Non-invasive and minimally-invasive measurements for lung health status have been applied in relevant *in vivo* studies, including air-blood barrier or endothelium permeability (Jones and McAteer, 1990; Matthay et al., 2010), lung capacity and quasistatic compliance (Huang, 2008; LaBrie et al., 1996; Nolen-Walston et al., 2008), level of lung related biomarkers in bronchoalveolar lavage fluid (BALF) and serum (Gupta et al., 2007; Meissner et al., 2005; Pan et al., 2002). However, extensive applications of these methods are limited by sensitivity (Pan et al., 2002), complexity (Jones and McAteer, 1990), and requirements for special equipments (Nolen-Walston et al., 2008). Most common evaluation for lung tissue damage remains as lung histology (Hoag et al., 2008; Narasaraju et al., 2009; Reynolds et al., 2004; Suliman et al., 2001). Some lung histology analyses utilize semi-quantitative grading system to classify different levels of lung damage based on sickness scores of inflammation, edema, fibrosis etc (Aguilar et al., 2009; Atzori et al., 2004; Cargnoni et al., 2009; Gupta et al., 2007; Hagood et al., 2005; Longhi et al., 2007). Such systems also acquire inherent drawbacks such as inter- and intra-observer variability and the discreteness of the measurement, so that small differences among samples are impractical to be distinguished. A series of imaging-based tissue informatics methods were developed in this paper in substitution of the conventional histology analysis, which significantly enhanced the accuracy and sensitivity of measurement and eliminated the inter- and intra-observer variability in interpretation. These methods

included indirect assessment of lung damage repair at tissue level based on immune cell infiltration, direct measurement of lung endogenous progenitor Clara cell and AT2 cellular death and recovery in terms of the relative cell density, and evaluation of lung repair potential based on the appearance frequency of SBEC.

Quantitative study of the damage and repair of the entire lung requires high throughput tissue information from images. Trade-off between the resolution and acquisition time for images needs to be optimized in order to acquire images over considerably large areas of lung tissue with sufficient quality of image information. As a result, virtual microscopy systems using automatic slide scanner bears apparent advantage in this high throughput image informatics study comparing to the conventional and confocal microscopy. The concept of digital slides has been gradually adopted in both laboratory and clinical applications for its advantage in storage, imaging speed and feasibility for spatial quantification due to large tissue area (Roignot et al., 2011; Steinberg and Ali, 2001). Whole-slide image quantification methods for whole-slide imaging have been recently developed to analyse multiple types of pathological samples (Hadi et al., 2010; Isse et al., 2010; Konsti et al., 2011; Lopez et al., 2009; Velez et al., 2008).

Automated quantification algorithms were applied to extract information of immune cell, Clara cell, AT2 and SBEC from large number of images taken from a time course of *in vivo* influenza induced lung injury model. Quantitative analysis of the information revealed new evidences in support of Clara cell to AT2

trans-differentiation in lung repair process and the temporal correlation between tissue repair and immune response.

3.3 Method

3.3.1 Animal and tissue sample preparation

Female C57BL/6 mice were purchased from Centre for Animal Resources, Singapore and housed in specific pathogen-free BSL2 facilities at National University of Singapore (NUS). Mice were anesthetized with ketamine (100mg/kg body weight) and infected with sub-lethal dose (100 PFU/mouse) influenza virus A/Puerto Rico/8/34 (H1N1) by intratracheal instillation. Five mice were sacrificed at each time point: before infection (control) and 1, 3, 5, 7, 9, 11, 13, 15, 17, 19, 21, 28 days post infection (dpi). Lung tissues were collected. The left lobes were fixed in 10% neutral buffered formalin solution (Sigma) overnight and processed with Tissue Processor (Leica) and embedded in paraffin blocks. For each lobe, 15 transverse sections were cut with microtome (Leica RM2165) from the middle part of the lobe and with 50μm in between sections. Sections were mounted on polylysine coated slides (Thermal Scientific). Ten sections were used for H&E and 5 sections for immunofluorescent staining. The right lobes were used for lavage, measuring virus titer and other analysis. All animal protocols were approved by the Institutional Animal Care and Use Committee at NUS and Massachusetts Institute of Technology.

3.3.2 Histological staining

Paraffin sections were de-waxed in Histo-Clear solutions twice (National Diagnostics, HS-200) and rehydrated first in absolute ethanol three times, and then once each in 90% ethanol, 70% ethanol and 50% ethanol. H&E staining was processed according to standard protocol. For immunofluorescent staining, antigen retrieval was performed by incubating the lung section with proteinase K solution (Sigma, 20mg/ml, in 50mM Tris-Cl,1mM EDTA, pH 8.0) at 37^{o}C for 30 min. Sections were then blocked in blocking buffer (3% BSA, 0.2% Triton X-100 in PBS) for 1hr. Polyclonal rabbit anti-CCSP antibody (USbiology, C5828) was used in 1:200 dilution, and goat anti-pro-SPC (Santa Cruz sc-7706) antibody was used in 1:50 dilution. Incubation was performed at 4^{o}C overnight in blocking buffer. Secondary Alexa Fluor 488-labeled donkey anti-rabbit antibody (Invitrogen, A21206) or Alexa Fluor 546-labeled donkey anti-goat antibody (Invitrogen, A11056) were used in 1:200 dilution. Incubation was performed at 4^{o}C for 1hr. Cover slips were mounted on stained section with antifade reagent containing DAPI (Invitrogen S36939).

3.3.3 Image acquisition

High-resolution MIRAX MIDI system (Carl Zeiss) equipped with bright field and fluorescence illumination was used to scan the stained lung sections. Images were captured with Axiocam MR(m) (Carl Zeiss), processed and converted to TIF format with Miraxviewer software (Carl Zeiss). The original resolution of all images is 1.68 μm ×1.68 μm per pixel. The images used for quantification were down sampled eight times from the original images to reduce the computation time and the use of memory

space.

3.3.4 Histology analysis

Digital images of H&E stained lung sample from different time points post infection were evaluated blindly by three independent researchers. Semi-quantitative grading system was applied as previously reported (Cargnoni et al., 2009), in which subjective scores from 0 to 3 were given to reflect absent, mild, moderate and extensive cell infiltration, respectively. Scores from the three researchers were averaged to obtain the average score of cell infiltration at each time point post infection.

3.3.5 Feature extraction and quantification

Automated algorithms were developed to compute four indices for quantitative evaluation of lung damage and repair based on image analysis.

3.3.5.1 Infiltration index

Infiltration Index

Infiltration index was defined as the percentage of infiltrated areas to total alveolar area in H&E stained lung section images. The infiltration index was calculated by infiltration algorithm as follows: The original H&E stained RGB image was first converted to greyscale. The image pyramid of greyscale image was then created by subsample the image by a factor of one, two, four and eight respectively along each spatial dimension (Burt, 1981). A threshold was applied to identify low intensity

pixels in each level of the image pyramid. A pixel was identified within infiltrated area if it was selected as low intensity pixels in all levels of the image pyramid. The mask of infiltrated area was generated by dilating all pixels identified within infiltrated area to connect small regions. Total alveolar area was segmented from original image by excluding large empty blood vessels and bronchioles with a threshold on size. The percentage of infiltrated area to total alveolar area was then computed as infiltration index and used as an index of general lung damage and repair at tissue level (Figure 24).

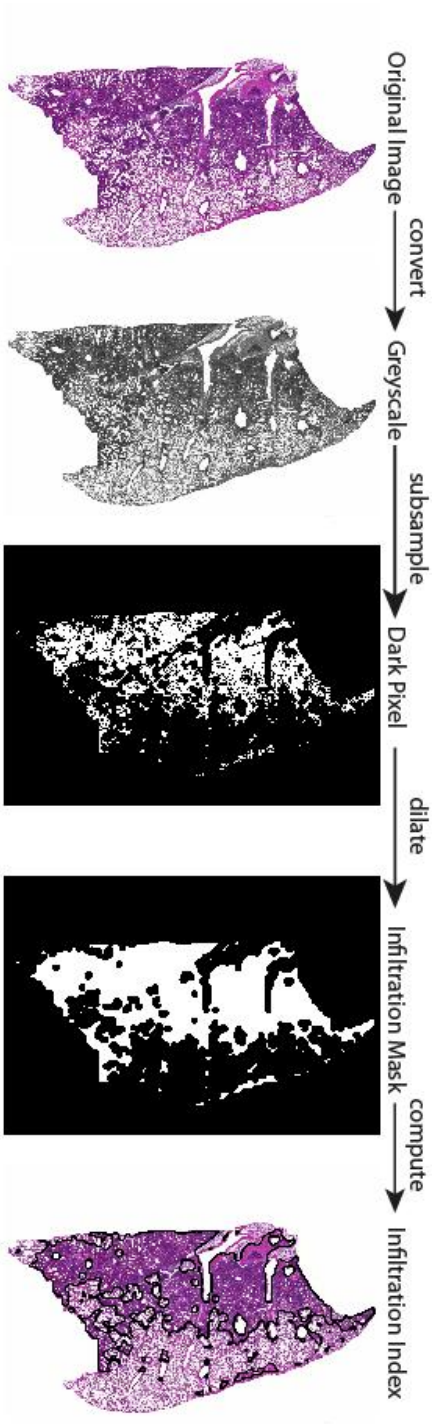

Figure 24. Flowchart of the feature extraction and quantification algorithm for infiltration index

3.3.5.2 Clara cell coverage index

Clara cell coverage index reflected the coverage density of Clara cell on the interior

wall of bronchioles. Bronchioles were automatically recognized from immunofluorescent images as empty spaces with no nuclei inside and surrounded by CCSP-expressing Clara cells (Figure 25A). Nuclei were segmented from original image by thresholding DAPI fluorescence intensities. Centres of each nucleus were located and denoted as nodes. Delaunay triangulation diagram was generated by introducing all nodes to connect neighbouring nodes while none was inside the circumcircle of any triangle formed (O'Rourke, 1994) (Figure 25B). Nodes at boundary of bronchioles (bronchiolar epithelium) tended to have longer average edge length than others, and non-boundary nodes with shorter average edge length were neglected accordingly. Boundary nodes belonged to the same bronchiole were then clustered together based on their connectivity in the original triangulation. Centres of each boundary node cluster were located and region growing (Gonzalez and Woods, 2002) was performed from the centres to determine the exact boundaries of potential bronchioles (Figure 25C). To further recognize bronchioles from all candidates, Clara cells were identified from original image by thresholding CCSP fluorescence intensities. The Clara cell coverage ratios around the boundary area were calculated for each candidate, and a minimum threshold (1%) was applied to exclude false ones with completely no Clara cells surrounded (Figure 25D). The remaining true bronchioles were then clustered into the high-Clara-cell-coverage ones (HC) and low-Clara-cell-coverage ones (LC) using Otsu method (Otsu, 1979) based on the Clara cells coverage ratio calculated. The Clara cell coverage index was defined as the ratio of HC frequency to LC frequency and used for evaluation of the lung

bronchiolar damage and repair.

3.3.5.3 Relative density of AT2

The two-dimension density of AT2s in lung tissue sections changes over the course of damage and repair post infection. Since AT2s were depleted in damaged areas, they were identified in healthy areas only. It was observed from the image that healthy lung tissue expressed dim auto-fluorescence in pro-SPC channel, while damaged areas emitted much brighter auto-fluorescence due to the highly condensed tissue where infiltrating cells accumulated (Figure 25E). Accordingly, k-means clustering algorithm was performed to group the pixels into four categories based on pro-SPC fluorescent intensities (Pham et al., 2000). The brightest cluster with the highest pixel intensities represented SPC expressing cells, including AT2s in healthy areas and SBECs in damaged areas. The second and third brightest clusters referred to areas with bright auto-fluorescence and dim auto-fluorescence signals, respectively. The last cluster with minimum fluorescence intensity represented empty spaces in the lung tissue such as bronchioles, blood vessels and alveolar sacs. Therefore, the group of pixels representing areas emitting bright auto-fluorescence were selected to create the mask of damaged areas (Figure 25F). Damaged areas were then subtracted from total tissue section to form the mask of healthy areas. Pixels from the first cluster were then selected and overlapped with the mask of healthy areas to create mask of AT2s. Watershed method (Meyer, 1994) was performed on the AT2 cell mask to separate co-joint cells and the number of AT2s was counted. Relative AT2 density was

estimated by computing the number of AT2s per unit tissue area, and used as an indicator for lung alveolar damage and repair.

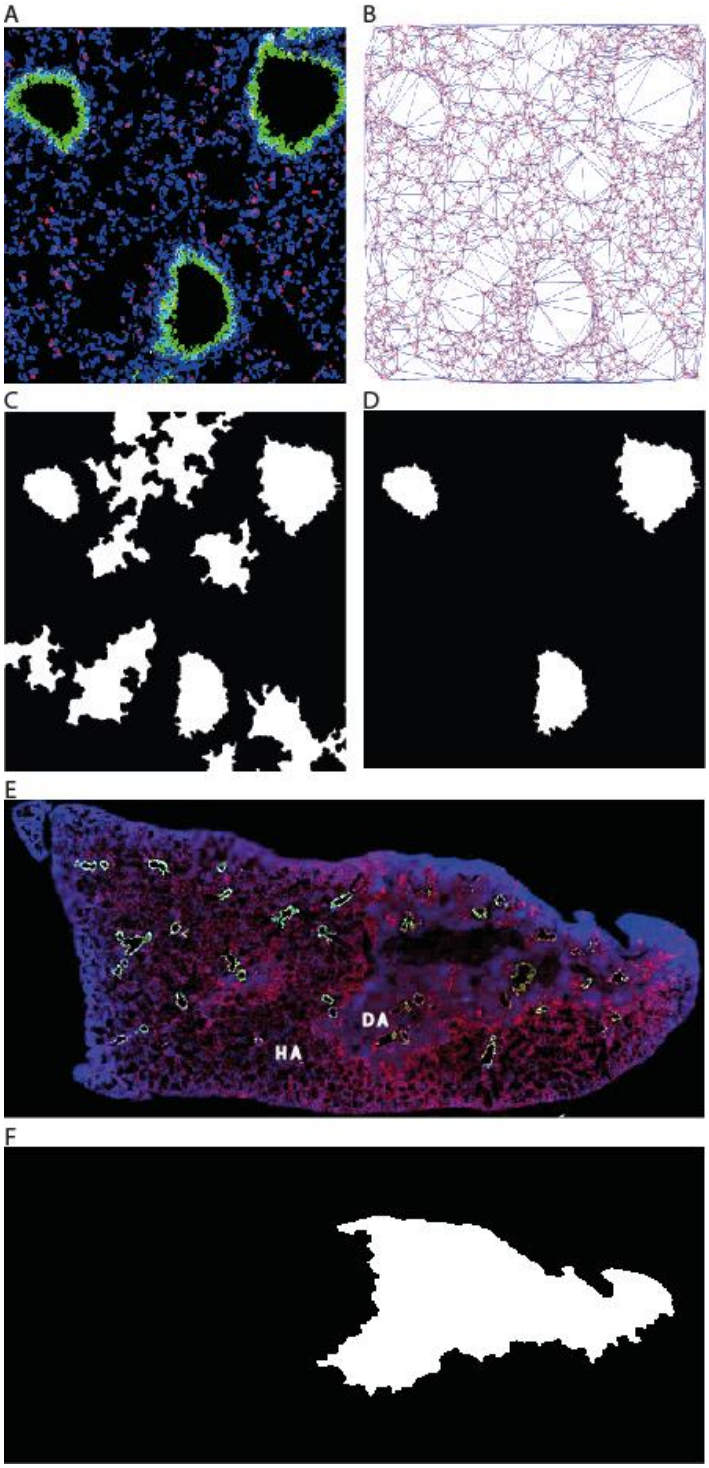

Figure 25. Illustration of algorithms for quantification with immuno-fluorescent images (A) Snapshot of lung tissue area containing three bronchioles to be

automatically identified. Nuclei was stained in blue colour, Clara cell were stained in green colour and AT2s were stained in red colour (B) Delaunay triangulation diagram generated with the centres of each nuclei to define boundary nodes around bronchiole. (C) Candidates of potential bronchioles identified after region growing performed from centres of clusters of boundary nodes. (D) Bronchioles identified after exam for Clara cell coverage along the boundaries. (E) Global view of the scanned image of one entire left lobe of infected mouse lung, consisting healthy area (HA) with normal alveolar structure and damaged area (DA) with condensed infiltrated immune cells. (F) Damaged area from the tissue section segmented with K-means clustering algorithm.

3.3.5.4 Occurrence frequency of SEBCs

Frequency of SEBCs in bronchioles was defined as the percentage of SBECs-containing bronchioles to total bronchioles. Bronchioles were identified as described in Clara Cell Coverage Index. SBEC-containing bronchioles were identified as bronchioles in the damaged areas that contained pro-SPC expressing cells. Frequencies of Scgb1a1^{+} and Scgb1a1^{-} SBEC-containing bronchioles were quantified by examining the co-localization of Scgb1a1 and pro-SPC signals in the identified bronchioles in the damaged areas.

All image processing and computation algorithms were implemented with Matlab (The Math Works, Inc., Natick, Massachusetts). The Matlab codes are available on request.

3.4 Results and Discussion

3.4.1 Immune cell infiltration: an indirect index for lung damage repair at tissue level

Vigorous immune response in the lung was triggered by influenza infection. Different

immune cells infiltrated and accumulated in damaged areas from blood circulation by chemotaxis. Generally, more severe tissue damage induces more chemokines and results in more infiltrating immune cells for prolonged time. The amount of the infiltrating immune cells in the lung can be evaluated from H&E stained tissue sample (Figure 2C). It was observed that immune cells in the lung gradually increased with time post infection, reached maximum amount around day 14, and significantly recovered by day 21.

Several H&E stained image-based quantitative analyses were developed for hyperoxia (Thebaud et al., 2005; van Haaften et al., 2009) and bleomycin (Rojas et al., 2005) induced injury models targeting size of alveolar sac and tissue thickness. Following influenza infection, condensed tissue in infiltrated areas contained high density of immune cells. Since nuclei are stained in dark purple by hematoxilin, the heavily infiltrated areas could be easily distinguished from healthy areas for their dark colour. An algorithm was developed to segment dark infiltrated areas from the healthy areas in H&E stained lung sections, and compute the infiltration index by averaging the percentage of infiltrated area to total alveolar area in each lung sections (Figure 24).

The algorithm was applied to H&E stained lung sections over the time course of infection to compute infiltration index. The result consistently reflected the observed trend in H&E stained images (Figure 26A). Small areas around bronchioles and blood vessels with high cell density were mistakenly identified as infiltrated areas, leading to a basal level of less than 10% infiltration in uninfected control. This value could be

affected by tissue processing and staining as well, but it is reasonable to be assumed constant over the entire time course with standardized tissue processing and staining protocol.

To compare performance of the automatic algorithm to that of traditional scoring method, a reported semi-quantitative grading system was applied to the same set of images for evaluation of immune cell infiltration (Cargnoni et al., 2009). The quantification result was able to clearly reveal the differences among remote time points and reflected the trend of tissue damage and repair; however, relatively subtle differences between day 13 to day 19 cannot be resolved (Figure 26B).

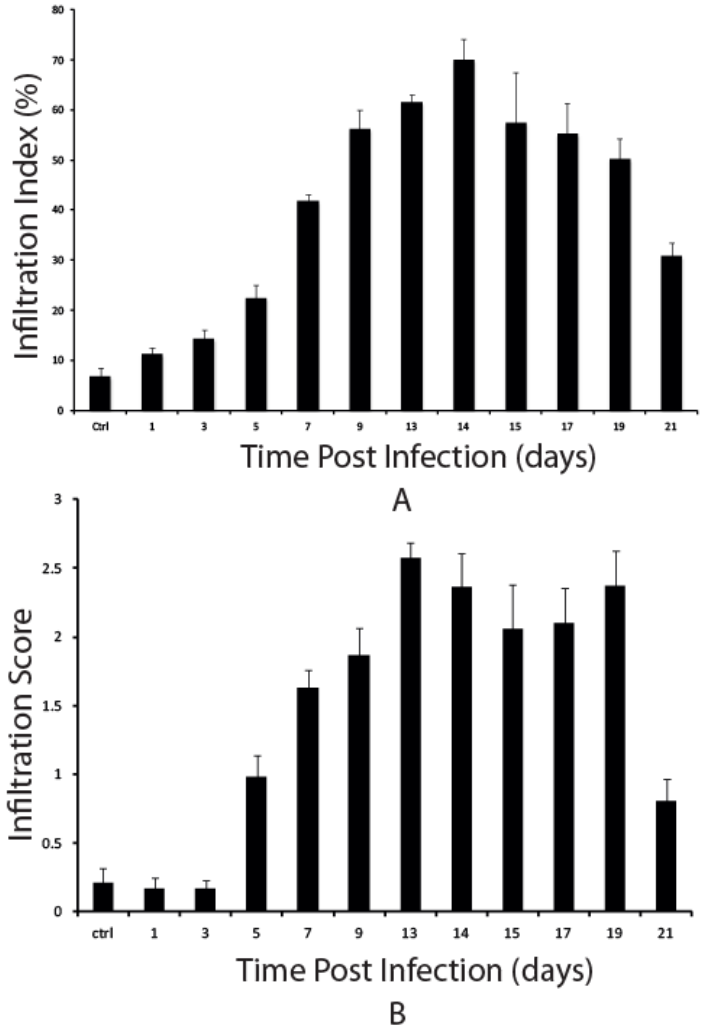

Figure 26. Quantification of lung damage and repair based on infiltration of immune cells (A) Infiltration index calculated at corresponding time points post infection using automatic algorithm. (B) Infiltration score (means ± S.E) estimated at corresponding time points post infection using classic semi-quantitative grading system.

3.4.2 Damage and repair of lung bronchiolar and alveolar epithelium

H1N1 type of influenza preferentially targets Clara cells in the bronchiolar epithelium and AT2s in the alveolar epithelium (van Riel et al., 2007). Known as lung progenitors, Clara cell and AT2 not only are capable of differentiating into other lung cell types in response to injury, but also possess important function of secreting surfactant proteins.

Therefore, it is reasonable to consider that the loss and recovery of Clara cell and AT2 represent the damage and repair of lung bronchiolar and alveolar epithelium respectively.

In healthy lung, AT2 are abundant in the alveolar region; and Clara cells cover all the bronchioles. Gradual losses of both cell types were observed post infection. Lose of Clara cell were most obvious on day 5 when they sloughed off from bronchioles. Large areas depleted with AT2 appeared on day 7, but high density of AT2s was found in some areas around bronchioles. SBECs appeared in bronchioles on day 7 and significantly increased by day 14. As the lung was almost repaired by day 21, although still small amount of SBECs could be observed, most of the bronchioles were covered by $CCSP^{+}$ cells only (Figure 27).

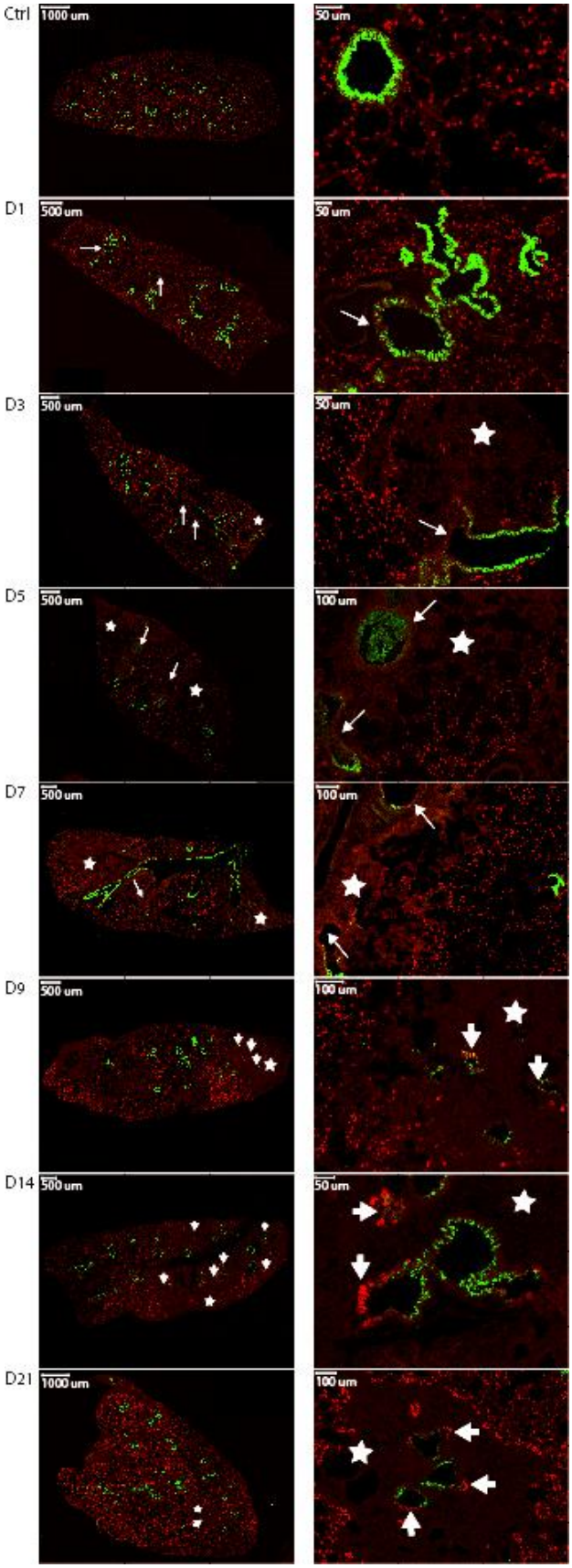

Figure 27. Response of lung progenitor cells post influenza infection Clara cell were stained in green colour and AT2s were stained in red colour.

We developed computational algorithms to quantify the loss and recovery of Clara cell and AT2s post infection with immune-fluorescence stained lung section images. Bronchioles were automatically identified in the images, and the coverage of Clara cell was computed for each bronchiole (Figure 25A-25D). Clara cell coverage index was defined as the ratio of frequency of high coverage bronchioles to low coverage bronchioles in each lung sections, and computed over the course of infection (Figure 28A). The result showed a gradual increase of bronchiolar damage till day 5 post infection, and the damage was repaired by day 14. AT2s were segmented with SPC staining and distinguished from SBECs by firstly identifying the healthy and damaged areas of the lung. Relative density of AT2 was calculated as the number of AT2s per unit tissue section area (Figure 28B). The result indicated that the most severe alveolar damage was around 7 days post infection and substantial recovery was completed by day 21.

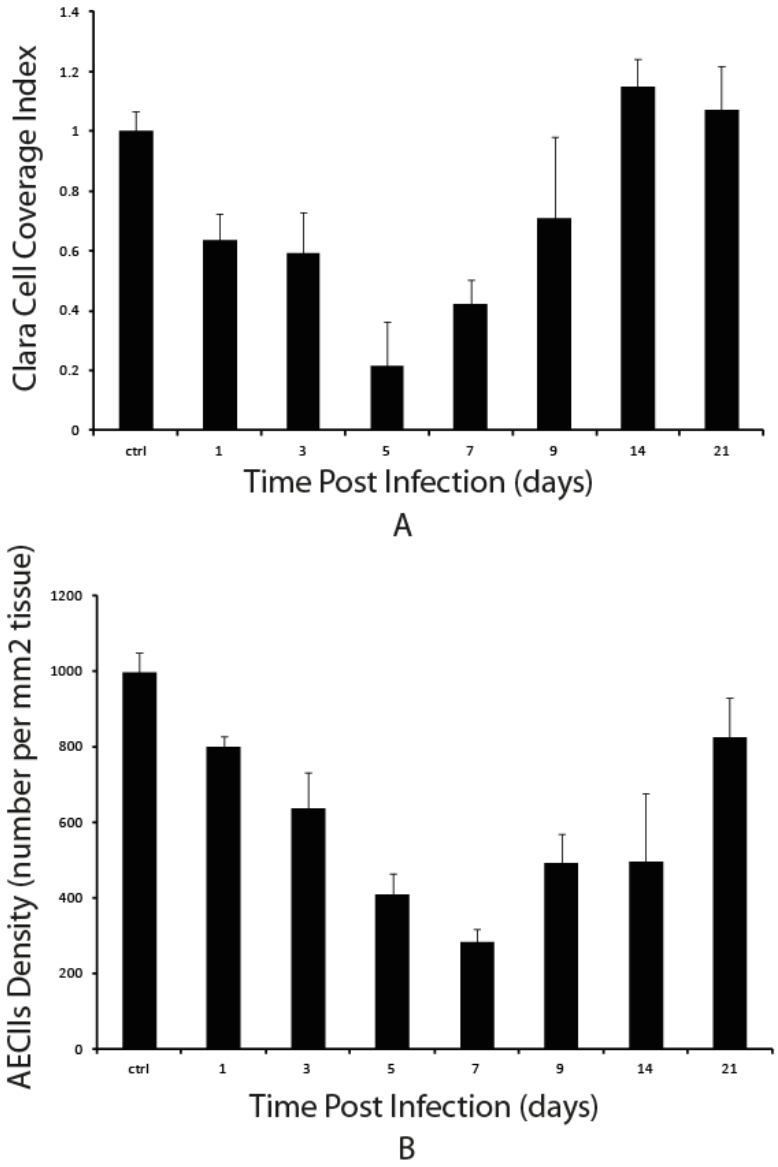

Figure 28. Quantification of Clara cell and AT2 response post infection (A) Clara cell coverage index (means ± S.E.) over time course of infection (B) AT2 density (means ± S.E.) over time course of infection.

Considerable amount of the terminal bronchioles exist in images of large lung tissue section area, which turned into the major difficulty in quantifying Clara cell coverage. The described algorithm identified all bronchioles as closed structures, based on which the ratio of Clara cell coverage was computed, and Clara cell coverage index was computed as described to estimate the damage and repair of bronchiolar

epithelium. Inaccuracy of the algorithm was mainly caused by mistakenly identifying alveolar structures as bronchioles in cases where open terminal bronchioles were connecting to alveoli. This issue could be overcome by segmenting Clara cells in terminal bronchioles from connecting alveolar structures based on their differences in nuclei morphology. Sophisticated algorithms extracting morphological features for training might possibly achieve this with satisfactory accuracy (Al-Kofahi et al., 2010; Ali et al., 2011; Cheng and Rajapakse, 2009; Jung and Kim, 2010; Jung et al., 2010), but the complexity of such algorithms would render them highly computationally expensive and impractical in this study, considering the size and requirement on resolution of the whole-slide images.

Both AT2s and SBECs expressed SPC. In the described algorithm, AT2s and SBECs were separated by defining SPC expressing cells in healthy area as AT2s and those in bronchioles of damaged areas as SBECs. SPC expressing cells in damaged alveolar areas forming ring structures reported previously was considered as newly generated AT2s instead of Clara cells in this study, due to their lack of bronchiolar cell morphology.

3.4.3 Quantitative analysis reveals new evidence in support of Clara cell to AT2 transition in lung repair

The responses of progenitor cells and immune response over time post infection were normalized to the same scale between 0 to 1 with the assumption of normal distribution. Systematic analysis on different responses revealed insights on dynamic

progression of lung tissue repair. Both initiation and completion of Clara cell recovery happened earlier than those of AT2s (Fig 17A) and previous studies reported much higher proliferation rate in Clara cell than AT2s during repair of influenza induced lung damage, which enhanced the possibility of transition from Clara cell to AT2s during lung repair. It was also worth noticing that the cellular repair process took place simultaneously with vigorous immune responses (Figure 29A). Automatic algorithm was developed for quantifying the occurrence frequencies of $CCSP^{+}SPC^{+}$ and $CCSP^{+}SPC^{-}$ SBECs with immuno-fluorescent images (Figure 29B). The results showed that $CCSP^{+}SPC^{+}$ SBECs first appeared by day 7, peaked around day 14 and an apparent decrease occurred by day 21 post infection. $CCSP^{+}SPC^{-}$ SBECs were observed at later time points than $CCSP^{+}SPC^{+}$ SBECs and experienced similar dynamic profile, which strongly implied that the direction of differentiation was from Clara cells to AT2s. Together, all these evidences led to the repair mechanism that bronchiolar Clara cell undergoes proliferation and trans-differentiate into AT2s to restore the alveolar structure after influenza induced lung damage.

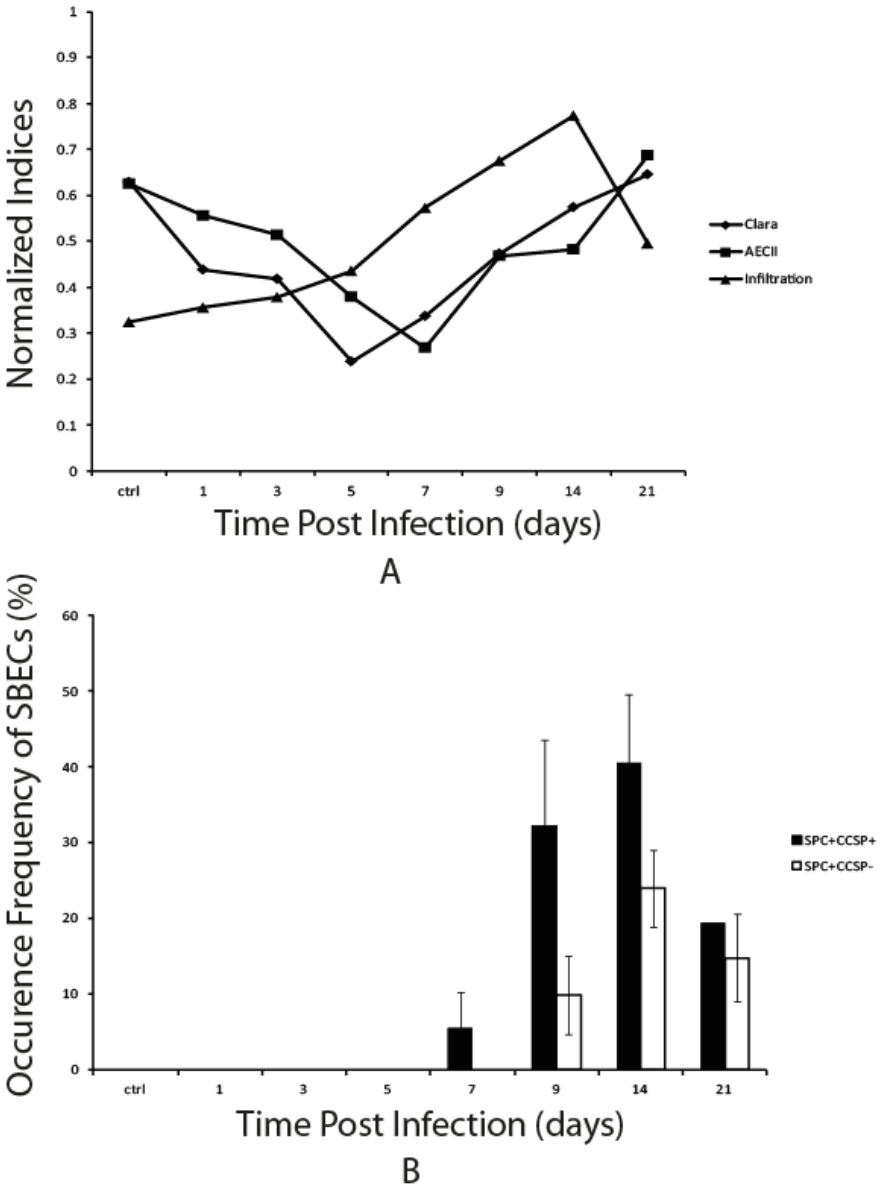

Figure 29. Systematic analysis on progenitor cell responses (A) Normalized responses of Clara cell (round dot), AT2 (square dot) and infiltrated immune cells (triangular dot). (B) Responses of single (white column) and double (black column) positive statuses of SBECs (means ± S.E.).

3.4.4 Features and applications of quantification methods

The quantification methods we developed for lung injury model in this study used images acquired with slide scanner. Large scanning area acquired by slide scanner of the entire transverse tissue cross-section with adequate image resolution enabled us to

acquire significant amount of information on the overall circumstance in the lung with described image analysis algorithms. Information over entire tissue cross-sections allowed us to investigate spatial-related features. Two phases of SBECs could be accurately traced and quantified in bronchioles in damaged areas. To obtain the same information with confocal microscopy would be impractical because substantial manual allocation of features is required. Quantification methods described in this study adequately took advantage of the high-throughput characteristic of images acquired from slide scanner, extracted specific features with fast speed, and were designed for tissue informatics study.

In this study, we analyzed the images by extracting specific features such as nucleus density and spatial distribution of molecular markers. Same features could be used in other lung injury models for evaluation of lung damage and repair with minor modifications of the existing methods. In addition to common advantages that automatic computational quantification acquires, such us accuracy, consistency, and time consumption, another distinct superiority of our quantification method for histology was its ability to give continuous assessments instead of discrete stages which traditional histology analysis normally achieved. As a result, small intra-stage difference could be distinguished, which implies its potential and validity to be applied to studies where relatively subtle differences are needed to be compared.

3.5 Conclusions

We established influenza-infected lung model to study the repair of lung tissue

following injury. Automatic computational algorithms were developed to quantify the extent of lung damage and repair at tissue and cellular levels. The algorithms were based on analysis of H&E and immuno-fluorescent images of the entire animal lung lobe sections. Comprehensive image analysis on overall responses of the animal lung over time post infection revealed the dynamic progression of immune responses and progenitor cell responses. This quantitative study provided evidences to the potential lung repair process in which bronchiolar Clara cell differentiate into AT2s to restore alveolar structure. The quantification methods we described greatly reduced the artificial variations that traditional microscopy-based histology analysis bear; and significantly ameliorated sensitivity and time consumption. The methods were not limited to this study, but could potentially be applied to other related lung injury models.

CHAPTER 4 – CHARACTERIZATION OF THE EFFECT OF AGING ON LUNG REPAIR FOLLOWING INFLUENZA-INDUCED LUNG INJURY

4.1 Summary

Aging is known to make lung susceptible to infection and suffer lingering injury. Studies have characterized the negative effect of aging on activation of immune system during influenza infection; however, little is reported on the delayed repair of damaged lung tissue post infection in the elderly. We utilized imaging-based quantitative analysis to compare the response of multiple lung epithelial progenitor cells to influenza infection in adult and aged mice. We characterized the impaired repair of alveoli but not bronchioles in aged group, and observed lower frequency of SBECs over prolonged period of time in damaged parenchyma. Together, these evidences implied degenerative capacity of Clara to AT2 transition in the elderly being a non-negligible cause of slow recovery of lung tissue from influenza infection.

4.2 Introduction

Influenza infection harms 5-10% of human population globally and causes approximately 500000 death annually. Children, pregnant women, the elderly (>65 years), and people with chronic respiratory diseases are the most susceptible populations (Russell et al., 2008; Stohr, 2002). The speedy pace of improvements made in medicine and health care have resulted in dramatic growth of the world senior population in recent decades. Studies have attempted to interpret the high

morbidity and mortality rate in the elderly when infected by influenza virus. Clinically, impairment of immune response activation and degradation in maintenance of immune memory have been observed in senescent immune system (Bender et al., 1991; Bender et al., 1995). Cell mediated immune responses to vaccinations were reduced in elderly group (Powers and Belshe, 1993; Simonsen et al., 2007).

Influenza-infected mice models have been widely used to further investigate the compromised immune systems in aged population for their high resemblance with human situation. In these systems, delayed viral clearance was observed as well as decreased T cell response (Dong et al., 2000; Murasko and Jiang, 2005). The delayed activation of adaptive immunity were likely to be caused by alterations in antigen presenting cell (APC) priming and activation, which lead to delayed production of cytokines and chemokines (Toapanta and Ross, 2009).

Alterations in immunity could be one critical cause which prevents the elderly from recovery following influenza infection. However, our previous work indicated that cellular repair in the lung happened simultaneously with immune responses (Chapter 3.4.3), suggesting another important factor for lung tissue regeneration in the elderly. With alternative injury models, studies have showed difference in DNA damage between adult and aged animal groups (Hudson et al., 2011; Lopez-Diazguerrero et al., 2005; Wang and Wang, 2012). Since DNA damage could be induced by the oxidative stress during influenza infection (Aldridge et al., 2009; Oda et al., 1989), the function of progenitor or stem cells in regeneration of lung tissue could be impaired.

Senescence-related changes of bone marrow-derived mesenchymal stem cell were reported to be responsible for the higher susceptibility of lung fibrosis in the elderly (Mora and Rojas, 2008) . BrdU-induced Clara cell senescence could result in impaired epithelial regeneration (Zhou et al., 2011).

With the imaging-based quantification algorithms developed in previous study, we compared the severity of lung tissue damage, as well as Clara cells, AT2s and SBECs responses to influenza infection between adult and aged animal groups at high accuracy over the time course of lung repair. The alterations in regeneration of bronchiolar and alveolar epithelium were characterized and degenerative capacity for Clara cell to trans-differentiate into AT2 was observed in the elderly. The result also highlighted Clara cell to AT2 transition being a critical cellular mechanism in regeneration of lung tissue following influenza infection.

4.3 Method

4.3.1 Animal and tissue sample preparation

8-12 weeks old and 8-10 months old female special pathogen free C57/BL6 mice were purchased from Centre for Animal Resources of Singapore and housed in BSL2 facilities at Center for Life Science of National University of Singapore (NUS). The 8-12 weeks old mice were directly infected as adult group, 8-10 months old mice were grow to 16-18 months old before infection as aged group. All animal-related protocols were approved by the NUS Institutional Animal Care and Use Committee.

Each mouse was infected with sub-lethal dose of 30 PFU influenza virus A/Puerto Rico/8/34 (H1N1) by intratracheal instillation after anesthetization with Ketamine (100mg/kg body weight). Five mice were randomly grouped and sacrificed before infection (control) and at 3, 6, 9, 12, 15, 18, 21 days post infection. Right lung bronchioalveolar lavage fluid was taken with 1ml PBS for 2 times following tracheotomy while the left lung was prevented from flush by placing haemostat at bifurcation point. The lavage fluid was centrifuged (Thermo Scientifc HERAEUS Pico 17) at $5000min^{-1}$ for 5mins for cells. Red blood cells were removed by resuspending the pellets in 200µl ACK lysing buffer (GIBCO A10492) for 90s. The remaining cells were washed 3 times before counting number with hemocytometer using standard protocol. Left lung tissues were collected and fixed in 10% neutral buffered formalin solution (Sigma) overnight. The tissues were then processed with Tissue Processor (Leica) and embedded in paraffin blocks. 5µm tissue transverse sections of mice left lung lobe were cut with microtome (Leica RM2165) and mounted on polylysine coated slides (Thermal Scientific). For each animal lung, 10 transverse sections in middle depth were cut with a distance of 50µm between each other for H&E and immuno- fluorescent staining respectively.

4.3.2 Histological staining

Paraffin sections were de-waxed in Xylene solutions 2 times (Sigma 534056-4L) and rehydrated in absolute ethanol 2 times, 90% ethanol and 70% ethanol 1 time each for 1 minute. H&E staining was processed according to standard protocol. For

immune-fluorescent staining, antigen retrieval was performed by incubating the tissue section with proteinase K solution (Sigma, 20mg/ml, in 50mMTris-Cl,1mM EDTA, pH 8.0) at 37^{o}C for 30 min. Sections were then blocked in blocking buffer (3% BSA, 0.2% Triton X-100 in PBS) for 1h. Primary antibody polyclonal Rabbit anti CCSP antibody (USbiology, C5828) was used in 1:100 dilution, and goat anti SPC (Santa Cruz sc-7706) were used in 1:100 dilution. Incubation was performed at 4^{o}C overnight in blocking buffer. Secondary Donkey anti rabbit Alexa Fluor 488 (Invitrogen, A21206) and donkey anti goat Alexa Fluor 546 (Invitrogen, A11056) were used in 1:100 dilution. Incubation was performed at 4^{o}C for 1h. Cover slips were mounted to stained tissue section slides with antifade reagent containing DAPI (Invitrogen S36939).

4.3.3 Image acquisition, processing and quantification

All images were acquired with the same slide scanner and camera used in previous study. All image processing and quantification of Clara cell, AT2, SBECs followed the same algorithm developed in previous study (Chapter 3.3.5).

4.4 Results and Discussion

4.4.1 Aging leads to more severe illness post influenza infection

To examine the difference between aged and adult groups in response to influenza infection, change in body weight and survival rate were monitored at multiple time points over the course of infection and recovery (Figure 30). The adult group showed

maximum ~25% loss in body weight at 9 dpi and complete recovery was observed at 21 dpi, while the aged group experienced progressive body weight loss till 21 dpi with peak of ~35%, and no clear trend of recovery was observed (Figure 30A). The sublethal influenza infection for the adult group caused death from 12 dpi in the aged group, and the death rate reached maximum of ~40% at 21 dpi (Figure 30B).

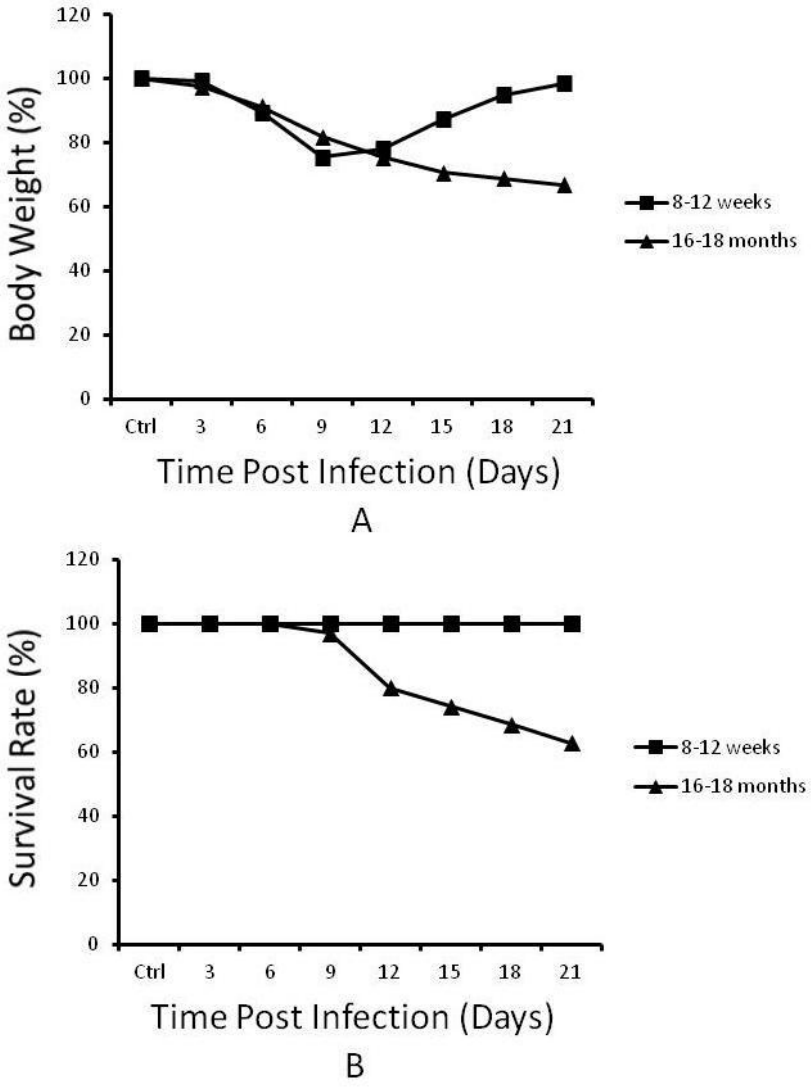

Figure 30. Aged mice experience more severe disease post influenza infection (A) Body weight change post influenza infection in adult (square dot) and aged group (triangular dot). (B) Survival in adult (square dot) and aged (triangular dot) group post influenza infection. (Percentages calculated as the average at each time points over average before infection.)

The results showed that a significantly more sever disease was caused by influenza infection in aged mice compared to adult. The severity was displayed in both the extent and time duration of body weight loss. No apparent trend of recovery in body weight till 21 dpi in the aged group suggested that the infection could probably cause long term damage in the elderly.

4.4.2 Aging leads to prolonged immune cell infiltration in the lung post influenza infection

Immune cell infiltration was quantitatively accessed in adult and aged groups using previously developed imaging-based quantification algorithm (chapter 3.3.5.1), to compare the general immune response and lung injury (Figure 31A). The adult group showed maximum infiltration of immune cells over 75% of alveolar region at 12 dpi, followed by fast regression, and more than 80% of the alveolar region was cleared of infiltration at 21 dpi (Figure 31A). The aged group exhibited ~80% infiltration in alveolar area at 12 dpi, and the number increased to ~85% at 15 dpi. A slower regression of infiltration was observed afterwards, and a considerable level of ~35% infiltration could still be detected at 21 dpi (Figure 31A).

General infiltration of immune cells was also assayed by counting the cell numbers in the BALF after removal of red blood cells (RBC) over the time course of infection (Figure 31B). Peak of BALF cell count in both groups reached maximum at 12 dpi with the aged group showing a slightly higher number, but the cell count persist high through 15 to 18 dpi in the aged group, while in the adult group a fast reduction was

detected (Figure 31B). At 28 dpi, cell count in the BALF in adult group recovered to the level before infection (data not shown).

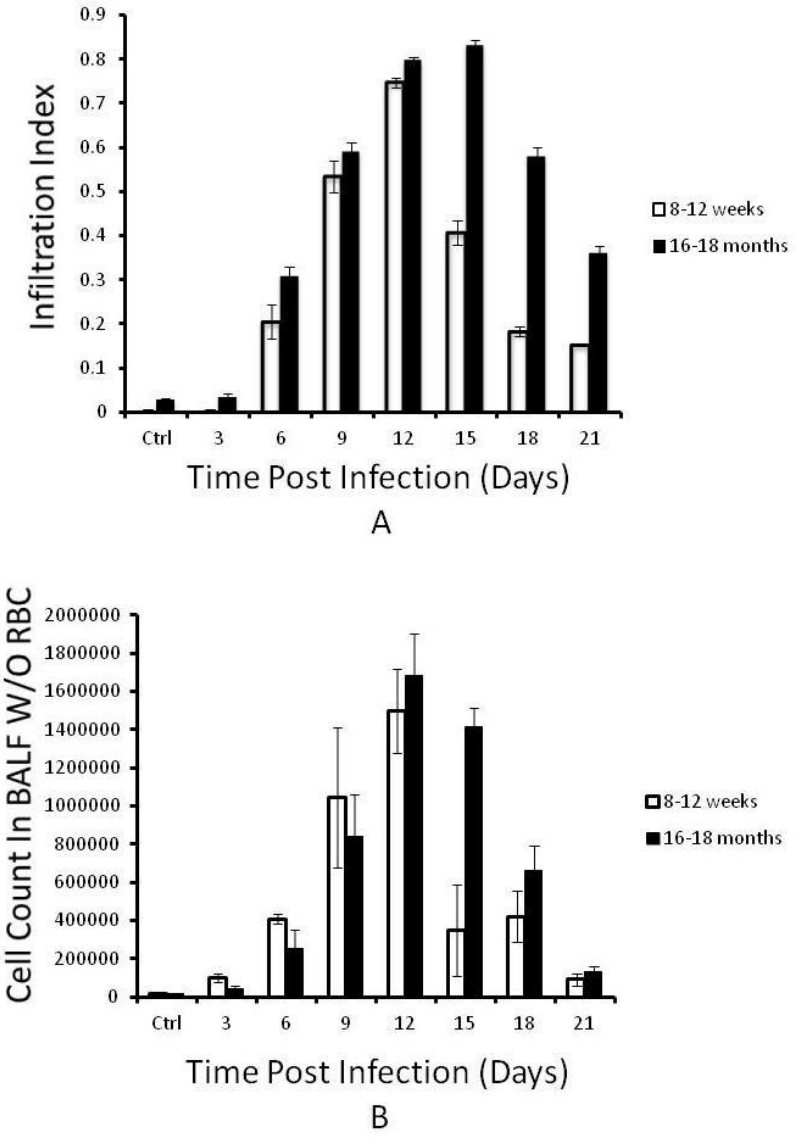

Figure 31. Prolonged immune response in aged mice experience post influenza infection (A) Infiltration Index (means ± S.E.) in adult (white column) and aged (black column) mice over time course of infection. (B) Cell count (means ± S.E.) in BALF in adult (white column) and aged (black column) mice over time course of infection (after removal of RBC).

The Infiltration Index calculated was based on the amount of immune cells retained in the alveolar region after formalin fixation, tissue processing and reflected in the H&E

stained image. BALF cell count measured the number of cells that were flushed out from the lung, among which majority were immune cells after removal of RBC. Both methods could give reasonable estimation on the level of immune cell infiltration; although the targets that each method measured were not completely identical, the trend obtained with both methods displayed reasonable consistency, which further verified each other.

The peak of immune cell infiltration estimated with both methods showed insignificant difference between adult and aged mice. BALF cell count showed a sequential difference in commence of immune cell accumulation in the lung between the groups through 3-6 dpi, which was consistent with previous report (Toapanta and Ross, 2009). The difference was not resolved by the imaging-based quantification, suggesting its limitations in identifying innate immune cells within the first week of influenza infection. Nevertheless, both methods clearly demonstrated that the aged group experienced prolonged immune response, which was consistent with the reported delay in activation of adaptive immunity (Dong et al., 2000; Murasko and Jiang, 2005; Toapanta and Ross, 2009).

4.4.3 Effect of aging on repair of bronchiolar and alveolar epithelium post influenza infection

To compare the damage and repair of bronchiolar and alveolar epithelium in adult and aged mice, imaging-based quantification methods developed previously for computing Clara cell Coverage Index (chapter 3.3.5.2) and relative AT2 cell density

(chapter 3.3.5.3) were applied to quantitatively compare the response of Clara cell and AT2 (Figure 32). Maximum Clara cell damage was observed at 6 dpi in both adult and aged group with the aged group showing a slightly more severe injury, and complete recovery was reached at 15 dpi (Figure 32A). No significant difference was detected in repair of bronchiolar epithelium (Figure 32A). Maximum damage of alveolar epithelium was observed at 9 dpi with ~50% drop in AT2 density, and repair was completed at 21 dpi in adult group. However, extensive loss of AT2 in alveolar epithelium progressed till 15 dpi in the aged group followed by a slow recovery (Figure 32B). The density of AT2 persisted at low level of ~40% of normal situation till 21 dpi (Figure 32B). The delayed repair in alveolar epithelium in aged group was consistent with compromised ability in clearance of virus (Dong et al., 2000; Murasko and Jiang, 2005) and prolonged immune response (Figure 31). It also partly verified our previous finding that repair of alveolar epithelium tended to complete after immune response regressed (Figure 29A).

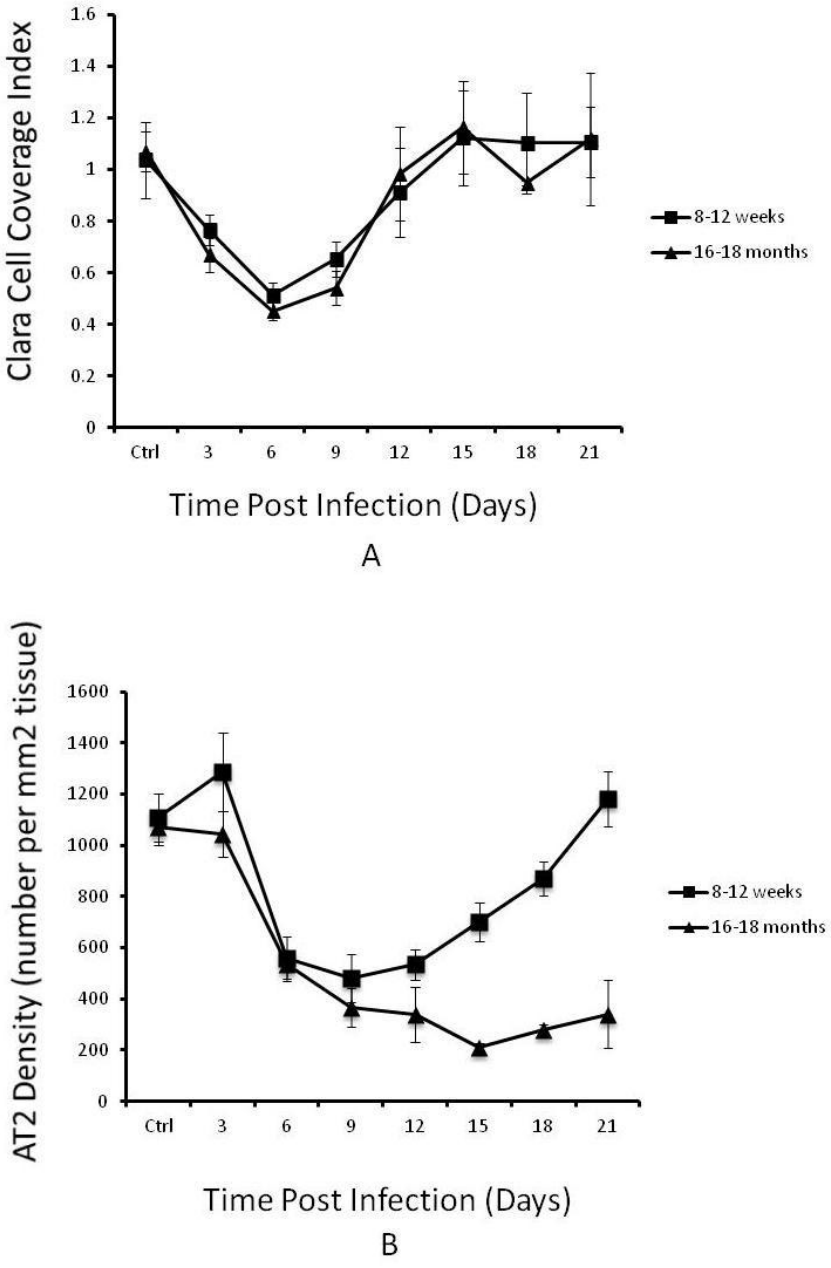

Figure 32. Repair of bronchiolar and alveolar epithelium in adult and aged mice (A) Clara Cell Coverage Index (means ± S.E.) in adult (square dot) and aged (triangular dot) mice over time course of infection. (B) Relative AT2 Density (means ± S.E.) in adult (square dot) and aged (triangular dot) mice over time course of infection.

Previous reports explored two possible cellular mechanisms for repair of bronchiolar epithelium. Clara cell has self-renewal capacity in response to bronchiolar damage (Hong et al., 2001; Rawlins et al., 2009a), and Clara^{v} is able to give rise to other Clara

cell in response to naphthalene-induced injury (Giangreco et al., 2002; Hong et al., 2001; Reynolds et al., 2000). Both mechanisms imply that in the case of influenza infection, it was the remaining Clara cell that proliferated to regenerate the damaged bronchiolar epithelium. Our result showed that the repair of bronchiolar epithelium was not significantly affected by aging, suggesting that the proliferation capacity of Clara cell (Figure 4F) in response to influenza infection was not influenced much by aging; as a result, the total amount of Clara cell at any time during this process was similar in both groups.

Since 1970s, common understanding on repair of alveolar epithelium believes that AT2 could renew itself and give rise to AT1 to repair alveolar damage; this conclusion was mainly derived from microscopy-based imaging (Adamson, 1976; Aso et al., 1976). This concept was recently challenged by a study performing genetic tracing, which revealed that the regenerated AT2s are not from the pre-existing AT2s (Chapman et al., 2011). The possibility that bronchiolar cells give rise to alveolar cells was raised in early study, but was not widely accepted (Aso et al., 1976). Our previous study supported this notion, and investigated in detail the capacity for Clara cell to become AT2 in repair of alveolar epithelium (chapter 2). Relating this cellular mechanism to the impaired repair of alveolar epithelium post influenza infection observed in aged mice, we infer that the differentiation capacity of Clara cell in aged mice was weakened since the total amount of Clara cell did not suffer significant reduction.

4.4.4 Aging diminishes the frequency and extends the duration of SBEC occurrence post influenza infection

We previous showed that repair of alveolar epithelium structure in response to severe injury involves Clara cell to AT2 trans-differentiation through SBECs (Figure 23). To verify whether this differentiation process was affected by aging, the occurrence frequency of SBECs were compared between adult and aged mice using the developed imaging-based quantification method (chapter 3.3.5.4). In both groups, SBECs appeared at 6 dpi (Figure 33A). The frequency in the adult group increased rapidly to peak at 12 dpi with ~35% of total bronchioles containing SBECs; while in the aged group, maximum frequency appeared later at 15 dpi with only ~28% of total bronchioles containing SBECs (Figure 33A). After peak, the adult group showed a fast decay in SBEC frequency, and SBEC-containing bronchioles was less than 5% of total by 21 dpi; while SBEC frequency in aged group experienced a slow decay, more than 10% of bronchioles could still be detected to contain SBECs by 21 dpi (Figure 33A).

The frequencies of SPC^+CCSP^+ and SPC^+CCSP^- SBECs were quantified respectively to compare the kinetics in adult and aged group. In both groups, The SPC^+CCSP^+ SBECs started to appear at 6 dpi, and SPC^+CCSP^- SBECs first appeared at 9 dpi (Figure 33). Frequencies of both phases of SBECs in the adult group reached maximum at 12 dpi with ~20% of total bronchioles containing double positive phase and ~27% containing single positive phase (Figure 33). While in the aged group, the

frequency of $SPC^{+}CCSP^{+}$ SBECs was peaked at 12 dpi at ~17%, and the maximum frequency of $SPC^{+}CCSP^{-}$ SBECs was appeared at 15 dpi at ~25% (Figure 33). Both phases of SBECs decreased fast in the adult group after peak; at 21 dpi, less than 5% of the bronchioles still contained single positive phase of SBECs, and double positive SBECs were almost non-detectable (Figure 33). In the aged group, the high frequency of double positive SBECs persisted till 15 dpi followed by a fast drop, however, the frequency of single positive SBECs experienced a slow regression after peak; they could still be observed in more than 10% of total bronchioles at 21 dpi (Figure 33).

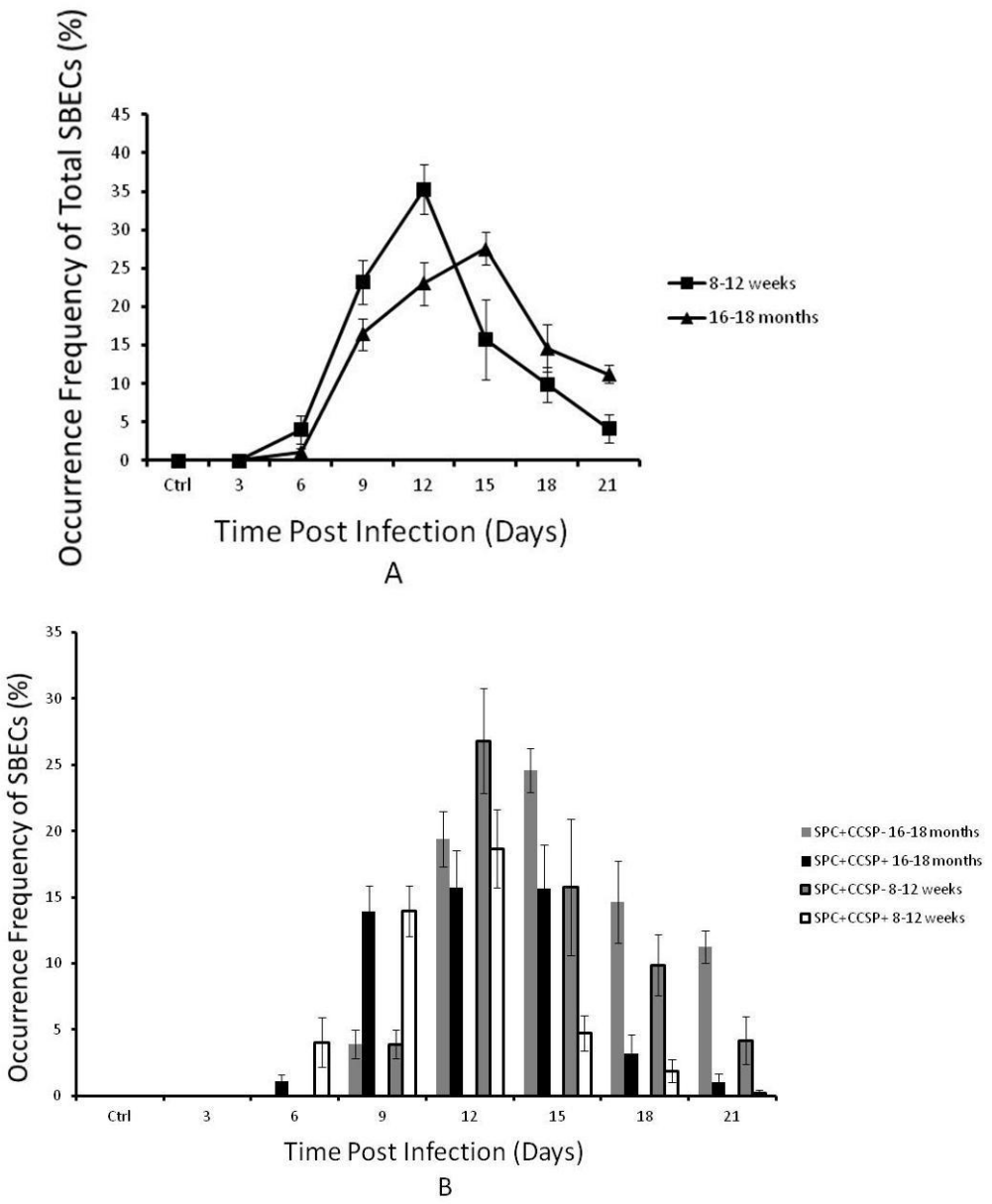

Figure 33. Frequency of SBECs induction in adult and aged mice (A) The occurrence frequency of total SBECs (means ± S.E.) in adult (square dot) and aged (triangular dot) mice over time course of infection (B)The occurrence frequency (means ± S.E.) of single (gray column with black boarder) and double (white column) positive SBECs in adult mice, and the occurrence frequency (means ± S.E.) of single (gray column without boarder) and double (black column) positive SBECs in aged mice over time course of influenza infection are shown.

The frequency of SBECs in both adult and aged groups gradually reduced (Figure 33A and 33B) while recovery from infection (Figure 31A), showing close correlation with the repair of AT2s (Figure 32B). Lower frequency of total SBECs at peak were

detected in the aged group, demonstrating the compromised capacity for Clara cell to differentiate into SBEC (Figure 33A). The duration of SBEC appearance tended to last longer (Figure 33A), especially for the $CCSP^-$ stage (Figure 33B), implying that $CCSP^-$ SBECs to AT2 transition were interrupted in aged group.

4.5 Conclusion

Comparative study was performed to characterize the alterations in lung repair post influenza infection in adult and aged mice. We utilized imaging-based quantification methods developed in previous study (chapter 3) to trace the immune response, damage and repair of bronchiolar and alveolar epithelium, as well as the induction of SBECs over the time course of influenza infection and recovery in adult and aged mice. The impaired immunity leading to a delayed repair of alveolar epithelium in the elderly was quantitatively documented. It was interesting to observe that aging has less effect on repair of bronchiolar epithelium than alveolar epithelium, implying that the proliferation capacity of Clara cell is maintained to considerable extent in the elderly. However, maximum induction of SBECs was observed lower in aged mice than adult mice, and the appearance period of SBECs last longer, indicating that the differentiation capacity of Clara cell is decayed in the elderly. The tight correlation discovered between impaired repair of alveolar epithelium and altered ability of SBEC induction demonstrated Clara cell to AT2 trans-differentiation being a critical mechanism for alveolar regeneration.

CHAPTER 5 - CONCLUSION AND FUTURE PERSPECTIVE

To study the role of lung progenitor and stem cell in repairing the lung, we established an influenza virus-induced recoverable model by infecting groups of mice with sub-lethal dose of influenza virus. The animals were sacrificed at multiple time points over the course of infection and recovery for comprehensive immunohistochemistry analysis (Figure 2, 3 and 4). The dynamics of multiple types of cells in the lung are quantified with automated image analysis algorithms that we developed (Figure 28).

The breakthrough observation was the induction of a novel cell type named SBECs in bronchioles in damage parenchyma post influenza infection (Figure 5). SBECs shared similar cytomorgphology of Clara cell, but express AT2 specific marker SPC, leading us to hypothesize that there was a trans-differentiation between Clara cell and AT2 in lung repair, with SBEC being the intermediate status. With imaging-based quantification (Figure 28 and 29) and observations from chemical challenge study (Figure 6 and 9), we believed the trans-differentiation was from Clara cell to AT2, and this conclusion was further demonstrated by genetic tracing using transgenic mice (Figure 10, 13 and 15). In another experiment when we utilized the imaging-based quantification tools to compare the lung repair between adult and aged mice, clear delay of repair was observed in alveoli, but not bronchioles in the elderly (Figure 32), together with lower frequency of SBECs over prolonged period of time (Figure 33), suggesting the inability for Clara cell to trans-differentiate into AT2 being a non-negligible cause of slow repair.

Another interesting phenomenon was the appearance of p63+ cell forming lumen-like structures in damaged parenchyma (Figure 19). p63 is a common stem cell marker, and in healthy lung it is specific to basal cell in the bronchiolar epithelium, which is known to be the ancestor of Clara cell. However, the p63+ lumen-like structures in damaged parenchyma also expressed Clara cell marker CYP450 (Figure 20), and can also be genetically traced back to the pre-existing Clara cells (Figure 22), implying that they are the regenerated bronchioles in damaged parenchyma.

In conclusion, influenza virus cause part of the lung damaged. In mildly damaged areas where only bronchioles were injured, the remaining Clara cells is known to repair the damaged bronchiolar epithelium (Hong et al., 2001; Rawlins et al., 2009a). In severely damaged areas where both bronchioles and alveoli were massively destroyed, two lung repair mechanisms were explored in this thesis. The restoration of alveolar structures involves Clara cell to AT2 trans-differentiation, and this process highly mimics embryo lung development (Figure 18). The restoration of bronchiolar structures possibly involves the differentiation of Clara cells to p63+ embryonic progenitor cells (Figure 21). Both cellular mechanisms were also demonstrated in bleomycin-induced injury model (Figure 12. 14. 17 and 19), making us believe that they would be activated by common alveolar injury. It is surprising to realize that Clara cells play all kinds of critical roles in lung regeneration post injury; we believe it might be the most crucial cell type in the lung whose function in lung repair has been underestimated over decades.

In next step of this study, two key issues need to be addressed. First, our study does not exclude the possibility of other parallel lung repair mechanisms. The contribution of the lung repair mechanisms initiated by Clara cell to total lung repair cannot be straightly calculated. However, with proper assumptions, this could be estimated with imaging-based quantification methods in *CCSP-CreER:ACTB-mT-EGFP* transgenic system by analyzing the correlation between maximum damaged area of lung parenchyma and the repaired area containing $EGFP^+$ regenerated AT2s. Second, our study has indisputably demonstrated Clara cell being the ancestor of SBEC, regenerated AT2 and AT1 in repair of lung alveolar damage by genetic tracing; however, the complicated cellular pathway of SBECs-AT2-AT1 differentiation was barely deduced from quantitative correlation analysis and evidence from embryonic lung study. To confirmatively verify this, lineage tracing on SBECs is required; however, it is complicated by the fact that SBEC is an induced transient cell type and it is so far lack of specific cellular marker. Another approach is to specifically deplete SBECs, and observe the condition of alveolar repair. This might be achieved by treating specific chemicals or inducing apoptosis. Both methods would require more understanding on metabolism and protein composition of SBECs.

In future studies, two important directions are worthwhile to pursue. First, with understanding of Clara's versatility in lung repair, it is significant to isolate and culture them for in vitro differentiation study and cell transplantation therapy. Isolation of Clara cell has encountered difficulties in purity and efficiency mainly due to lack of specific surface marker (Belinsky et al., 1995; Martin et al., 1993; Martin et al., 1990;

Oreffo et al., 1990); and no studies have reported successful long term culture of Clara cell while maintaining their function as progenitor cell. Clara cell transplantation would require identification of specific Clara cell surface marker for isolation by flow cytometry, and probably scaffold made of biocompatible materials to facilitate engraftment in the bronchiolar epithelium, since transplantation assays using cells from other sources showed poor engraftment rate in lung (Gupta et al., 2007; Kotton et al., 2001; Krause et al., 2001; Ortiz et al., 2003; Rojas et al., 2005). Second is to further investigate the underlying molecular mechanisms of the lung repair process, so that the explored cellular pathways can be intervened to examine their significance. Also, understanding of the underlying molecular mechanisms would guide therapeutic interventions in future. Research on molecular aspect of this study would require microarray, bioinformatics, pathway analysis and possibly knock-out mice. Considering the difficulties in isolation and culture of individual progenitor cell types, laser capture microdiscection might be used to isolate Clara, SBECS and AT2 based on both location and cell marker; and extract mRNA from each type of cells for characterization and bioinformatics and pathway analysis (Betsuyaku and Senior, 2004). This would also aid identification of novel surface markers for individual progenitor cells, so as to benefit many of the proposed future works above.

REFERENCES

Adamson, I.Y. (1976). Pulmonary toxicity of bleomycin. Environ Health Perspect *16*, 119-126.

Adamson, I.Y., and Bowden, D.H. (1974). The type 2 cell as progenitor of alveolar epithelial regeneration. A cytodynamic study in mice after exposure to oxygen. Lab Invest *30*, 35-42.

Aguilar, S., Scotton, C.J., McNulty, K., Nye, E., Stamp, G., Laurent, G., Bonnet, D., and Janes, S.M. (2009). Bone marrow stem cells expressing keratinocyte growth factor via an inducible lentivirus protects against bleomycin-induced pulmonary fibrosis. PLoS One *4*, e8013.

Al-Kofahi, Y., Lassoued, W., Lee, W., and Roysam, B. (2010). Improved automatic detection and segmentation of cell nuclei in histopathology images. IEEE Trans Biomed Eng *57*, 841-852.

Aldridge, J.R., Jr., Moseley, C.E., Boltz, D.A., Negovetich, N.J., Reynolds, C., Franks, J., Brown, S.A., Doherty, P.C., Webster, R.G., and Thomas, P.G. (2009). TNF/iNOS-producing dendritic cells are the necessary evil of lethal influenza virus infection. Proc Natl Acad Sci U S A *106*, 5306-5311.

Ali, S., Veltri, R., Epstein, J.I., Christudass, C., and Madabhushi, A. (2011). Adaptive energy selective active contour with shape priors for nuclear segmentation and gleason grading of prostate cancer. Med Image Comput Comput Assist Interv *14*, 661-669.

Alt, J.A., Bohnet, S., Taishi, P., Duricka, D., Obal, F., Jr., Traynor, T., Majde, J.A., and Krueger, J.M. (2007). Influenza virus-induced glucocorticoid and hypothalamic and lung cytokine mRNA responses in dwarf lit/lit mice. Brain Behav Immun *21*, 60-67.

Aso, Y., Yoneda, K., and Kikkawa, Y. (1976). Morphologic and biochemical study of pulmonary changes induced by bleomycin in mice. Lab Invest *35*, 558-568.

Atzori, L., Chua, F., Dunsmore, S.E., Willis, D., Barbarisi, M., McAnulty, R.J., and Laurent, G.J. (2004). Attenuation of bleomycin induced pulmonary fibrosis in mice using the heme oxygenase inhibitor Zn-deuteroporphyrin IX-2,4-bisethylene glycol. Thorax *59*, 217-223.

Azambuja, E., Fleck, J.F., Batista, R.G., and Menna Barreto, S.S. (2005). Bleomycin lung toxicity: who are the patients with increased risk? Pulm Pharmacol Ther *18*, 363-366.

Belinsky, S.A., Lechner, J.F., and Johnson, N.F. (1995). An improved method for the isolation of type II and Clara cells from mice. In Vitro Cell Dev Biol Anim *31*, 361-366.

Bender, B.S., Johnson, M.P., and Small, P.A. (1991). Influenza in senescent mice: impaired cytotoxic T-lymphocyte activity is correlated with prolonged infection. Immunology *72*, 514-519.

Bender, B.S., Taylor, S.F., Zander, D.S., and Cottey, R. (1995). Pulmonary immune response of young and aged mice after influenza challenge. J Lab Clin Med *126*, 169-177.

Betsuyaku, T., and Senior, R.M. (2004). Laser capture microdissection and mRNA characterization of mouse airway epithelium: methodological considerations. Micron *35*, 229-234.

Bigby, T.D., Allen, D., Leslie, C.G., Henson, P.M., and Cherniack, R.M. (1985). Bleomycin-induced lung injury in the rabbit. Analysis and correlation of bronchoalveolar lavage, morphometrics, and fibroblast stimulating activity. Am Rev Respir Dis *132*, 590-595.

Borthwick, D.W., Shahbazian, M., Krantz, Q.T., Dorin, J.R., and Randell, S.H. (2001). Evidence for stem-cell niches in the tracheal epithelium. Am J Respir Cell Mol Biol *24*, 662-670.

Brady, R.C. (2010). Influenza. Adolesc Med State Art Rev *21*, 236-250, viii.

Burt, P.J. (1981). Fast Filter Transforms for Image-Processing. Comput Vision Graph *16*, 20-51.

Cargnoni, A., Gibelli, L., Tosini, A., Signoroni, P.B., Nassuato, C., Arienti, D., Lombardi, G., Albertini, A., Wengler, G.S., and Parolini, O. (2009). Transplantation of allogeneic and xenogeneic placenta-derived cells reduces bleomycin-induced lung fibrosis. Cell Transplant *18*, 405-422.

Chagnon, F., Fournier, C., Charette, P.G., Moleski, L., Payet, M.D., Dobbs, L.G., and Lesur, O. (2010). In vivo intravital endoscopic confocal fluorescence microscopy of normal and acutely injured rat lungs. Lab Invest *90*, 824-834.

Chapman, H.A., Li, X., Alexander, J.P., Brumwell, A., Lorizio, W., Tan, K., Sonnenberg, A., Wei, Y., and Vu, T.H. (2011). Integrin alpha6beta4 identifies an adult distal lung epithelial population with regenerative potential in mice. J Clin Invest *121*, 2855-2862.

Cheng, J., and Rajapakse, J.C. (2009). Segmentation of clustered nuclei with shape markers and marking function. IEEE Trans Biomed Eng *56*, 741-748.

Dong, L., Mori, I., Hossain, M.J., and Kimura, Y. (2000). The senescence-accelerated mouse shows aging-related defects in cellular but not humoral immunity against influenza virus infection. J Infect Dis *182*, 391-396.

Doyle, S.E., O'Connell, R., Vaidya, S.A., Chow, E.K., Yee, K., and Cheng, G. (2003). Toll-like receptor 3 mediates a more potent antiviral response than Toll-like receptor 4. J Immunol *170*, 3565-3571.

Dubaybo, B.A., Crowell, L.A., and Thet, L.A. (1991). Changes in tissue fibronectin in elastase induced lung injury. Cell Biol Int Rep *15*, 675-686.

Eccles, R. (2005). Understanding the symptoms of the common cold and influenza. Lancet Infect Dis *5*, 718-725.

Evans, M.J., Cabral, L.J., Stephens, R.J., and Freeman, G. (1973). Renewal of alveolar epithelium in the rat following exposure to NO2. Am J Pathol *70*, 175-198.

Evans, M.J., Cabral, L.J., Stephens, R.J., and Freeman, G. (1975). Transformation of alveolar type 2 cells to type 1 cells following exposure to NO2. Exp Mol Pathol *22*, 142-150.

French, L.E., Chonn, A., Ducrest, D., Baumann, B., Belin, D., Wohlwend, A., Kiss, J.Z., Sappino, A.P., Tschopp, J., and Schifferli, J.A. (1993). Murine clusterin: molecular cloning and mRNA localization of a gene associated with epithelial differentiation processes during embryogenesis. J Cell Biol *122*, 1119-1130.

Giangreco, A., Reynolds, S.D., and Stripp, B.R. (2002). Terminal bronchioles harbor a unique airway stem cell population that localizes to the bronchoalveolar duct junction. Am J Pathol *161*, 173-182.

Gonzalez, R.C., and Woods, R.E. (2002). Digital image processing, 2nd edn (Upper Saddle River, N.J., Prentice Hall).

Gothelf, A., Mir, L.M., and Gehl, J. (2003). Electrochemotherapy: results of cancer treatment using enhanced delivery of bleomycin by electroporation. Cancer Treat Rev *29*, 371-387.

Gupta, N., Su, X., Popov, B., Lee, J.W., Serikov, V., and Matthay, M.A. (2007). Intrapulmonary delivery of bone marrow-derived mesenchymal stem cells improves survival and attenuates endotoxin-induced acute lung injury in mice. J Immunol *179*, 1855-1863.

Hadi, A.M., Mouchaers, K.T., Schalij, I., Grunberg, K., Meijer, G.A., Vonk-Noordegraaf, A., van der Laarse, W.J., and Belien, J.A. (2010). Rapid quantification of myocardial fibrosis: A new macro-based automated analysis. Anal Cell Pathol (Amst) *33*, 257-269.

Hagood, J.S., Prabhakaran, P., Kumbla, P., Salazar, L., MacEwen, M.W., Barker, T.H., Ortiz, L.A., Schoeb, T., Siegal, G.P., Alexander, C.B., *et al.* (2005). Loss of fibroblast Thy-1 expression correlates with lung fibrogenesis. Am J Pathol *167*, 365-379.

Hoag, J.B., Liu, M., Easley, R.B., Britos-Bray, M.F., Kesari, P., Hassoun, H., Haas, M., Tuder, R.M., Rabb, H., and Simon, B.A. (2008). Effects of acid aspiration-induced acute lung injury on kidney function. Am J Physiol Renal Physiol *294*, F900-908.

Hong, K.U., Reynolds, S.D., Giangreco, A., Hurley, C.M., and Stripp, B.R. (2001). Clara cell secretory protein-expressing cells of the airway neuroepithelial body microenvironment include a label-retaining subset and are critical for epithelial renewal after progenitor cell depletion. Am J Respir Cell Mol Biol *24*, 671-681.

Hong, K.U., Reynolds, S.D., Watkins, S., Fuchs, E., and Stripp, B.R. (2004). In vivo differentiation potential of tracheal basal cells: evidence for multipotent and unipotent subpopulations. Am J Physiol Lung Cell Mol Physiol *286*, L643-649.

Huang, Y.C. (2008). Lung compliance measurement in mice. Am J Physiol Lung Cell Mol Physiol *294*, L815; author reply L816.

Hudson, D., Kovalchuk, I., Koturbash, I., Kolb, B., Martin, O.A., and Kovalchuk, O. (2011). Induction and persistence of radiation-induced DNA damage is more pronounced in young animals than in old animals. Aging (Albany NY) *3*, 609-620.

Inada, A., Nienaber, C., Katsuta, H., Fujitani, Y., Levine, J., Morita, R., Sharma, A., and Bonner-Weir, S. (2008). Carbonic anhydrase II-positive pancreatic cells are progenitors for both endocrine and exocrine pancreas after birth. Proc Natl Acad Sci U S A *105*, 19915-19919.

Isse, K., Grama, K., Abbott, I.M., Lesniak, A., Lunz, J.G., Lee, W.M., Specht, S., Corbitt, N., Mizuguchi, Y., Roysam, B., *et al.* (2010). Adding value to liver (and allograft) biopsy evaluation using a combination of multiplex quantum dot immunostaining, high-resolution whole-slide digital imaging, and automated image analysis. Clin Liver Dis *14*, 669-685.

Izbicki, G., Segel, M.J., Christensen, T.G., Conner, M.W., and Breuer, R. (2002). Time course of bleomycin-induced lung fibrosis. Int J Exp Pathol *83*, 111-119.

Jones, J.G., and McAteer, E.M. (1990). The quantitative evaluation of acute lung

injury. Clin Phys Physiol Meas *11 Suppl A*, 127-131.

Jung, C., and Kim, C. (2010). Segmenting clustered nuclei using H-minima transform-based marker extraction and contour parameterization. IEEE Trans Biomed Eng *57*, 2600-2604.

Jung, C., Kim, C., Chae, S.W., and Oh, S. (2010). Unsupervised segmentation of overlapped nuclei using Bayesian classification. IEEE Trans Biomed Eng *57*, 2825-2832.

Kajstura, J., Rota, M., Hall, S.R., Hosoda, T., D'Amario, D., Sanada, F., Zheng, H., Ogorek, B., Rondon-Clavo, C., Ferreira-Martins, J., *et al.* (2011). Evidence for human lung stem cells. N Engl J Med *364*, 1795-1806.

Kim, C.F., Jackson, E.L., Woolfenden, A.E., Lawrence, S., Babar, I., Vogel, S., Crowley, D., Bronson, R.T., and Jacks, T. (2005). Identification of bronchioalveolar stem cells in normal lung and lung cancer. Cell *121*, 823-835.

Konsti, J., Lundin, M., Joensuu, H., Lehtimaki, T., Sihto, H., Holli, K., Turpeenniemi-Hujanen, T., Kataja, V., Sailas, L., Isola, J., *et al.* (2011). Development and evaluation of a virtual microscopy application for automated assessment of Ki-67 expression in breast cancer. BMC Clin Pathol *11*, 3.

Kotton, D.N., Ma, B.Y., Cardoso, W.V., Sanderson, E.A., Summer, R.S., Williams, M.C., and Fine, A. (2001). Bone marrow-derived cells as progenitors of lung alveolar epithelium. Development *128*, 5181-5188.

Krause, D.S., Theise, N.D., Collector, M.I., Henegariu, O., Hwang, S., Gardner, R., Neutzel, S., and Sharkis, S.J. (2001). Multi-organ, multi-lineage engraftment by a single bone marrow-derived stem cell. Cell *105*, 369-377.

Kumar, P.A., Hu, Y., Yamamoto, Y., Hoe, N.B., Wei, T.S., Mu, D., Sun, Y., Joo, L.S., Dagher, R., Zielonka, E.M., *et al.* (2011). Distal airway stem cells yield alveoli in vitro and during lung regeneration following H1N1 influenza infection. Cell *147*, 525-538.

LaBrie, L.J., 2nd, Palladino, J.L., Grant, E.J., Bronzino, J.D., and Thrall, R.S. (1996). Automated in-vivo measurement of quasi-static lung compliance in the rat. Biomed Instrum Technol *30*, 51-54.

Li, W.C., Rukstalis, J.M., Nishimura, W., Tchipashvili, V., Habener, J.F., Sharma, A., and Bonner-Weir, S. (2010). Activation of pancreatic-duct-derived progenitor cells during pancreas regeneration in adult rats. J Cell Sci *123*, 2792-2802.

Lipatov, A.S., Govorkova, E.A., Webby, R.J., Ozaki, H., Peiris, M., Guan, Y., Poon, L., and Webster, R.G. (2004). Influenza: emergence and control. J Virol *78*, 8951-8959.

Liu, X., Driskell, R.R., and Engelhardt, J.F. (2006). Stem cells in the lung. Methods Enzymol *419*, 285-321.

Longhi, M.P., Williams, A., Wise, M., Morgan, B.P., and Gallimore, A. (2007). CD59a deficiency exacerbates influenza-induced lung inflammation through complement-dependent and -independent mechanisms. Eur J Immunol *37*, 1266-1274.

Lopez-Diazguerrero, N.E., Luna-Lopez, A., Gutierrez-Ruiz, M.C., Zentella, A., and Konigsberg, M. (2005). Susceptibility of DNA to oxidative stressors in young and aging mice. Life Sci *77*, 2840-2854.

Lopez, A.M., Graham, A.R., Barker, G.P., Richter, L.C., Krupinski, E.A., Lian, F., Grasso, L.L., Miller, A., Kreykes, L.N., Henderson, J.T., *et al.* (2009). Virtual slide telepathology enables an innovative telehealth rapid breast care clinic. Semin Diagn Pathol *26*, 177-186.

Lu, Y., Okubo, T., Rawlins, E., and Hogan, B.L. (2008). Epithelial progenitor cells of the embryonic lung and the role of microRNAs in their proliferation. Proc Am Thorac Soc *5*, 300-304.

Marcos, M.A., Esperatti, M., and Torres, A. (2009). Viral pneumonia. Curr Opin Infect Dis *22*, 143-147.

Martin, J., Dinsdale, D., and White, I.N. (1993). Characterization of Clara and type II cells isolated from rat lung by fluorescence-activated flow cytometry. Biochem J *295 (Pt 1)*, 73-80.

Martin, J., Legg, R.F., Dinsdale, D., and White, I.N. (1990). Isolation of Clara cells from rat lung using flow cytometry. Biochem Soc Trans *18*, 664.

Mason, R.J., Williams, M.C., Moses, H.L., Mohla, S., and Berberich, M.A. (1997). Stem cells in lung development, disease, and therapy. Am J Respir Cell Mol Biol *16*, 355-363.

Matthay, M.A., Thompson, B.T., Read, E.J., McKenna, D.H., Jr., Liu, K.D., Calfee, C.S., and Lee, J.W. (2010). Therapeutic potential of mesenchymal stem cells for severe acute lung injury. Chest *138*, 965-972.

McQualter, J.L., Brouard, N., Williams, B., Baird, B.N., Sims-Lucas, S., Yuen, K., Nilsson, S.K., Simmons, P.J., and Bertoncello, I. (2009). Endogenous fibroblastic progenitor cells in the adult mouse lung are highly enriched in the sca-1 positive cell

fraction. Stem Cells *27*, 623-633.

Meissner, N.N., Lund, F.E., Han, S., and Harmsen, A. (2005). CD8 T cell-mediated lung damage in response to the extracellular pathogen pneumocystis is dependent on MHC class I expression by radiation-resistant lung cells. J Immunol *175*, 8271-8279.

Meyer, F. (1994). Topographic Distance and Watershed Lines. Signal Process *38*, 113-125.

Min, B.H., Jeong, S.Y., Kang, S.W., Crabo, B.G., Foster, D.N., Chun, B.G., Bendayan, M., and Park, I.S. (1998). Transient expression of clusterin (sulfated glycoprotein-2) during development of rat pancreas. J Endocrinol *158*, 43-52.

Modelska, K., Pittet, J.F., Folkesson, H.G., Courtney Broaddus, V., and Matthay, M.A. (1999). Acid-induced lung injury. Protective effect of anti-interleukin-8 pretreatment on alveolar epithelial barrier function in rabbits. Am J Respir Crit Care Med *160*, 1450-1456.

Mora, A.L., and Rojas, M. (2008). Aging and lung injury repair: a role for bone marrow derived mesenchymal stem cells. J Cell Biochem *105*, 641-647.

Murasko, D.M., and Jiang, J. (2005). Response of aged mice to primary virus infections. Immunol Rev *205*, 285-296.

Narasaraju, T., Sim, M.K., Ng, H.H., Phoon, M.C., Shanker, N., Lal, S.K., and Chow, V.T. (2009). Adaptation of human influenza H3N2 virus in a mouse pneumonitis model: insights into viral virulence, tissue tropism and host pathogenesis. Microbes Infect *11*, 2-11.

Nolen-Walston, R.D., Kim, C.F., Mazan, M.R., Ingenito, E.P., Gruntman, A.M., Tsai, L., Boston, R., Woolfenden, A.E., Jacks, T., and Hoffman, A.M. (2008). Cellular kinetics and modeling of bronchioalveolar stem cell response during lung regeneration. Am J Physiol Lung Cell Mol Physiol *294*, L1158-1165.

O'Rourke, J. (1994). Computational geometry in C (Cambridge ; New York, Cambridge University Press).

Oda, T., Akaike, T., Hamamoto, T., Suzuki, F., Hirano, T., and Maeda, H. (1989). Oxygen radicals in influenza-induced pathogenesis and treatment with pyran polymer-conjugated SOD. Science *244*, 974-976.

Oreffo, V.I., Morgan, A., and Richards, R.J. (1990). Isolation of Clara cells from the mouse lung. Environ Health Perspect *85*, 51-64.

Ortiz, L.A., Gambelli, F., McBride, C., Gaupp, D., Baddoo, M., Kaminski, N., and Phinney, D.G. (2003). Mesenchymal stem cell engraftment in lung is enhanced in response to bleomycin exposure and ameliorates its fibrotic effects. Proc Natl Acad Sci U S A *100*, 8407-8411.

Otsu, N. (1979). A threshold selection method from gray-level histograms. IEEE Transactions on Systems, Man, and Cybernetics *9(1)*, 62-66.

Pan, T., Nielsen, L.D., Allen, M.J., Shannon, K.M., Shannon, J.M., Selman, M., and Mason, R.J. (2002). Serum SP-D is a marker of lung injury in rats. Am J Physiol Lung Cell Mol Physiol *282*, L824-832.

Parsons, D.W., Morgan, K., Donnelley, M., Fouras, A., Crosbie, J., Williams, I., Boucher, R.C., Uesugi, K., Yagi, N., and Siu, K.K. (2008). High-resolution visualization of airspace structures in intact mice via synchrotron phase-contrast X-ray imaging (PCXI). J Anat *213*, 217-227.

Perl, A.K., Wert, S.E., Loudy, D.E., Shan, Z., Blair, P.A., and Whitsett, J.A. (2005). Conditional recombination reveals distinct subsets of epithelial cells in trachea, bronchi, and alveoli. Am J Respir Cell Mol Biol *33*, 455-462.

Perl, A.K., Wert, S.E., Nagy, A., Lobe, C.G., and Whitsett, J.A. (2002). Early restriction of peripheral and proximal cell lineages during formation of the lung. Proc Natl Acad Sci U S A *99*, 10482-10487.

Pham, D.L., Xu, C., and Prince, J.L. (2000). Current methods in medical image segmentation. Annu Rev Biomed Eng *2*, 315-337.

Potter, C.W. (2001). A history of influenza. J Appl Microbiol *91*, 572-579.

Powers, D.C., and Belshe, R.B. (1993). Effect of age on cytotoxic T lymphocyte memory as well as serum and local antibody responses elicited by inactivated influenza virus vaccine. J Infect Dis *167*, 584-592.

Randell, S.H. (1992). Progenitor-progeny relationships in airway epithelium. Chest *101*, 11S-16S.

Rawlins, E.L., Clark, C.P., Xue, Y., and Hogan, B.L. (2009b). The Id2+ distal tip lung epithelium contains individual multipotent embryonic progenitor cells. Development *136*, 3741-3745.

Rawlins, E.L., and Hogan, B.L. (2006). Epithelial stem cells of the lung: privileged few or opportunities for many? Development *133*, 2455-2465.

Rawlins, E.L., Okubo, T., Xue, Y., Brass, D.M., Auten, R.L., Hasegawa, H., Wang, F., and Hogan, B.L. (2009a). The role of Scgb1a1+ Clara cells in the long-term maintenance and repair of lung airway, but not alveolar, epithelium. Cell Stem Cell *4*, 525-534.

Reynolds, S.D., Giangreco, A., Hong, K.U., McGrath, K.E., Ortiz, L.A., and Stripp, B.R. (2004). Airway injury in lung disease pathophysiology: selective depletion of airway stem and progenitor cell pools potentiates lung inflammation and alveolar dysfunction. Am J Physiol Lung Cell Mol Physiol *287*, L1256-1265.

Reynolds, S.D., Giangreco, A., Power, J.H., and Stripp, B.R. (2000). Neuroepithelial bodies of pulmonary airways serve as a reservoir of progenitor cells capable of epithelial regeneration. Am J Pathol *156*, 269-278.

Reynolds, S.D., and Malkinson, A.M. (2010). Clara cell: progenitor for the bronchiolar epithelium. Int J Biochem Cell Biol *42*, 1-4.

Rock, J.R., Gao, X., Xue, Y., Randell, S.H., Kong, Y.Y., and Hogan, B.L. (2011). Notch-dependent differentiation of adult airway basal stem cells. Cell Stem Cell *8*, 639-648.

Rock, J.R., and Hogan, B.L. (2011). Epithelial progenitor cells in lung development, maintenance, repair, and disease. Annu Rev Cell Dev Biol *27*, 493-512.

Rock, J.R., Onaitis, M.W., Rawlins, E.L., Lu, Y., Clark, C.P., Xue, Y., Randell, S.H., and Hogan, B.L. (2009). Basal cells as stem cells of the mouse trachea and human airway epithelium. Proc Natl Acad Sci U S A *106*, 12771-12775.

Rock, J.R., Randell, S.H., and Hogan, B.L. (2010). Airway basal stem cells: a perspective on their roles in epithelial homeostasis and remodeling. Dis Model Mech *3*, 545-556.

Roignot, P., Donzel, J.P., and Brunaud, M.D. (2011). [The use of virtual slides in the daily practice of a pathology laboratory]. Ann Pathol *31*, 73-77.

Rojas, M., Xu, J., Woods, C.R., Mora, A.L., Spears, W., Roman, J., and Brigham, K.L. (2005). Bone marrow-derived mesenchymal stem cells in repair of the injured lung. Am J Respir Cell Mol Biol *33*, 145-152.

Russell, C.A., Jones, T.C., Barr, I.G., Cox, N.J., Garten, R.J., Gregory, V., Gust, I.D., Hampson, A.W., Hay, A.J., Hurt, A.C., *et al.* (2008). The global circulation of seasonal influenza A (H3N2) viruses. Science *320*, 340-346.

Schoch, K.G., Lori, A., Burns, K.A., Eldred, T., Olsen, J.C., and Randell, S.H. (2004).

A subset of mouse tracheal epithelial basal cells generates large colonies in vitro. Am J Physiol Lung Cell Mol Physiol *286*, L631-642.

Simonsen, L., Taylor, R.J., Viboud, C., Miller, M.A., and Jackson, L.A. (2007). Mortality benefits of influenza vaccination in elderly people: an ongoing controversy. Lancet Infect Dis *7*, 658-666.

Smith, L.J. (1985). Hyperoxic lung injury: biochemical, cellular, and morphologic characterization in the mouse. J Lab Clin Med *106*, 269-278.

Steinberg, D.M., and Ali, S.Z. (2001). Application of virtual microscopy in clinical cytopathology. Diagn Cytopathol *25*, 389-396.

Stohr, K. (2002). Influenza--WHO cares. Lancet Infect Dis *2*, 517.

Stripp, B.R., and Reynolds, S.D. (2008). Maintenance and repair of the bronchiolar epithelium. Proc Am Thorac Soc *5*, 328-333.

Suliman, H.B., Ryan, L.K., Bishop, L., and Folz, R.J. (2001). Prevention of influenza-induced lung injury in mice overexpressing extracellular superoxide dismutase. Am J Physiol Lung Cell Mol Physiol *280*, L69-78.

Taubenberger, J.K., and Morens, D.M. (2008). The pathology of influenza virus infections. Annu Rev Pathol *3*, 499-522.

Teisanu, R.M., Lagasse, E., Whitesides, J.F., and Stripp, B.R. (2009). Prospective isolation of bronchiolar stem cells based upon immunophenotypic and autofluorescence characteristics. Stem Cells *27*, 612-622.

Ten Have-Opbroek, A.A. (1979). Immunological study of lung development in the mouse embryo. II. First appearance of the great alveolar cell, as shown by immunofluorescence microscopy. Dev Biol *69*, 408-423.

Thebaud, B., Ladha, F., Michelakis, E.D., Sawicka, M., Thurston, G., Eaton, F., Hashimoto, K., Harry, G., Haromy, A., Korbutt, G., *et al.* (2005). Vascular endothelial growth factor gene therapy increases survival, promotes lung angiogenesis, and prevents alveolar damage in hyperoxia-induced lung injury: evidence that angiogenesis participates in alveolarization. Circulation *112*, 2477-2486.

Theise, N.D., Henegariu, O., Grove, J., Jagirdar, J., Kao, P.N., Crawford, J.M., Badve, S., Saxena, R., and Krause, D.S. (2002). Radiation pneumonitis in mice: a severe injury model for pneumocyte engraftment from bone marrow. Exp Hematol *30*, 1333-1338.

Toapanta, F.R., and Ross, T.M. (2009). Impaired immune responses in the lungs of aged mice following influenza infection. Respir Res *10*, 112.

van Haaften, T., Byrne, R., Bonnet, S., Rochefort, G.Y., Akabutu, J., Bouchentouf, M., Rey-Parra, G.J., Galipeau, J., Haromy, A., Eaton, F., *et al.* (2009). Airway delivery of mesenchymal stem cells prevents arrested alveolar growth in neonatal lung injury in rats. Am J Respir Crit Care Med *180*, 1131-1142.

van Riel, D., Munster, V.J., de Wit, E., Rimmelzwaan, G.F., Fouchier, R.A., Osterhaus, A.D., and Kuiken, T. (2007). Human and avian influenza viruses target different cells in the lower respiratory tract of humans and other mammals. Am J Pathol *171*, 1215-1223.

Van Winkle, L.S., Johnson, Z.A., Nishio, S.J., Brown, C.D., and Plopper, C.G. (1999). Early events in naphthalene-induced acute Clara cell toxicity: comparison of membrane permeability and ultrastructure. Am J Respir Cell Mol Biol *21*, 44-53.

Velez, N., Jukic, D., and Ho, J. (2008). Evaluation of 2 whole-slide imaging applications in dermatopathology. Hum Pathol *39*, 1341-1349.

Wang, J.L., and Wang, P.C. (2012). The effect of aging on the DNA damage and repair capacity in 2BS cells undergoing oxidative stress. Mol Biol Rep *39*, 233-241.

Woolfenden, J.M., Alberts, D.S., Hall, J.N., and Patton, D.D. (1979). Cobalt-57 bleomycin for imaging head and neck tumors. Cancer *43*, 1652-1657.

Wuenschell, C.W., Sunday, M.E., Singh, G., Minoo, P., Slavkin, H.C., and Warburton, D. (1996). Embryonic mouse lung epithelial progenitor cells co-express immunohistochemical markers of diverse mature cell lineages. J Histochem Cytochem *44*, 113-123.

Zhou, F., Onizawa, S., Nagai, A., and Aoshiba, K. (2011). Epithelial cell senescence impairs repair process and exacerbates inflammation after airway injury. Respir Res *12*, 78.